CUKUROVA UNIVERSITY

INSTITUTE OF NATURAL AND APPLIED SCIENCES

MSc THESIS

Design of A Hybrid PV-Fuel Cell System with Active Reactive Power Control Capabilities

Ramazan MACİT

Electrical and Electronics Engineering Department

August 2023

CUKUROVA UNIVERSITY
INSTITUTE OF NATURAL AND APPLIED SCIENCES

MSc THESIS APPROVAL

Design of A Hybrid PV-Fuel Cell System with Active Reactive Power Control Capabilities

---

Ramazan MACİT

Electrical and Electronics Engineering Department

This Master's Thesis was evaluated by the following Jury Members on 28/08/2023 and was approved by unanimity / majority of votes.

Jury : Prof. Dr. Ahmet TEKE (Advisor) …………

: Asst. Prof. Dr. Oğuzhan TİMUR …………

: Asst. Prof. Dr. Kasım ZOR …………

This Thesis was written in the Department of Electrical and Electronics Engineering Institute of Natural and Applied Sciences.

Thesis Number:

Prof. Dr. Sadık DİNÇER
Institute Director

This work was supported by the Scientific Research Project Unit of Çukurova University.
Project ID: FYL-2022-15330

CONTENTS

CUKUROVA UNIVERSITY
INSTITUTE OF NATURAL AND APPLIED SCIENCES

MSc THESIS

Design of A Hybrid PV-Fuel Cell System with Active Reactive Power Control Capabilities

Ramazan MACİT

Advisor: Prof. Dr. Ahmet TEKE
Co-advisor: Asst. Prof. Dr. Özgür ÇELİK

Department of Electrical and Electronics Engineering

ABSTRACT

The increasing use and integration of renewable energy into the electricity grid has started to have impacts on power system security and stability. Hence, grid integration needs have become a major concern as the share of renewable energy sources in the electricity grid is gradually increasing and replacing conventional power plants. The sudden disconnection of large renewable power plants during outages can lead to problems with power stability, reliability, and overall system operation. Grid codes are rules that developed by transmission system operators to address integration requirements. An important aspect of grid codes is the low voltage ride-through (LVRT) feature. Recent regulations require renewable power systems to remain connected to the grid during faults, providing/frequency support like conventional installations and contributing to grid stability and reliability. Different countries have specific grid code requirements, but overall, the objective is to ensure stable and reliable operation of the power system. In this thesis, Türkiye's LVRT requirements are considered. The fulfillment of LVRT requirements for renewable power plants requires overcoming important issues such as the prevention of overcurrent at the AC side and overvoltage on the DC side of the inverter. In this thesis, a flexible active power control approach using an artificial neural network (ANN) is developed to improve DC voltage stabilization of photovoltaic (PV)- fuel cell (FC) hybrid power system to overcome overcurrent at the AC side during grid faults. A detailed simulation of proposed grid-connected PV-FC hybrid power system is carried out using MATLAB/Simulink to evaluate the performance of the suggested control scheme. The performance of the proposed system is evaluated by subjecting it to symmetric and asymmetric faults in four different fault types to improve the LVRT capabilities of the PV-FC hybrid system. This approach improves DC-link voltage stability and provides consistent voltage levels by limiting voltage deviation to between 12.9 % dip and 10.1 % peak in all fault types.

Key Words: LVRT, Grid code, PV-FC hybrid system, Renewable energy

ÇUKUROVA ÜNİVERSİTESİ
FEN BİLİMLERİ ENSTİTÜSÜ

YÜKSEK LİSANS TEZİ

Aktif Reaktif Güç Kontrol Özelliklerine Sahip Hibrit FV-Yakıt Hücreleri Sisteminin Tasarımı

Ramazan MACİT

Danışman: Prof. Dr. Ahmet TEKE
İkinci danışman: Dr. Öğr. Üyesi Özgür ÇELİK

Elektrik Elektronik Mühendisliği Anabilim Dalı

ÖZ

Yenilenebilir enerji kaynaklarının elektrik şebekesindeki payı giderek artmakta ve geleneksel enerji santrallerinin yerini almaktadır, dolayısıyla şebeke entegrasyon ihtiyaçları önemli bir endişe kaynağı haline gelmiştir. Hata durumlarında büyük yenilenebilir enerji santrallerinin şebeke bağlantısının aniden kesilmesi, güç istikrarı, güvenilirlik ve genel sistem işletimi ile ilgili sorunlara yol açabilir. Şebeke yönetmelikleri, iletim sistemi operatörleri tarafından entegrasyon gereksinimlerini karşılamak için geliştirilen yönergeler ve kuralları içerir. Şebeke yönetmeliklerinin önemli bir gerekliliği düşük gerilim geçiş (DGG) özelliğidir. Bu özellik, yenilenebilir enerji sistemlerinin arızalar sırasında şebekeye bağlı kalmasını, geleneksel tesisler gibi voltaj/frekans desteği sağlamayarak ve şebeke istikrarına ve güvenilirliğine katkıda bulunmasını gerektirmektedir. Farklı ülkelerin özel şebeke yönetmelikleri vardır, ancak genel olarak amaç, güç sistemlerinin istikrarlı ve güvenilir çalışmasını sağlamaktır. Bu tezde Türkiye'nin DGG gereksinimleri dikkate alınmıştır. Yenilenebilir enerji sistemlerinin LVRT gereksinimlerinin karşılanması, alternatif akım alternatif akım (AA) tarafında aşırı akımın önlenmesi ve eviricinin doğru akım (DA) tarafında aşırı gerilimin engellenmesi gibi önemli sorunların üstesinden gelmeyi gerektirir. Bu tezde, fotovoltaik (FV)-yakıt hücreli (YH) hibrit güç sisteminin DA voltaj stabilizasyonunu iyileştirmek ve şebeke arızaları sırasında AA tarafında aşırı akımı sınırlandırmak amacıyla yapay sinir ağı kullanan esnek bir aktif güç kontrol yöntemi geliştirilmiştir. Önerilen kontrol yönteminin performansını değerlendirmek için FV-YH hibrit sisteminin MATLAB/Simulink ortamında detaylı bir modeli geliştirilmiştir. Geliştirilen model FV-YH hibrit sisteminin DGG yeteneklerini test etmek amacıyla için dört farklı arıza tipinde simetrik ve asimetrik arızalara maruz bırakılarak analiz edilmiştir. Analizler sonucunda önerilen yöntemin DA-bara gerilim kararlılığını iyileştirdiği ve tüm arıza türlerinde gerilim sapmasını % 12.9 dip ve % 10.1 tepe arasında sınırladığı gözlemlenmiştir.

Anahtar Kelimeler: DGG, Şebeke yönetmeliği, FV-YH hibrit sistem, yenilenebilir enerji

GENİŞLETİLMİŞ ÖZET

Günümüzde, çevresel kaygıların artmasıyla birlikte yenilenebilir enerji kaynaklarının kullanımı ve elektrik şebekesine entegrasyonu önemli bir odak noktası haline gelmiştir. Yenilenebilir enerji kaynaklarının artan kullanımı, enerji sektörünü dönüştürerek geleneksel fosil yakıt tabanlı enerji üretiminin yerine daha temiz ve sürdürülebilir alternatiflerin getirilmesini sağlamaktadır. Ancak, bu geçiş süreci beraberinde bazı zorlukları da getirmektedir. Yenilenebilir enerji kaynaklarının elektrik şebekesine entegrasyonu, güç sistemi güvenliği ve istikrarı açısından yeni dinamikleri ortaya çıkarmıştır. Geleneksel enerji santrallerinin aksine, yenilenebilir enerji kaynakları kesintilidir ve hava koşullarına bağlı olarak üretimleri değişebilir. Bu durum, enerji arzının istikrarını etkileyebilir ve ani güç dalgalanmalarına neden olabilir. Şebekelerdeki arıza durumlarında büyük ölçekli yenilenebilir enerji santrallerinin şebekeden bağlantılarının aniden kesilmesi, güç istikrarı ve genel sistem işletimi ile ilgili sorunlara yol açabilir.

İletim sistemi operatörleri yenilenebilir enerji kaynaklı sistemlerini etkin bir şekilde elektrik şebekelerine entegrasyonunu düzenlemek amacıyla şebeke yönetmelikleri yayınlamaktadır. Şebeke yönetmelikleri, enerji iletimi ve dağıtımının sürdürülebilirliği için kritik öneme sahip, modern enerji sektörünün düzenleyici temel unsurlarını belirler. Bu yönetmelikler, enerji üreticileri, dağıtım şirketleri ve tüketiciler arasındaki ilişkileri ve etkileşimleri düzenlemekte ve enerji sistemlerinin güvenilirliğini ve istikrarını sağlamak amacıyla oluşturulmaktadır. Farklı ülkelerin enerji altyapıları, kendilerine özgü şebeke yönetmelikleri çerçevesinde şekillenir; ancak temel amaç, güç sisteminin sürekli istikrar ve güvenilirlik içinde işlemesini sağlamaktır.

Şebeke yönetmeliklerinin önemli bir gerekliliği, DGG özelliğidir. Bu özellik yenilenebilir enerji sistemlerinin şebeke arızalar sırasında belirli bir süre şebekeye bağlı kalmasını, geleneksel tesisler gibi şebekeye destek sağlamasını, şebeke istikrarına ve güvenilirliğine katkıda bulunmasını gerektirmektedir. Yenilenebilir enerji santrali DGG gereksinimlerine yanıt vermek, iki kritik sorunu ele almayı içerir.

İlk olarak, eviricinin AA tarafında aşırı akım ve DA tarafında aşırı gerilim oluşmasını önlemek önemlidir. Şebekedeki ani voltaj düşüşünün neden olduğu aşırı akım, giriş ve çıkış gücü arasındaki farkın bir sonucu olarak DA geriliminin dalgalanmasına neden olmaktadır. DA tarafındaki gerilim dalgalanmaları ve dengesizlikler, sistem performansını olumsuz etkileyebilir ve ekipmana zarar verebilir. Yenilenebilir enerji santrallerinin DGG gereksinimlerinin karşılanması, eviricinin AA tarafında aşırı akımın önlenmesi ve DA bağlantı noktasında aşırı gerilimin engellenmesi gibi önemli sorunlar, modern yenilenebilir enerji sistemlerinin verimli ve güvenilir bir şekilde çalışabilmesi için ele alınması gereken kritik konulardandır.

İkinci olarak, gerilim düşmeleri sırasında yenilenebilir enerji sistemi, şebeke gerilimini dengelemeye yardımcı olmak için reaktif güç desteği sağlamalıdır. Bu, gerilimi kabul edilebilir

sınırlar içinde tutmak için reaktif güç enjekte etmeyi veya emmeyi içerir. Reaktif güç desteği, gerilim düşüşünü hafifletmeye ve gerilim iyileştirmesine yardımcı olabilir.

Bu sorunların üstesinden gelmek için, evirici sistemleri ve güç elektroniği teknolojileri geliştirilmekte ve iyileştirilmektedir. Bu çalışmada, önerilen FV-YH hibrit sistemin hata durumlarında DA gerilim kararlılığını artırmak için yapay sinir ağları kullanan esnek bir aktif güç kontrol stratejisi geliştirilmiştir. Geliştirilen kontrol stratejisi, sistemin kararlılığını ve verimliliğini artırmak amacıyla bu tür dalgalanmaları tespit edip düzenlemeyi hedefler. Aynı zamanda, sistemin güvenilirliğini ve şebekeye uyumunu iyileştirmek amacıyla güç çıkışını düzenler ve aşırı akımı belirli sınırlar altında tutar.

Önerilen kontrol yönteminin performansını değerlendirmek için FV-YH hibrit sisteminin MATLAB/Simulink ortamında detaylı bir modeli geliştirilmiştir. Tasarlanan modelin performansı, kararlı ve geçici koşullar altında yapılan testlerle değerlendirilmiştir. Geliştirilen model FV-YH hibrit sisteminin DGG yeteneklerini test etmek amacıyla için dört farklı arıza tipinde simetrik ve asimetrik arızalara maruz bırakılarak analiz edilmiştir. Analizler sonucunda önerilen yöntemin DA-bara gerilim kararlılığını iyileştirdiği ve tüm arıza türlerinde gerilim sapmasını % 12.9 dip ve % 10.1 tepe arasında sınırladığı gözlemlenmiştir.

Önceki çalışmaların aksine, sistem geçici durumlar sırasında dinamik tepkisini analiz etmek için ardışık hatalara maruz bırakılarak davranışının kapsamlı bir şekilde incelemesi yapılmıştır. Elde edilen sonuçlar, geliştirilen yapay sinir ağı tabanlı kontrol yönteminin, tasarlanan FV-YH hibrit güç sisteminde istikrarlı bir şekilde çalıştığını göstermektedir.

Bu hibrit sistemin en önemli özelliklerinden biri, aktif ve reaktif güç kontrol kabiliyetleridir. Sistem, aktif güç üreterek elektrik şebekesine enerji sağlar ve reaktif güç üreterek gerilimi düzenler. Bu özellik, şebekenin kararlılığını sağlamak için önemlidir. Özellikle büyük endüstriyel tesislerde, güç faktörünün düzeltilmesi gerekebilir ve bu sistem bu gereksinimi karşılayabilir. Sistem aynı zamanda çoklu mod kontrol stratejisi ve enerji yönetimi şeması ile optimize edilmiştir. Bu, enerji üretimi ve tüketiminin akıllıca yönetilmesini sağlar. Tasarlanan enerji yönetim sistemi, enerji ihtiyaçlarına göre FV-YH kaynakların gücünü ayarlayabilme özelliğine sahiptir, bu sayede enerji verimli bir şekilde yönetilebilmektedir.

Sonuç olarak, önerilen FV-YH hibrit yenilenebilir enerji sistemi, aktif ve reaktif güç kabiliyetleriyle elektrik şebekesi kararlılığını katkıda bulunmaktadır. Aynı zamanda şebeke hataları durumunda yenilenebilir enerji kaynağının belirli bir süre bağlı tutarak sistemin hata direncini artırmaktadır. Tasarlanan sistemin dinamik tepki kabiliyetleri ve gerilim düşmeleri ve bozulmaları sırasında çalışmaya devam etme yeteneği simülasyonlar aracılığıyla doğrulanmıştır. Çoklu mod kontrol stratejisi ve enerji yönetimi şemasının entegrasyonu, normal ve arıza senaryolarında verimli çalışmayı sağlayarak güç üretimini ve kullanımını optimize eder. Sistem ayrıca Türkiye'nin yenilenebilir enerji yönetmeliğinde bulunan aktif güç kontrol kabiliyeti ve DGG gereksinimlerine uygun olacak şekilde tasarlanmıştır.

Türkiye, enerji talebinin arttığı ve iklim değişikliğinin etkilerini hissettiği bir dönemden geçmektedir. Geleneksel fosil yakıtlara dayalı enerji üretimi, çevresel ve iklimsel sorunların önde gelen nedenlerinden biri olarak kabul edilmektedir. Buna karşılık yenilenebilir enerji sistemleri, güneş, rüzgâr, hidroelektrik, biyokütle ve hidrojen enerjisi gibi çevre dostu kaynakları kullanarak enerji üretir. Bu bağlamda, yenilebilir enerji kaynaklarının elektrik şebekelerinde geleneksel fosil yakıtlı kaynaklarının yerine kullanımı sera gazı emisyonlarını azaltmaya ve iklim değişikliği etkilerinin azaltılmasına yardımcı olabilir.

Özellikle hidrojen FV-YH enerji kaynakları teknolojik gelişmelerle birlikte ucuzlamakta ve giderek daha fazla ilgi görmektedir. Bu tür kaynakların sabit güç uygulamalarında kullanımı temiz enerji için büyük umut vaat etmektedir. Yenilenebilir enerji kaynaklarının en büyük eksikliklerinden biri kesintili enerji üretim yapmalarıdır. Bu eksikliği gidermek için birden fazla kaynak türünü hibrit olarak kullanan sistemler tasarlanmaktadır. Son yıllarda hidrojen enerjisine olan ilgi artmaktadır. Hidrojen YH hücreleri, yakıt olarak hidrojen kullanmaktadır ve hidrojen beslendiği sürece enerji üretimine devam edebilmektedir, yakıt hücrelerinin bu özelliği onları enerji üretiminde güvenli bir kaynak haline getirmektedir. Sonuç olarak yakıt hücresi teknolojisinin birincil güç ve yedek güç uygulamaları sistemlerine entegre edilmesi, daha yeşil bir enerji sektörüne geçişi hızlandırabilir. Sözü geçen avantajlarından dolayı bu sistemin tasarımında FV-YH hibrit kaynaklar kullanılmıştır.

Gelecekte, yenilenebilir enerji kaynaklarının elektrik şebekelerinde kullanımının artmasıyla birlikte, bu tür çalışmaların önemi daha da artacaktır. Enerji sektörü, güvenli ve istikrarlı bir şekilde yenilenebilir enerjiye geçiş için yeni teknolojiler ve kontrol sistemleri üzerinde çalışmaya devam edecektir.

ACKNOWLEDGMENTS

First of all, I would like to express my deepest gratitude to Prof. Dr. Ahmet TEKE and Asst. Prof. Dr. Özgür ÇELİK for their guidance, invaluable expertise, endless support, and patience throughout the journey of this thesis. Their scientific approach has enabled me to accomplish this thesis.

In addition, I would like to extend my sincere gratitude to the members of the jury Asst. Prof. Dr. Oğuzhan TİMUR and Asst. Prof. Dr. Kasım ZOR for many generous and helpful suggestions.

I would like to acknowledge the Scientific Research Project Unit of Çukurova University for their generous financial support in conducting the research titled “Design of Hybrid PV-Fuel Cell System with Active Reactive Power Control Capabilities” (Project Number: FYL-2022-15330).

I also would like to express my sincere thanks to Asst. Prof. Dr. Altan ONAT, Res. Asst. Ali SOLAK, Res. Asst. Kerim ÖRÜKLÜ, and my roommate Res. Asst. Dr. Özge EROL, and my other colleagues. Their moral support and constant encouragement contributed significantly to the successful completion of this thesis.

Finally, I would like to express my deepest gratitude to my family for their unwavering support throughout my thesis and my life journey.

LIST OF TABLES

LIST OF FIGURES

SYMBOLS AND ABBREVIATIONS

AC : Alternating Current
AFC : Alkaline Fuel Cell
ANFIS : Adaptive Neuro-Fuzzy Inference System
DC : Direct Current
DCM : Discontinuous Conduction Mode
DDSRF : Decouple Double Synchronous Reference Frame
DLG : Double Line to Ground
EMC : Electromagnetic Compatibility
EMS : Energy Management Scheme
FC : Fuel Cell
FCTO : Fuel Cell Technology Office
FRT : Fault Ride Through
GW : Giga Watt
INC : Incremental Conductance
IAE : International Energy Agency
IEEE : Institute of Electrical and Electronics Engineers
IRENA : International Renewable Energy Agency
KOSPO : Korean Southern Power
LL : Line-to-Line
LVRT : Low Voltage Ride Through
MLI : Multilevel Inverter
MPP : Maximum Power Point
MPPT : Maximum Power Point Tracking
NPC : Neutral Point Clamped
PAFC : Phosphoric Acid Fuel Cell
PV : Photovoltaic
PEMFC : Proton-Exchange Membrane Fuel Cell
PMSG : Permanent Magnet Synchronous Generator
P&O : Perturb and Observe
SAPP : Stand-Alone Power Plants
SCADA : Supervisory Control and Data Acquisition
SBP : Strategy Budget Planning
SLG : Single Line to Ground
SRF : Synchronous Reference Frame

STC : Standard Test Conditions

THD : Total Harmonic Distortion

TLG : Three Lines to Ground

VRT : Voltage Ride Through

1. INTRODUCTION

In this section, topics such as the world energy capacity, the energy profile in Türkiye, the importance of renewable energy sources, the share of renewable energy resources in the world electricity capacity, hybrid renewable energy systems, the role of renewable energy sources in grid stabilization and the grid integration of renewable energy resources are discussed. The background and motivation, purpose and outline of the thesis, and contributions of the thesis are also given in this section.

1.1. Background and Motivation

1.1.1. Energy in the World

The growth of the world's electricity generation capacity has been on a steady upward trend in recent years, driven by the increasing demand for energy to power homes, businesses, and industrial processes. This growth is being driven by a combination of factors, including population growth, urbanization, and the increasing use of technology and electrification in many areas of life. Annual global power capacity increase between 2000-2022 is given in Figure 1.1, according to IRENA data, world energy capacity has reached over 8000 GWs at the end of 2022 and this capacity is expected to increase (IRENA, 2023). The global increase in energy demands and increasing environmental concerns have led to a significant increase in power generation from RES (Bonthagorla and Mikkili, 2022).

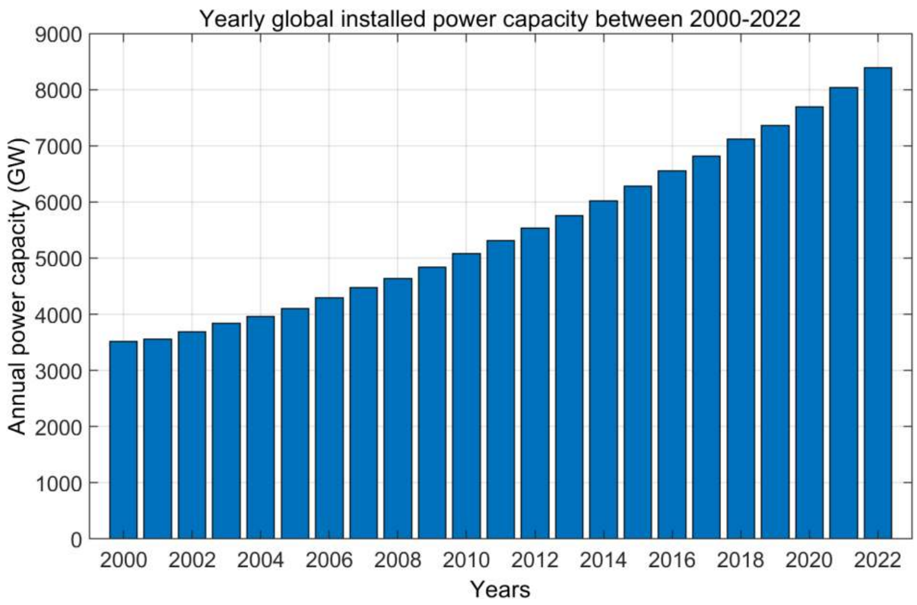

Figure 1.1. Global installed power capacity growth between 2000-2022 (IRENA, 2023)

1.1.2. Energy in Türkiye

Türkiye has a diverse energy mix, with significant sources of both conventional and renewable energy. Türkiye is heavily dependent on imported oil and gas to meet its energy needs, with domestic production of these fuels being limited (IEA, 2021). As a result, Türkiye is planning a roadmap to diversify its energy mix and increase the use of renewable energy sources. Türkiye also has significant hydroelectric, solar, and wind power potential, and the government has been promoting the development of these renewable energy sources in recent years to increase the efficiency and competitiveness of the sector (SBP, 2022). This has included the privatization of state-owned energy companies, the liberalization of energy markets, and the development of a legal framework to encourage investment in the sector. According to the Turkish Energy Transmission Corporation (TETC, 2023) report, Türkiye's total installed power capacity reached 103.809 GWs at the end of 2022. In 2016, renewable sources installed power capacity was at a level of 44%. By the end of 2022, Türkiye's renewable energy installed power capacity reached 54% and dominated by a steady increase in investments in these sources over the years. Türkiye's installed power capacity growth by sources between 2016-2022 is presented in Figure 1.2.

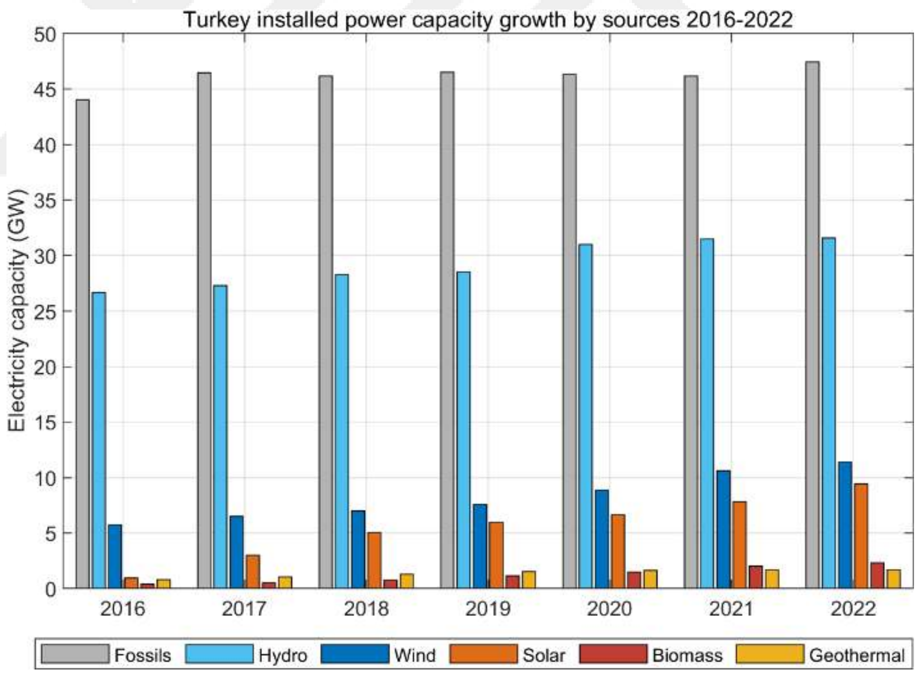

Figure 1.2. Türkiye energy growth by sources 2016-2022 (TETC, 2023)

1.1.3. Renewable Energy

The consumption of fossil fuels for electricity generation has several drawbacks, such as emitting harmful pollutants, contributing to air pollution and global warming (Hosseini et al., 2022; Velvizhi et al., 2023). Additionally, the extraction and transportation of fossil fuels lead to environmental degradation and vulnerability to price fluctuations and supply disruptions (Alizadeh and Avami, 2021).

The declining costs of renewables make them an attractive option for decarbonizing electricity production and limiting global temperature rise (Osman et al., 2023). They are environmentally friendly, producing minimal greenhouse gas emissions and pollutants, thus mitigating climate change. Moreover, renewables are sustainable, naturally replenished, and provide a more secure energy solution for the future. By transitioning to renewable energy, we can achieve a cleaner, more sustainable, and cost-effective energy future while reducing dependence on imported fossil fuels and enhancing energy security (OECD, 2022).

Renewable energy sources such as solar, wind, and hydropower, offer numerous advantages over fossil fuels. Among renewable sources, PV power generation systems have grown exponentially and are expected to play a crucial role in the energy systems of the future (Morey et al., 2023). The power generation of PV energy systems relies on solar irradiation. Hence, suitable environmental conditions are crucial for continuous energy production from these systems (Maradin, 2021). To ensure consistent energy production, it is advisable to consider utilizing these resources in hybrid configurations with other complementary energy sources (Huang et al., 2022). Hydrogen FC technology shows great promise for clean energy in stationary power applications. Integrating FC technology into primary power, backup power, and combined heat-power applications systems can accelerate the shift towards a greener energy sector (Bizon and Thounthong, 2021; Felseghi et al., 2019). The world's largest hydrogen FC facility, the 78.96MW Shinincheon Bitdream FC Power Plant in Incheon, South Korea, built by Korean Southern Power, supplies power to 250,000 homes, heats an additional 44,000 house, and absorb 24,000 tons of fine dust each year purifies air for 700,000 people in the vicinity (KOSPO, 2021). This instance serves as a notable illustration of the combined heat-power application potential of FC technology. Hydrogen's production cost decreases annually (Marqusee et al., 2021). In the next five years, the capacity for producing hydrogen from renewable sources is expected to increase 100 times, providing a chance to decrease carbon emissions in industry and transportation (IEA, 2022). The PV-FC hybrid system was chosen due to its numerous mentioned advantages and suitability.

1.1.4. Grid Integration

The share of RES in the electricity grid is increasing as countries transition towards clean and sustainable energy sources. Strong policy support and high electricity prices are expected to drive record global renewable electricity installations in 2023 and 2024. Renewable capacity is expected to increase by 107 GW to more than 440 GW in 2023, with solar and wind power overcoming challenges and remaining competitive. Solar PV will lead 2024's renewable capacity growth (IEA, 2023). Figure 1.3. illustrates the share of annual power capacity expansion, reflecting this ongoing transition.

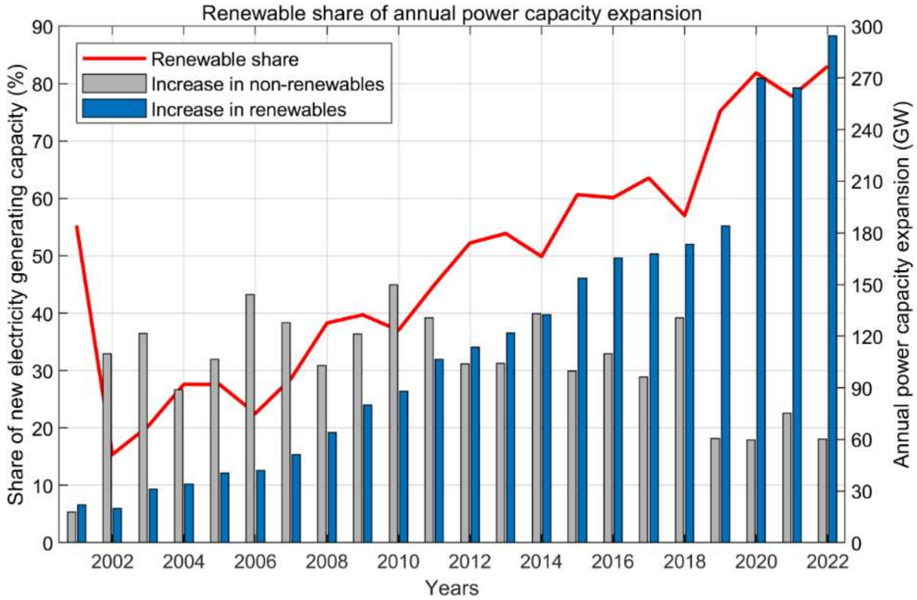

Figure 1.3. Renewable share of annual power capacity expansion (IRENA, 2023)

The stability of utility grids can be adversely affected by sudden disconnections of large-scale renewable energy sources (Soto et al., 2022). As the penetration of renewable energy increases, concerns arise about power quality and system security. To address these issues, various countries such as Türkiye, Malaysia, Denmark, Germany, other European countries, Japan, China, and the United States have introduced new grid codes that offer ancillary services to enhance stability and power quality (Çelik et al., 2022; Rahman et al., 2022; Zeb et al., 2022). Collaboration between government agencies, utilities, and renewable energy developers drives the development and implementation of grid codes (IRENA, 2022). Grid codes also are essential for integrating renewable energy into the power grid, ensuring compliance with safety, reliability, and efficiency standards. These codes impose specific requirements on RES, varying based on type, location, and specific grid code. Among these services, the LVRT feature holds significant importance. LVRT allows renewable energy systems to remain connected to the grid during voltage dips, mitigating grid instability issues and ensuring a reliable power supply.

Addressing renewable power plant LVRT requirements involves tackling two critical issues (Al-Shetwi et al., 2019). Firstly, it is essential to prevent over-current on the AC side and over-voltage on the DC side of PV inverters. Over-current and over-voltage occurrences can lead to system instability and potential damage to equipment. Secondly, to ensure grid stability during grid failures, reactive current injection is employed. This process involves injecting controlled reactive power to support grid voltage recovery, mitigating the impact of disruptions, and enabling renewable power plants to remain connected during voltage dips or faults, enhancing grid resilience.

Figure 1.4 represents a typical LVRT graph, which specifies certain requirements such as voltage thresholds and time intervals that the power generation system must comply with during grid faults. These requirements may include voltage levels at which the system must continue to operate, time limits for remaining connected during voltage dips, and conditions that trigger disconnection. During normal operation, the power generation system functions between v_{lim2} and v_{lim3}. If the voltage dips below v_{lim2} (blue zone), the system remains connected, if falls into the red area system should disconnect for safety. These limits vary according to transmission operators and country regulations (Hagh and Khalili, 2019). The Turkish Energy Market Regulatory Authority (EMRA, 2022) LVRT operation limits are given in Figure 1.4. The LVRT criteria include firstly, the power system must maintain connection for 150 milliseconds under all conditions and stay within the limits of the blue area, secondly, if the grid voltage drops below the set threshold (red area), PV systems can disconnect for safety.

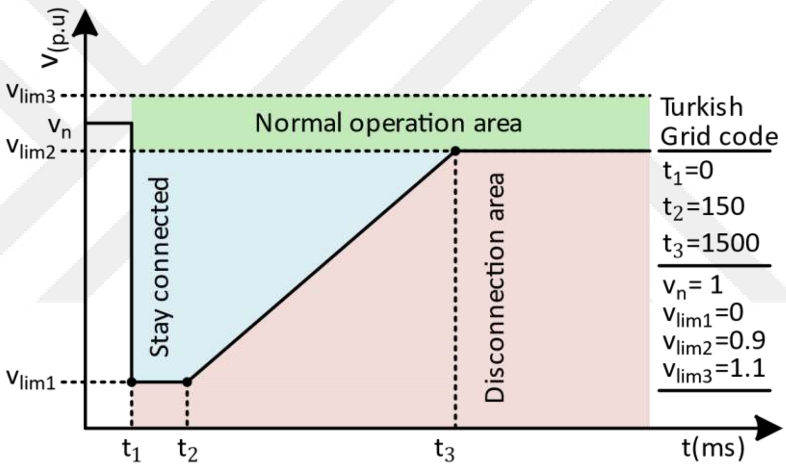

Figure 1.4. LVRT graph-Turkish grid code

To address LVRT requirements papers propose several innovative approaches to improve the performance and stability of PV inverters during grid faults. The paper by (Ding et al., 2016) presents an adaptive DC-link voltage control method to manage voltage fluctuation during faults, (Ma et al., 2022) propose an LVRT strategy incorporating a crowbar circuit to address DC capacitance voltage instability and improve stability, (Nasiri et al., 2022) present an LVRT strategy for single-stage PV systems using a breaker chopper, (Nithya and Roselyn, 2022) proposes a multimode inverter control with fault driving scheme and integrated DC chopper, (Mohamed et al., 2019) proposes a hybrid control approach with braking chopper to regulate DC-link overvoltage, (Huka et al., 2018; Mirhosseini et al., 2015; Yang et al., 2014) introduces an LVRT strategy with a power reduction method to control the DC-link voltage by shifting the PV operating point to the non-MPPT point.

The current literature investigates a wide range of source combinations in PV-FC systems, but there is limited research on the FRT capabilities of PV-FC systems. Existing LVRT methods utilize fixed duty cycles for the boost stage, which may cause unstable DC-link voltage during severe sags, potentially leading to instability due to discontinuous conduction mode. To address these challenges, there is a pressing need for the development of adaptive duty cycle strategies. Adaptive duty cycles can help avoid issues during severe sags, ensuring a safe and continuous boost operation. Further research in this direction will contribute to the improved stability and performance of PV-FC systems under grid faults.

1.2. Objective of the Thesis

The objective of this study is to develop and implement a hybrid RES system in LVRT version in accordance with the Turkish electricity grid regulations. The system is designed considering the following key contributions:

- Maintain boost converter operation safely without external circuitry, ensuring a variable power approach independent of voltage severity LVRT strategy.
- Develop a flexible power control strategy employing adaptive duty cycles to stabilize the DC-link voltage during severe sags.
- Implement over-current limitation according to the German grid code during voltage sags to protect the system.
- Employ a multilevel inverter to achieve low THD and reduced switching frequency, enhancing overall system efficiency.
- Conduct comprehensive simulations on a 300-kW system to evaluate and optimize the proposed approach.
- Propose a comprehensive design and simulation approach for PV-FC hybrid RES system, integrating theoretical analysis and simulation studies for enhanced renewable energy system efficiency.
- Evaluate system performance under symmetrical and asymmetrical voltage sags, while subjecting it to sequential faults, to analyze the dynamic response of the proposed approach.

1.3. Contributions of the Thesis

The contributions of the proposed PV-FC hybrid RES system with active and reactive power are summarized below:

- An innovative approach is presented with a flexible active power control method using ANN. This method significantly improves DC-link voltage stability by effectively managing PV array power during grid disturbances.
- The system is equipped with LVRT capacity in various sag levels, enabling it to withstand and continue operation during voltage dips or disturbances in the grid including symmetrical and asymmetrical faults. The system exhibits dynamic response during LVRT operation, responding quickly to grid variations.
- The PV-FC hybrid power plant achieves active and reactive power capabilities for enhanced grid support and stability.
- An energy management scheme efficiently handles faults and normal operation scenarios, optimizing power generation and utilization.
- The system is compatible with Türkiye's latest renewable energy sources grid integration regulations.
- A comprehensive LCL filter design is performed.
- The system operates within the required THD limits, ensuring the injected power meets IEEE quality standards and Turkish grid regulations.
- A multimode control strategy enhances the system's flexibility and adaptability under different conditions.
- Safe DC-link voltage limits are maintained during voltage dips to ensure reliable operations and system stability.
- A multilevel converter improves power quality by delivering lower THD on voltage and current waveforms. It reduces switch power dissipation, making it suitable for high voltage applications, and provides high efficiency thanks to lower switching frequencies.
- Components of the system are modeled using MATLAB/Simulink for reliable design and simulation.
- By implementing a sustainable hybrid RES system, the project aims to reduce pollution and emissions, contributing to environmental preservation.
- A comprehensive design and simulation are established to support future research and studies in the field of hybrid renewable energy systems.

1.4. Organization of the Thesis

Chapter 1: This chapter consists of background and motivation, grid integration, objective and outline of the thesis, and organization of the thesis.

Chapter 2: This chapter covers preliminary work for renewable energy systems, studies based on hybrid systems being standalone and grid-connected, grid codes, and literature-based information about LVRT are all discussed in this section.

Chapter 3: This chapter covers the design of PV-FC hybrid system, MPPT, boost DC-DC converter, inverter, LCL filter, energy management, the utility grid, and mathematical modeling.

Chapter 4: This chapter covers simulation results for the proposed grid-connected PV-FC system, summarizing results and evaluating the study's findings.

Chapter 5: This chapter summarizes the obtained results, findings, addresses research questions, and provides closure to the study's objectives and recommendations for future investigations.

1.5. Summary

In this chapter, the thesis's organization, research objectives, contributions, and the research approach are presented. After briefly reviewing PV-FC hybrid systems, the significance of renewable energy is first discussed. The importance of grid codes and grid connection standards for grid-connected PV-FC hybrid power systems are comprehensively covered.

2. PRELIMINARY WORK

2.1. Renewable Energy Sources

Renewable energy is increasingly being adopted globally for power generation due to environmental concerns associated with conventional electricity methods, and it helps to protect the environment by reducing greenhouse gas emissions and dependence on finite natural resources (Mohsin et al., 2021). RES such as solar, wind, and hydropower are replenished naturally and produces clean, emission-free energy (Zhao et al., 2022). Solar, hydro, wind, bioenergy, and geothermal energy are the major renewable energy categories, each with its own operational requirements, and conversion efficiencies, making technology choices location and environment-dependent (Ang et al., 2022). Explanation of common RES is given in Table 2.1.

Table 2.1. Renewable energy sources

Source	Explanation of the sources
PV	PV panels convert sunlight into DC electricity, which is then converted into AC for use in homes and businesses. Due to land availability onshore and offshore (on the sea surface) PV installations can be considered (Trapani and Millar, 2013).
Wind	Wind turbines convert the kinetic energy from wind into mechanical energy, which is then converted into electricity using a generator. Wind farms come in two types: onshore, situated on land, and offshore, located in sea or freshwater, offering sustainable energy solutions (Rashad et al., 2017).
Bioenergy	Biomass and biogas are converted into electricity through incineration or anaerobic digestion, generating heat for steam and powering a turbine connected to a generator (Pishvaee et al., 2021). Traditional and modern methods include a variety of biomass sources and thermal conversion techniques (Sun et al., 2014).
Hydropower	Hydroelectric power plants generate electricity by using the water flow to turn a turbine, which drives a generator. Hydroelectric systems are categorized as run-of-river, with river-dependent generation; reservoir, storing water for flexible generation; and pumped storage, offering grid stability via off-peak pumping and peak-time generation (IRENA, 2012).
Geothermal	Geothermal power plants generate electricity by using heat from the Earth's core to produce steam, which drives a turbine connected to a generator (Breeze, 2018).
Hydrogen	Hydrogen's rising importance in energy systems, driven by its clean combustion, makes it a vital player alongside electricity. Its high energy capacity and use in FCs drive diverse applications (Falcone et al., 2021).

2.2. Hybrid Power Systems

Hybrid RES power systems are facilities that combine two or more sources of renewable energy sources for power generation, such as PV, wind, FC, geothermal energy, and other renewable sources to provide a reliable and stable source of electricity (Paska et al., 2009). RES offers an important alternative, but dependence on factors such as solar irradiation and wind speed poses challenges. Individual RES struggle to provide stable power due to unpredictability (Arar Tahir et al., 2023). Hybrid RES addresses this by combining sources for stability and eco-friendliness (Paliwal et al., 2014). Hybrid RES can function independently or grid-connected, composed of single/multiple RES and possibly conventional energy (Bajpai and Dash, 2012). Key elements of hybrid RESs include loads, AC/DC converters, and diverse energy sources (renewable/non-renewable) alongside energy storage systems, illustrated in Figure 2.1.

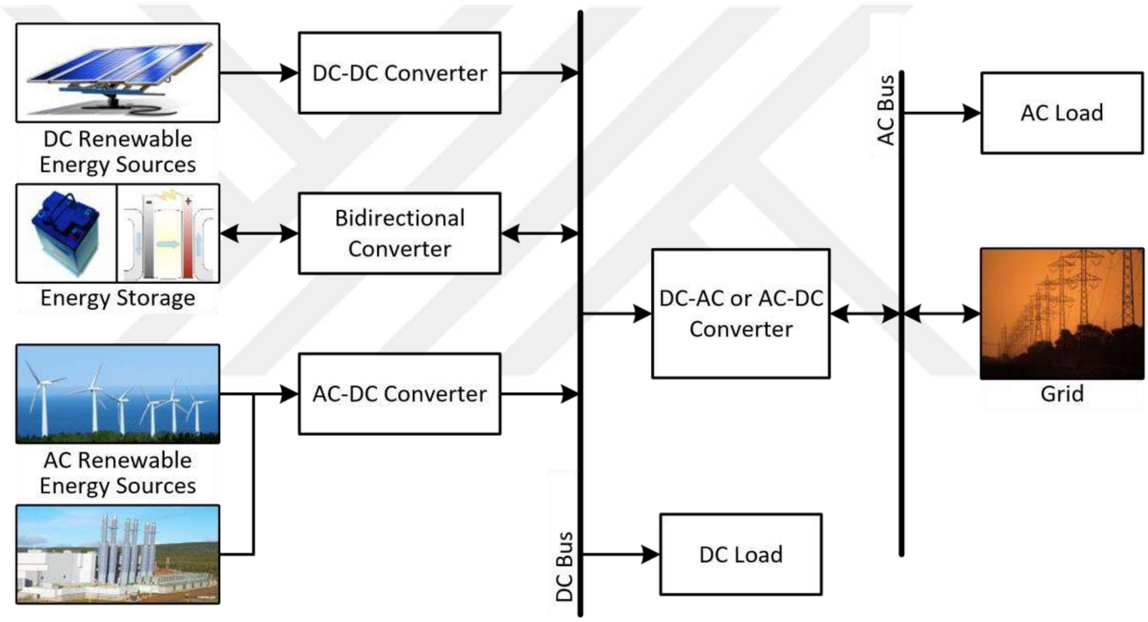

Figure 2.1. Elements of hybrid energy system

There is various type of hybrid energy system in literature. The classification of hybrid renewable power systems can be done in various ways, based on energy source combination, based on location: on-grid, off-grid, based on application: residential, commercial, industrial, etc. These classifications help to identify the specific type of hybrid power plant and its suitability for different energy needs and requirements. In this thesis, hybrid power system classification based on energy sources combination and grid connection (grid-tied or off-grid) is summarized in Table 2.2.

Table 2.2. Hybrid energy sources

Sources, Capacity	Explanation of the sources
PV: 500 kW PEMFC: 100 kW	An optimized grid-tied PV-FC hybrid RES for a university building, aiming for high renewable penetration, low emissions, and low energy cost. (Ghenai and Bettayeb, 2019a)
PV: 1.025 MW SOFC: 200 kW DIESEL: 100 kW	An off-grid hybrid RES simulation optimizes the University of Sharjah administration building power with 73% solar PV, 24% SOFC, 3% Diesel Generator, ensuring 100% load coverage (Ghenai and Bettayeb, 2019b).
PV: 100 kW SOFC: 100 kW	A grid-tied hybrid PV-FC power source with LVRT features with an energy management algorithm is proposed. Validation is done in MATLAB-Simulink under normal and voltage sag conditions (Sabir, 2019).
PV: 200 kW FC: 40 kW BATT: 50 kW	A grid-tied PV, FC, Battery hybrid system supplying power to a small community in NEOM city, Saudi Arabia (Rezk et al., 2020).
PMSG: 40 kW PEMFC: 1.2 kW	A grid-tied PV-Wind hybrid system that addresses FRT capability. Validation of the system is done in MATLAB-Simulink. (Roy et al., 2019)
PV: 40 kW FC: 6 kW WIND: 15 kW	A Hybrid RES consists of PV, FC, Wind source optimization for the AL-Arish Site (Attala et al., 2014).
PV: 18 kW WIND: 20 kw DIESEL: 15 kW BATT: 3 kW	An off-grid system addressing the energy challenge in remote, isolated areas like Malaysia's hilly terrain, a 56 kW solar-wind-diesel-battery hybrid system proposed for "KLIA Sepang station", aiming to provide sustainable power for more than 50 households and 6 shops (Shezan et al., 2015).
PV: 5.4 kW FC: 6 kW	A grid-tied PV-FC hybrid system integrates a 200V/10Ah battery into PV's DC bus within the FC system, utilizing FC power to balance variable PV and load demands in charge-sustained mode. (Bizon and Thounthong, 2021)
PV: 5.23 kW PEMFC: 4.77 kW	An off-grid hybrid RES combining PV and FC investigated for techno-economic viability in remote Jiaju Tibetan Village, China. A novel approach enhances HRES feasibility. (Xu et al., 2021).
PV: 0.95 kW PEMFC: 1.26 kW	A grid-tied system with a combination of PV and FC sources to meet load needs in various natural circumstances. Simulation in MATLAB/Simulink validates system performance (Reddy et al., 2023).
PV: 0.2 kW PEMFC: 0.2 kW	A grid-tied single-stage hybrid PV-FC system with a Lyapunov-based controller for optimal power extraction. Experimental results validate the effectiveness of the proposed controller (Priyadarshi et al., 2020).

In this section, the literature on hybrid systems based on source combinations, power ratings, and applications are summarized, and it is aimed to raise the awareness of the researchers about the current hybrid power system types, size, and applications.

2.3. PV Modules

PV modules, also known as solar panels, are made up of interconnected solar cells that convert sunlight into electricity. The basic model of the PV module is presented in Figure 2.2.

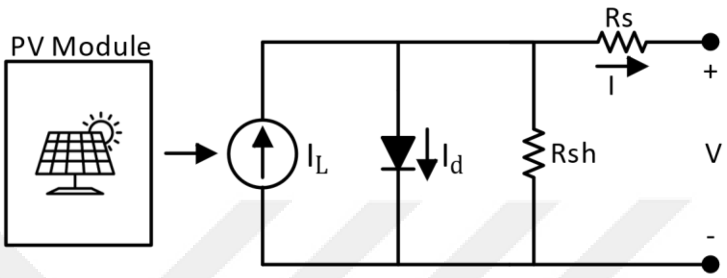

Figure 2.2. PV model

The I-V characteristics of a single module's diode are specified in Equation 2.3.1. Detailed equations of the PV model are presented in (Gilman et al., 2018).

$$I_d = I_0 * \left[\exp\left(\frac{V_d}{V_T}\right) - 1\right], V_T = \frac{k * T}{q} * nl * N_s \quad (2.3.1)$$

The parameters for the diode include: I_d - diode current (A), V_d - Diode voltage (V), nI - diode ideality factor (close to 1.0), I_0 - diode saturation current (A), k - Boltzmann constant (1.3806e-23 J.K-1), T - Cell temperature (K), q - Electron charge (1.6022e-19 C) and N_s- Number of cells connected in series in a module, Rs - series resistance, and Rsh - the shunt resistance.

Over time, researchers and engineers have focused on enhancing the performance of these modules to harness more energy from the sun. The development of PV modules has undergone significant advancements in recent years, leading to increased power ratings (Benda and Černá, 2020). Through advancements in materials, manufacturing processes, and design techniques, PV modules have become more efficient at converting sunlight into electricity (Alaaeddin et al., 2019). This has resulted in higher power ratings for solar panels, with modern modules ranging from a few watts to several hundred watts per panel. The continuous development and innovation in PV technology aim to maximize the power output and minimize the cost per watt, making solar energy a more viable and sustainable solution for global energy needs.

Table 2.3. Aiko-A460-MAH54Mb module parameters

Technical properties of utilized PV module	
No. of Cells	108 (6 x 18)
Dimensions	1722 x 1134 x 30 mm
Weight	20.5 kg
Nominal max. power (P_{max})	460 W
Opt. operating voltage (V_{mp})	34.21 V
Opt. operating current (I_{mp})	13.45 A
Open circuit voltage (V_{oc})	40.39 V
Short circuit current (I_{sc})	13.87 A
Module efficiency	23.6 %
Operating temperature	-40 °C ~ +85 °C
Max. system voltage	DC 1500 V
Power tolerance	0 ~ + 3 W

PV module efficiency is calculated by following formula in (Patil and Asokan, 2017). The P_{max} is the maximum power of the PV model under STC (1000 W/m², 25 °C), Panel area is (length*breadth) in meter squares. The efficiency (η) of the Aiko-A460-MAH54Mb module in Table 2.3 is calculated in Equation 2.3.2.

$$\eta = \frac{P_{max}}{1000(W/m^2) * \text{Panel area}(m^2)} = \frac{460}{1000 * 1.722 * 1.134} * 100 \approx 23.6\ \% \qquad (2.3.2)$$

In this thesis, the "Aiko-A460-MAH54Mb" black hole series PV modules, known for their high efficiency of up to 23.6 % (Aiko, 2023), were selected and utilized for modeling purposes. Detailed features of the module are given in Table 2.3 by use of the parameters MATLAB PV array block is used to generate the module model. This approach allowed us to accurately simulate and represent the features and characteristics of the PV module.

2.4. Fuel Cells

FCs are devices that convert chemical energy to electricity via electrolytic reaction, emitting only heat and water (Motapon et al., 2009). A fuel, such as hydrogen, is fed to the anode, and air is fed to the cathode. This reaction produces an electrical current through an external circuit, which can be used to energize an electric motor or to produce electricity. FCs work like batteries, but they do not run down or need recharging. They produce electricity and heat as long as fuel is supplied (Hawke et al., 2011). The structure of an FC is shown in Figure 2.3.

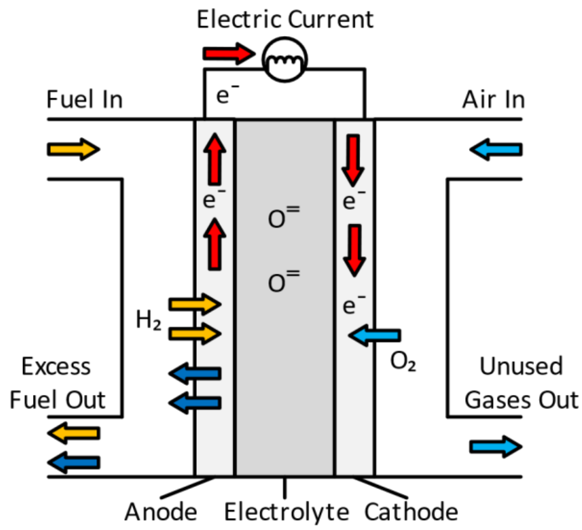

Figure 2.3. FC structure

The basic FC reactions are as follows (Barbir, 2006).

At the anode:

$$H_2 \rightarrow 2H^+ + 2e^- \tag{2.4.1}$$

At the cathode:

$$½O_2 + 2H^+ + 2e^- \rightarrow H_2O \tag{2.4.2}$$

Overall:

$$H_2 + ½O_2 \rightarrow H_2O \tag{2.4.3}$$

In general, FCs share a common basic structure consisting of an electrolyte and two electrodes. However, each type of FC is distinguished by the specific electrolyte used. For example, PEMFC's common electrolyte type is Perfluoro sulfonic acid. The type of electrolyte is critical as it governs the chemical reactions that occur in the FC, its operating temperature range, and other aspects that determine its most suitable applications (FCTO, 2016). This variability between FC types adds to their uniqueness and versatility in various energy-related fields.

The PEMFC operates below 120 °C, has a power range of <1 kW to 100 kW, and an electrical efficiency of 60 %. It finds applications in backup power, portable power, transportation, and more. The alkaline FC operates below 100 °C, with a power range of 1 kW to 100 kW and an electrical efficiency of 60 %, used in military, space, and backup power applications. The phosphoric aside FC operates at 150-200°C, with power ranges of 5-400 kW, or <10 kW in the polymer membrane variant, and an electrical efficiency of 40 %, commonly used for distributed generation. The molten carbonate FC operates at 600-700 °C, with power ranges of 300 kW to 3 MW and an electrical efficiency of 50 %, primarily for electric utility and distributed generation. The solid oxide FC operates at 500-1000 °C, with power ranges of 1 kW to 2 MW and an electrical efficiency of 60 %, used for auxiliary power and electric utility applications (FCTO, 2016).

2.5. Boost Converter

A boost converter is a type of DC-DC converter that steps up (increases) the input voltage to a higher output voltage level (Rashid, 2011). It is commonly used in various electronic systems, such as power supplies, battery chargers, and renewable energy applications. The boost converter operates based on the principle of storing energy in an inductor during a switching cycle and releasing it to the output during another cycle. A basic schematic of the boost converter is given in Figure 2.4.

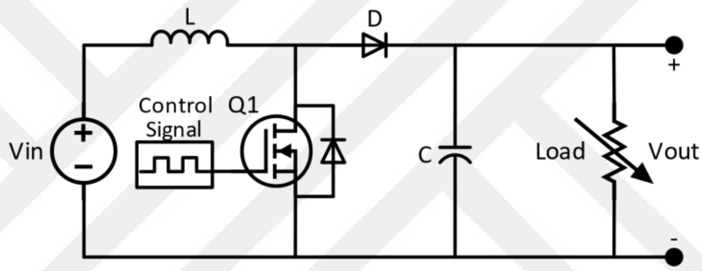

Figure 2.4. Basic schematic of a boost converter

Boost converter continuous mode operation mode parameters and equations are taken from Texas Instruments application notes (De Stasi, 2015; Hauke, 2022)
The output current is calculated in Equation 2.5.1.

$$I_{out} = \frac{P_{out}}{V_{out}} \tag{2.5.1}$$

The maximum duty cycle value is calculated in Equation 2.5.2.

$$D = 1 - \frac{V_{imin}}{V_{out}} * \eta \tag{2.5.2}$$

The desired inductor peak-to-peak current ripple for 10% ripple is calculated in Equation 2.5.3.

$$\Delta I_L = 0.1 * I_{out} * \frac{V_{out}}{V_{IN}} \tag{2.5.3}$$

The desired output voltage ripple for 1% ripple is calculated in Equation 2.5.4.

$$\Delta V_{out} = 0.01 * Vout \quad (2.5.4)$$

The inductor value is calculated in Equation 2.5.5.

$$L = \frac{V_{imin} * (V_{out} - V_{IN})}{\Delta I_L * f_s * V_{out}} \quad (2.5.5)$$

The minimum capacitor value is calculated in Equation 2.5.6.

$$C = \frac{I_{out} * D}{f_s * \Delta V_{out}} \quad (2.5.6)$$

Parameters: I_{out} desired output current, P_{out} desired output power, V_{imin} the minimum input voltage, V_{out} the desired output voltage, η efficiency of the converter, V_{IN} the typical input voltage, f_s converter minimum switching frequency.

2.6. Maximum Power Point Tracking

PV array output varies according to meteorological factors like irradiance and temperature. Therefore, PV array output is non-linear and leads to fluctuating current, voltage, and power (Shang et al., 2020). MPPT is a technique used in PV systems to extract the maximum usable power from a PV array therefore achieving MPPT is crucial for optimal real-time power extraction. A typical power-voltage curve of a standard solar panel is depicted in Figure 2.5. The MPPT algorithm continuously adjusts the operating voltage and current of the PV array to maintain maximum power output under varying conditions such as varying solar irradiation and temperature (Podder et al., 2019).

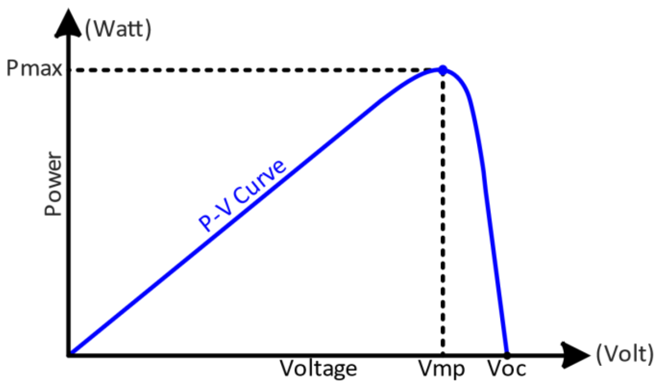

Figure 2.5. PV curve

A basic schematic for a PV system with MPPT consists of a PV array, a converter, and a load (Bollipo et al., 2021). Figure 2.6 shows a schematic PV system connected to a load. It comprises a solar PV array, employing either a DC/DC or DC/AC converter for power conversion.

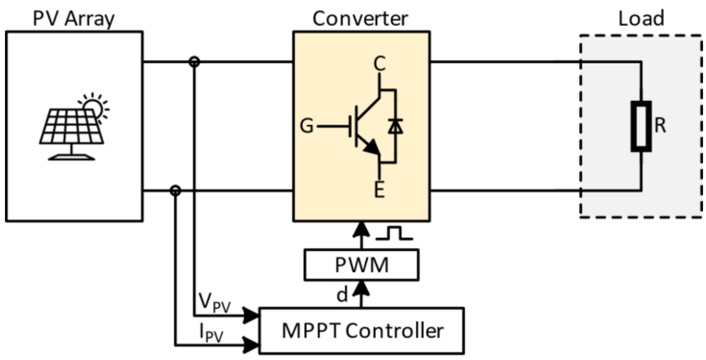

Figure 2.6. PV system with MPPT

Conventional MPPT techniques include perturb and observe, incremental conductance, fractional short circuit, and fractional open circuit methods (Brito et al., 2013). Intelligent approaches such as fuzzy logic control, ANN methods, and hybrid methods aim to optimize power extraction (Da Silva et al., 2017). In the paper by (Revathy et al., 2022), an ANFIS-based MPPT for optimizing PV power, in (Errouha et al., 2019) a variable step size P&O for PV, in thesis by (Çelik, 2015) a perturb and observe- ANN based hybrid MPPT, enhancing tracking capability of PV under partial shading conditions introduced, the paper by (Ali et al., 2020) investigates uniform, non-uniform irradiance and hybrid optimization MPPT methods adapted for challenging conditions such as partial shading and solar irradiation variations. Numerous MPPT techniques exist in the literature, mainly classified in four groups (Abidi et al., 2023): classic, optimization, advanced, and hybrid categories methods illustrated in Figure 2.7.

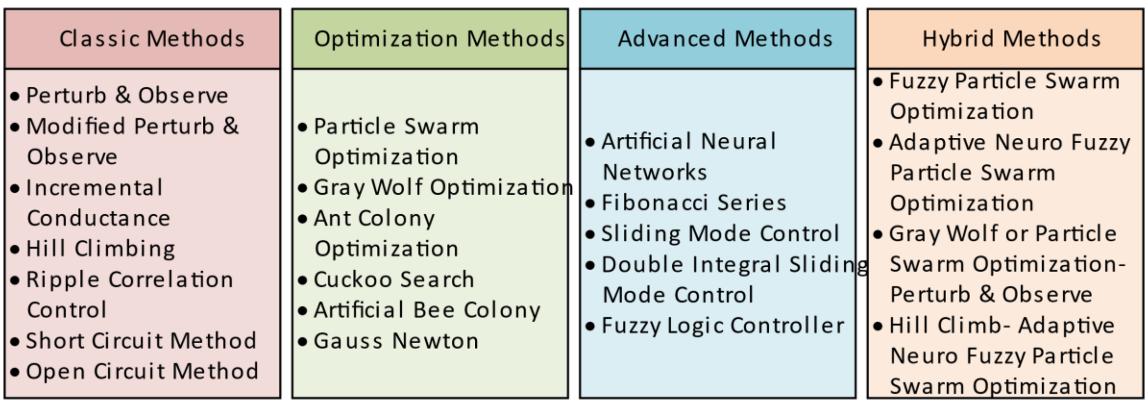

Figure 2.7. MPPT classification

2.6.1. Perturb and Observe Method

The perturb and observe method's algorithm operates by comparing past and present power and voltage values during each sampling step. It initializes PV voltage and current, calculates differences in power ΔP_{PV}, and voltage ΔV_{PV}. Adjustments of the duty cycle are made based on ΔP_{PV} and ΔV_{PV} to approach the maximum power point iteratively (Dorji et al., 2020).

2.6.2. Incremental Condutance Method

The incremental conductance method optimizes power output in PV systems by continuously tracking the P-V curve slope in Figure 2.5. The INC MPPT algorithm utilizes dP/dV, which equals zero at the MPP, ensuring accurate tracking even under rapidly changing conditions (Kish et al., 2012). Figure 2.8 shows the flowchart of the INC method, starting with measuring V(k) and I(k) at observation k. By comparing conductance (I/V) with incremental conductance (dP/dV), the algorithm tracks MPP and adjusts the control voltage reference to maintain the MPP effectively (Shang et al., 2020).

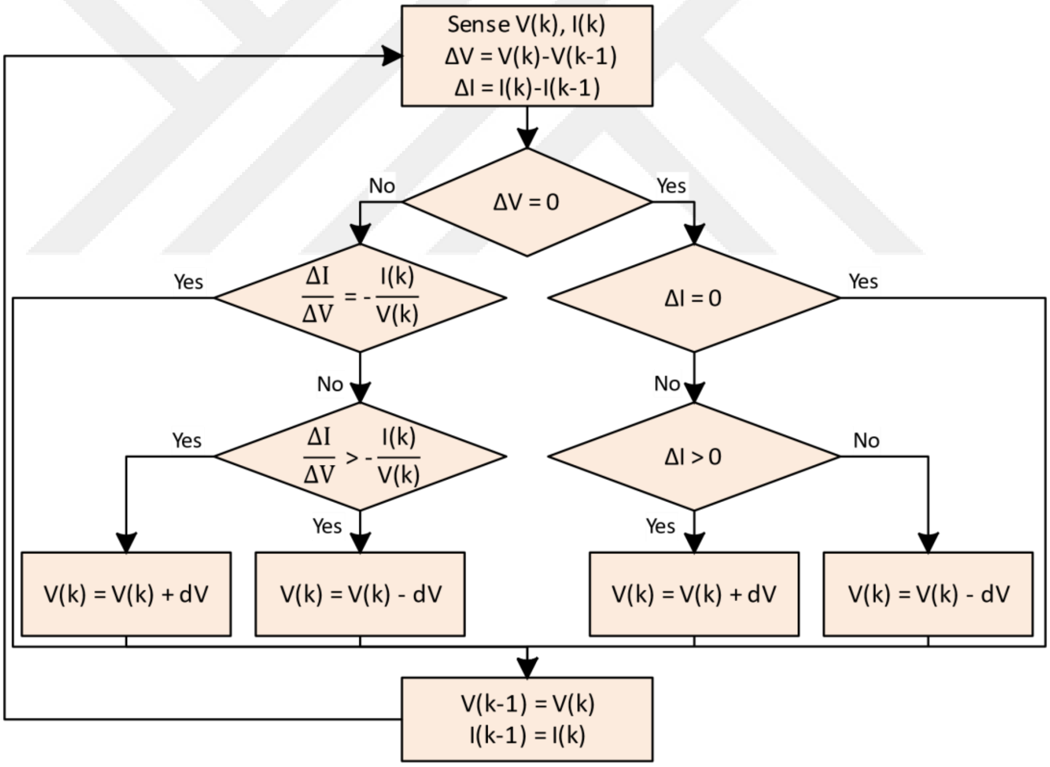

Figure 2.8. Incremental conductance flow chart

The mathematical approach to determine MPP position on the P-V curve for incremental conductance MPPT method is as in Equation 2.6.1 (Abidi et al., 2023).

$$\begin{cases} \frac{\Delta I_{PV}}{\Delta V_{PV}} > -\frac{I_{PV}}{V_{PV}}, & \text{left of MPPT} \quad (V_{MPPT} > V_{PV}), \text{ increase } V_{PV} \text{ value} \\ \frac{\Delta I_{PV}}{\Delta V_{PV}} = -\frac{I_{PV}}{V_{PV}}, & \text{at the MPPT} \quad (V_{MPPT} = V_{PV}), \text{ hold } V_{PV} \text{ value} \\ \frac{\Delta I_{PV}}{\Delta V_{PV}} < -\frac{I_{PV}}{V_{PV}}, & \text{right of MPPT } (V_{MPPT} < V_{PV}), \text{ decrease } V_{PV} \text{ value} \end{cases} \quad (2.6.1)$$

In this thesis, the incremental conductance method is used due to its algorithmic simplicity, high efficiency in obtaining peak power from PV panels, fast adaptation to changing conditions such as shading while ensuring minimal computation, and ease of design.

2.7. Three-Level NPC Inverter

Multilevel converters were first introduced by (Nabae et al., 1981) with their proposal for a three-level NPC. This innovative inverter demonstrates lower harmonic content compared to conventional inverters. Since then, various multilevel converter topologies have been developed. The basic idea behind multilevel converters is to use multiple low-voltage DC sources and an array of power semiconductor switches to synthesize a ladder voltage waveform (Kala and Arora, 2017). Compared to traditional two-level converters, multi-level converters offer several advantages. It includes reduced voltage stress on switches, improved power quality by reducing THD of voltage and current waveforms, lower power dissipation when on, applicability to high voltage applications, medium and high voltage generation, lower switching frequency precursor, reduced switching losses, higher efficiency, reduced dv/dt stress minimizing electromagnetic interference issues, and the ability to draw input current with low distortion. (Noman et al., 2017; Rodríguez et al., 2002). A study by (Kala and Arora, 2017) analyzes recent hybrid MLI topologies, addressing issues with classical MLIs. It reviews their impact on grid-connected renewable energy applications and presents simulation results in MATLAB/Simulink. The article by (Nyamathulla et al., 2023) focuses on the reliability analysis of grid-tied MLI topologies for PV systems. It covers motivational factors, properties, evaluation parameters, topologies, modulation schemes, selection process, and reliability evaluation using computational techniques and simulation methods. The structure of the three-level NPC inverter used in this thesis is shown in Figure 2.9 and the switching states of the inverter for one branch are given in Table 2.4.

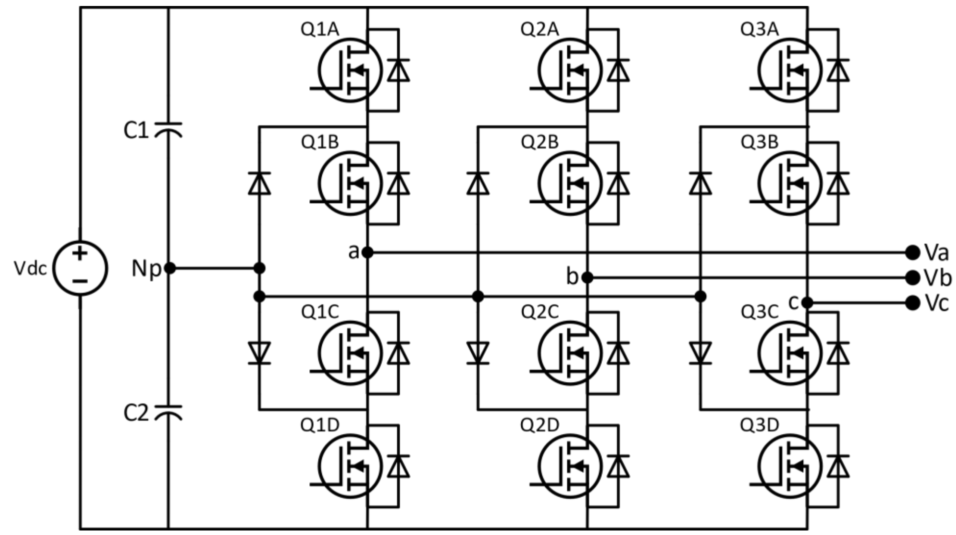

Figure 2.9. Three-level NPC inverter

Using Kirchhoff's laws and circuit analysis, Equation 2.7.1 represents the equation of state for a grid-connected NPC inverter connected to an RL filter system during typical operation derived by (Xu et al., 2023).

$$\begin{bmatrix} \frac{di_a}{dt} \\ \frac{di_b}{dt} \\ \frac{di_c}{dt} \end{bmatrix} = -\begin{bmatrix} \frac{R}{L} & 0 & 0 \\ 0 & \frac{R}{L} & 0 \\ 0 & 0 & \frac{R}{L} \end{bmatrix} \begin{bmatrix} i_a \\ i_b \\ i_c \end{bmatrix} - \begin{bmatrix} \frac{1}{L} & 0 & 0 \\ 0 & \frac{1}{L} & 0 \\ 0 & 0 & \frac{1}{L} \end{bmatrix} \begin{bmatrix} u_a \\ u_b \\ u_c \end{bmatrix} + \frac{U_{dc}}{6 * L} \begin{bmatrix} 2 & -1 & 1 \\ -1 & 2 & -1 \\ -1 & -1 & 2 \end{bmatrix} \begin{bmatrix} \delta_a \\ \delta_b \\ \delta_c \end{bmatrix} \qquad (2.7.1)$$

In Equation 2.7.1: i_a, i_b, and i_c represent the three-phase currents, R stands for total filter resistance, L for filter total inductance value, and U_{dc} represents the DC-side voltage of the NPC inverter. $\delta_X = \delta_{XA}\delta_{XB}\delta_{XC}'\delta_{XD}' - \delta_{XA}'\delta_{XB}'\delta_{XC}\delta_{XD}$, and δ_{XM} represents the gate signal of the power switch Q_{XM} (X=1, 2, 3; M=A, B, C, D). The value of δ_{XM}=1 indicates an active 'on' state for the switch Q_{XM}, while δ_{XM}=0 indicates an inactive 'off' state for the switch Q_{XM}. δ_X, has three states individually “-1,” “0”, “1”, lastly u_a, u_b, and u_c are the phase voltages of the grid side.

Table 2.4. The switching states of the NPC inverter

Voltage	Q1A	Q1B	Q1C	Q1D	Q2A	Q2B	Q2C	Q2D	Q3A	Q3B	Q3C	Q3D
$V_{DC/2}$	1	1	0	0	1	1	0	0	1	1	0	0
0	0	1	1	0	0	1	1	0	0	1	1	0
$-V_{DC/2}$	0	0	1	1	0	0	1	1	0	0	1	1

2.8. LCL Filter

Utilizing a filter at the output of the inverter is crucial. This is because the inverted signal, although having a high amplitude, contains harmonics at the switching frequency and its multiples (Reznik et al., 2014). The LCL filter is preferred due to its suitability for low switching frequencies, smaller size, lower voltage drop, and improved damping compared to conventional "L" and "LC" filters (Jayalath and Hanif, 2018). Figure 2.10 shows a single-phase reduced LCL filter model.

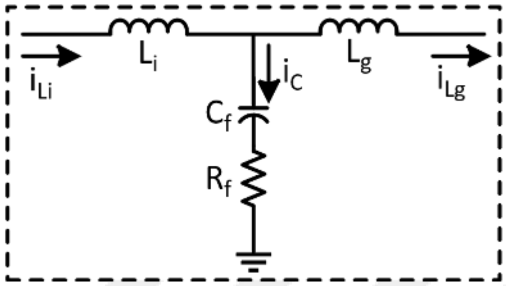

Figure 2.10. One-phase representation of LCL filter

The base impedance is calculated in Equation 2.8.1.

$$Z_b = \frac{V_n^2}{P_n} \tag{2.8.1}$$

The grid angular frequency is represented by ω_g, base capacitance is calculated in Equation 2.8.2.

$$C_b = \frac{1}{\omega_g * Z_b} \tag{2.8.2}$$

The sizing of the filter capacitance depends on power factor limits, typically ensuring a maximum 5% decrease in power (Büyük et al., 2016). Consider this criteria filter capacitor calculated as in Equation 2.8.3.

$$C_f = C_b * 0.05 \tag{2.8.3}$$

The maximum phase current is calculated in Equation 2.8.4.

$$I_{maxphase} = \frac{P_n * \sqrt{2}}{3 * V_{ph}} \tag{2.8.4}$$

The maximum phase current ripple is chosen as 0.1 (10%) as in Equation 2.8.5.

$$\Delta I_{max} = 0.1 * I_{maxphase} \tag{2.8.5}$$

The inverter side inductor value for three-level NPC (Araujo et al., 2007) is calculated formula in Equation 2.8.6.

$$L_{inv} = \frac{V_{DC}}{16 * f_{sw} * dImax} \tag{2.8.6}$$

The attenuation factor is represented by k_a, grid side inductor value (Dursun and Dosoglu, 2018) is calculated formula in Equation 2.8.7.

$$L_{grid} = \frac{\sqrt{\frac{1}{{k_a}^2}} + 1}{{\omega_{sw}}^2 * C_f} \tag{2.8.7}$$

The resonance frequency f_{res} is calculated formula in Equation 2.8.8.

$$f_{res} = \frac{1}{2 * \pi} * \sqrt{\frac{L_{inv} + L_{grid}}{L_{inv} * L_{grid} * C_f}} \tag{2.8.8}$$

The resonance avoiding criteria is defined in Equation 2.8.9.

$$10 * f_g < f_{res} < 0.5 * f_{sw} \tag{2.8.9}$$

The resistance in series with the filter capacitance is calculated formula in Equation 2.8.10.

$$R_f = \frac{1}{3 * (2 * \pi * f_{res}) * C_f} \tag{2.8.10}$$

The transfer function of the filter is represented in Equation 2.8.11 (Çelik, 2019).

$$\frac{I_{Lg}(s)}{V_o(s)} = \frac{R_f * C_f + 1}{\left(L_i * L_g * C_f\right) * s^3 + \left(L_g * R_f * C_f + L_i * L_g * C_f\right) * s^2 + \left(L_i + L_g\right) * s} \tag{2.8.11}$$

A detailed numerical design of LCL filter for proposed system is presented in Section 3.6.

2.9. Stand-Alone Renewable Power Plants

Stand-alone renewable power plants are electrical systems that operate independently of the main electrical grid, and they are commonly used in remote or isolated areas where access to the main grid is limited or unavailable (Reca-Cardeña and López-Luque, 2018). They are designed to generate and supply electricity locally, catering to the energy needs of a specific location or community (Kemp et al., 2023).

The basic structure of stand-alone renewable power plants involves utilizing renewable energy sources such as solar, wind, or hydro power. These sources are harnessed to generate electricity through appropriate technologies like solar panels, wind turbines, hydroelectric generators, or hybrid technologies (Basnet et al., 2023). To ensure a consistent power supply, stand-alone renewable power plants often incorporate energy storage systems such as FCs, which can store excess energy for later use (Thirunavukkarasu et al., 2023). A basic scheme of a stand-alone power system scheme is shown in Figure 2.11.

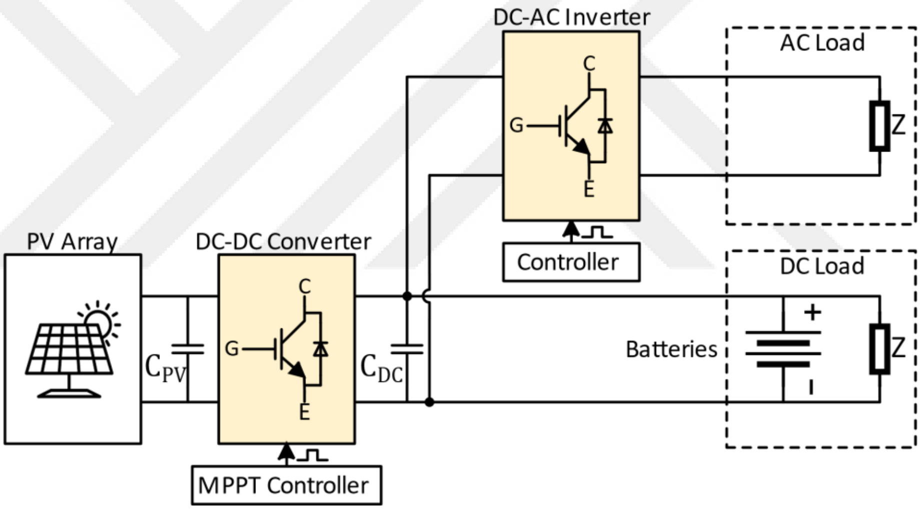

Figure 2.11. Stand-alone power system

2.10. Single-Stage Grid-Connected PV System

A grid-connected renewable power plant is a type of electrical power generation facility that is connected to the main electrical grid. Grid-connected renewable power plants generate electricity using renewable sources such as solar, wind, hydro power, geothermal, and biomass. A single-stage grid-connected system typically consists of a renewable energy source (such as solar panels or wind turbines), an inverter to convert DC power into AC power. The grid connection for power transfer is established via a line transformer or direct connection. The inverter is designed to handle double the nominal power (Kjaer et al., 2005). Figure 2.12 shows a basic schematic of a single-stage power processing structure.

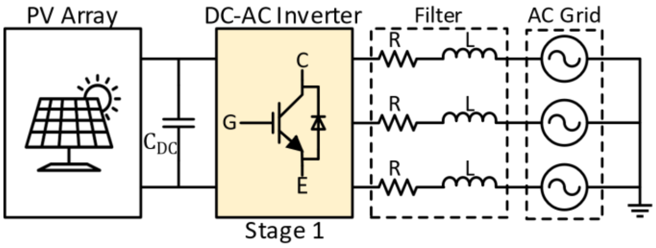

Figure 2.12. Single-stage power conversion for PV

2.11. Two-Stage Grid-Connected PV System

The two-stage power processing system consists of two critical stages: the DC-DC converter which is generally a boost converter and the DC-AC three-phase inverter (Anzalchi and Sarwat, 2017). The DC-DC converter utilizes MPPT to optimize power from PV arrays based on weather conditions, ensuring efficient DC voltage level adjustments. Meanwhile, the DC-AC inverter employs control mechanisms to regulate injected current, voltage, and power to meet grid and load demands, enabling smooth synchronization between the DC and AC components of the PV system. Furthermore, integrating an extra source, such as an FC or battery, into the DC bus via a DC-DC converter enables multi-stage conversion (Khalid et al., 2021). This enhances PV array control and facilitates a unified DC-AC inverter technology. thesis employs a multistage power conversion approach featuring a unified inverter topology for enhanced efficiency and control because mentioned advantages. The basic structure of a transformerless two-stage energy conversion scheme is illustrated in Figure 2.13.

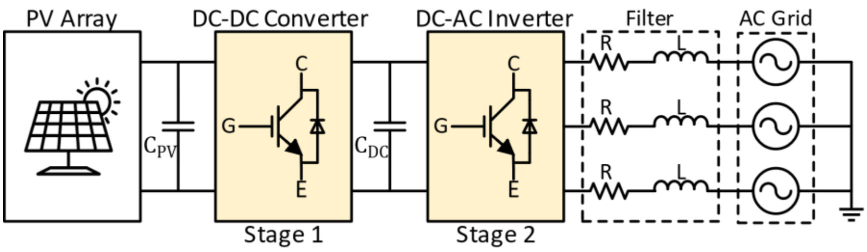

Figure 2.13. Two-stage power conversion for PV

2.12. Compliance of Grid Connection Codes

Grid connection requirements given in grid codes, are sets of minimum technical requirements that power plants must comply with to obtain grid access. These codes play a crucial role in coordinating various independent actors within power systems operating under diverse regulatory frameworks. By establishing rules for efficient collaboration towards shared objectives, grid codes govern grid access and network user operations, regardless of the operator's nature. Grid codes are frequently revised to accommodate technological advancements and operational capacities, grid codes are applied uniformly to all participants, promoting transparency and equal treatment (IRENA, 2022). They also provide valuable insights into future-generation technology needs.

Establishing a grid code is crucial in facilitating private sector participation and the smooth integration of distributed renewable energy generators, while regional grid codes further support the growth of regional energy markets.

It is important for renewable energy developers to be aware of and comply with the relevant grid codes, as failure to do so can result in technical issues, safety hazards, and increased costs. The European Network of Transmission System Operators for Electricity (ENTSO-E) has developed a set of pan-European grid codes, known as the ENTSO-E Guidelines, which provide a harmonized framework for the integration of renewable energy sources into the European power grid. Similarly, the United States Federal Energy Regulatory Commission (FERC) has established nationwide standards for interconnecting renewable energy projects to the power grid (Rahman et al., 2022). The Energy Market Regulatory Authority of the Republic of Türkiye (EMRA, 2022) plays an important role in shaping the Turkish grid codes.

Research by (Shafiullah et al., 2022) conducted a review of the challenges and solutions for integrating solar PV systems into electricity grids. The paper covers technical, socioeconomic, environmental, and market challenges, and proposes solutions like grid codes, advanced control strategies, energy storage, and renewable energy policies. The findings provide valuable insights for researchers and decision-makers.

In general, grid codes are developed based on system needs, requiring all generators to contribute according to their technical restrictions. The aim is to make variable renewable energy generators behave like synchronous machines, but they can also provide additional functionalities not easily achievable by conventional generators (Zeb et al., 2022). Grid codes typically include requirements for voltage and frequency control, reactive power provision, fault behavior, protection, and controllability of active and reactive power output. Power quality requirements limit harmonics distortion. Different countries have specific grid code requirements, but overall, the objective is to ensure stable and reliable operation of the power system (IRENA, 2022).

2.13. Turkish Grid Code

The Energy Market Regulatory Authority of the Republic of Türkiye (EMRA, 2022) plays an important role in shaping the Turkish grid code, defining roles for transmission system operators, generation facilities, and directly connected customers. The latest edition of the grid regulations published on 19.11.2022 highlights the guidelines for wind power plants and PV plants in Annex 18 (Çelik et al., 2022). The document specifies requirements such as the contribution of production facilities during faults, active power control, frequency response, reactive power capacity, reactive power support, responses to voltage changes, and post-fault system assistance. It also details the required features of the grid connection transformer for transmission-connected wind and solar facilities. These requirements apply to the following generation facilities:

- Wind and solar PV generation connected to the transmission system.
- PV generation facilities connected to the distribution system at medium voltage level.
- Wind power generation facilities connected to the distribution system, holding a license, and having a capacity of 10 MW or more.

2.13.1. Contribution of Production Facilities to the Post-Failure System

The profile of the LVRT code used at Türkiye (Çelik et al., 2022) is shown in Figure 2.14. The required criteria for LVRT are summarized as follows: i) When grid voltage drops to zero, it is essential for the PV system to maintain its connection for at least 150 milliseconds. ii) When the grid voltage drops below the specified threshold (red line), the PV system may be disconnected from the grid as a safety measure. ii) When the voltage drop remains within Zone 1 during a fault, the power generation facility should increase its active power immediately after the fault is cleared by at least 20% of the nominal active power per second, reaching the maximum achievable active power. 4) When the voltage drop remains within Zone 2 during a fault, the power generation facility should increase its active power immediately after the fault is cleared by at least 5% of the nominal active power per second, reaching the maximum achievable active power.

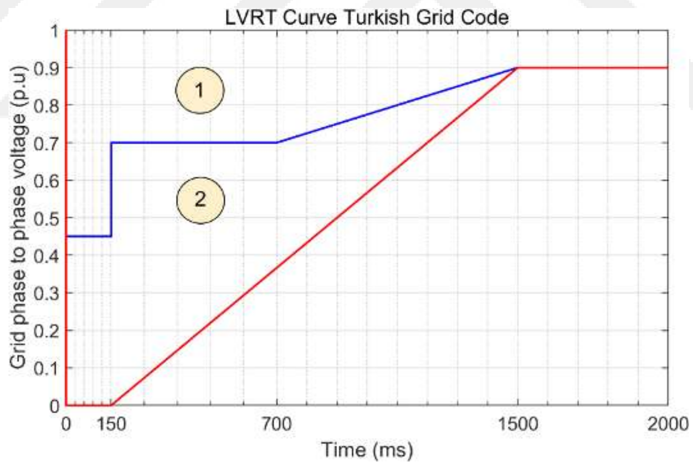

Figure 2.14. LVRT graph-Turkish grid code (EMRA, 2022)

Reactive Power Support

In case of voltage fluctuations greater than ±10% that will occur in fault conditions expressed at the grid connection point, each wind turbine generator and/or each inverter in PV power plants must provide maximum reactive current support in inductive or capacitive direction at levels up to 100% of the nominal current, if necessary, without exceeding the designed transient regime rated values. This transient regime must reach the maximum reactive current support value within 60 ms with a 10% margin of error and must be sustained for 1.5 s.

2.13.2. Active Power Control

The regulation outlines guidelines for active power control in wind and solar PV facilities connected to the grid. During emergencies, active power can be adjusted automatically (20-100% of current output) based on signals from the grid operator. In facilities producing wind and solar energy connected to the grid, specific load control measures are outlined as follows.

i) For generation facilities with an installed capacity of 100 MW or less, the load-taking rate should not exceed 5 % of the installed capacity of the power plant per minute, and the load-shedding rate should not be less than 5 % of the installed capacity of the power plant per minute.

ii) For generation facilities with an installed capacity of more than 100 MW, the load-taking rate shall not exceed 4 % of the installed capacity of the power plant per minute and the load-shedding rate shall not be less than 4 % of the installed capacity of the power plant per minute.

Similar adjustments can be made by distribution companies for licensed facilities using SCADA systems. The aim is to ensure compatibility with grid constraints and enable controlled power reduction when needed for grid stability.

2.13.3. Frequency Response

Wind and solar-based PV facilities must operate within the frequency ranges specified in Figure 2.15 during their operational period. Furthermore, generation facilities based on wind and solar energy should operate based on the frequency ranges and the time intervals specified in Table 2.5 during their operation.

Table 2.5. Frequency response criteria (EMRA, 2022)

Frequency Range	**Minimum Operating Time (sec)**
50,5 Hz ≤ f < 51,5 Hz	1 hour
49 Hz ≤ f < 50,5 Hz	Continuous
48,5 Hz ≤ f < 49 Hz	1 hour
48 Hz ≤ f < 48,5 Hz	20 minutes
47,5 Hz ≤ f < 48 Hz	10 minutes

Generation facilities based on wind and solar energy must be capable of generating their full rated power as long as the grid frequency ranges between 47.5 to 50.3 Hz. If the frequency exceeds 50.3 Hz, these facilities must follow active power-frequency characteristics in Figure 2.14, ensuring a 4 % speed reduction at 51.5 Hz and complete shutdown beyond. In addition to these operational conditions, additional wind turbines or solar panel systems should not be activated when the grid frequency is higher than 50.2 Hz. The total active output of the generation system should remain within the limits of the power-frequency curve outlined in Figure 2.14.

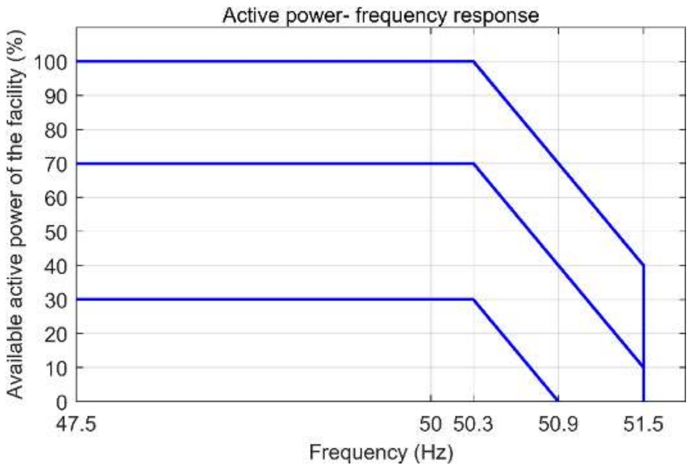

Figure 2.15. Active power-frequency response

2.13.4. Reactive Power Capacity

PV generation facilities based on solar energy must be continuously operable at each point for the reactive power values within the limits indicated by the blue lines in Figure 2.16 at the connection point of the transmission or distribution system.

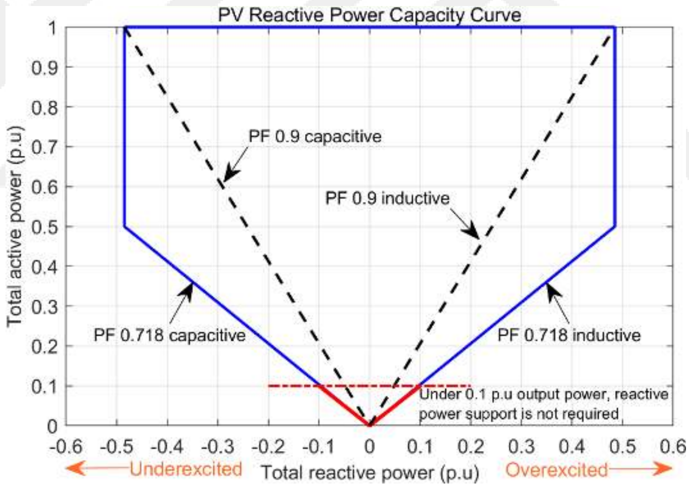

Figure 2.16. Reactive power capacity curve for PV production facilities

2.14. International Grid Regulations

International regulations, such as IEEE Std 929-2000, IEEE Std 519-1992, IEEE Std 1668-2017, IEEE Std 519-2022, IEEE Std 1547-2018, IEEE Std 2800-2022, EN50160 cover guidelines for grid-connected PV systems, harmonic control in power converters, testing equipment compatibility during voltage sags, electrical system design objectives, interconnection of distributed energy resources and inverter-based resource integration with power systems. These standards set safety, performance, and interoperability criteria for various aspects of electrical systems.

IEEE Std 929-2000 provides advice on the equipment and procedures required for the harmonized operation of grid-connected PV systems. It covers safety, equipment protection measures, power quality, and grid interaction, including islanding prevention and handling voltage/frequency control during grid disconnection.

IEEE Std 519-1992 standard is relevant to a variety of static power converters in industrial and commercial power systems. It addresses harmonic control, reactive compensation, and distortion limits, providing application information while excluding radio frequency interference effects.

IEEE Std 1668-2017 standard provides a recommended, non-industry specific approach for evaluating the ride through performance and compatibility of electrical and electronic equipment connected to low voltage power systems (below 1000 V). It addresses devices susceptible to malfunctions or shutdowns due to short-term voltage reductions. The application outlines voltage drop immunity criteria derived from real data and provides an in-depth examination of the voltage drops experienced by the user. Clear test protocols and equipment prerequisites are defined to cover various voltage drop scenarios, both balanced and unbalanced. The scope also covers certification, reporting, and characterization requirements.

IEEE Std 519-2022 standard outlines design objectives for electrical systems covering linear and non-linear loads. It sets disturbance targets for system designers by defining allowable voltage and current waveforms. The interface, known as a point of common coupling (PCC), reduces interference. While IEEE Std 1547™ and IEEE Std 2800™ specify current distortion limits for inverter-based sources, this standard only addresses steady-state constraints on the PCC. Radio frequency interference is not covered except for wired telephone systems. In particular, the limits specified are specific to the PCC and are not applicable for equipment evaluation elsewhere in the power system.

IEEE Std 1547-2018 standard sets universal criteria for the interconnection of distributed energy resources with electrical power systems, enabling interoperability, performance, safety, and security throughout installation and service, covering technical specifications, testing, operation, and maintenance.

IEEE Std 2800-2022 standard defines recommended interconnection technical requirements for inverter-based resource integration with transmission systems. It covers aspects like voltage and frequency stability and ride-through capabilities, active and reactive power control, dynamic voltage support during anomalies, power quality, and system protection, ensuring reliable integration into the bulk power system.

IEC 61727, 2004 covers related to grid-connected PV systems using static non-islanding inverters, detailing their interconnection requirements with the utility grid.

EN50160 defines the voltage characteristics for public European electricity networks, excluding industrial ones, under normal conditions. It is not applicable during faults, incompatibility situations, extreme weather conditions, third-party intervention, or force majeure.

2.14.1. Over/Under voltage limits

The inverter needs to function within specific voltage limits as outlined in the standards. If the grid voltage deviates beyond these limits, either exceeding or falling below them, the inverter must stop operating within a certain maximum trip time. This time frame is specified in Table 2.6 (IEC 61727; IEEE 1547)

Table 2.6. Over/Under voltage limits

Voltage maximum trip time	**Trip time (sec)**
$V < 0.5 \times V_{nominal}$	0.1
50 % ≤ V < 85 %	2.0
85 % ≤ V < 110 %	Unlimited operation
110 % < V < 135 %	2.0
135 % ≤ V	0.05

The inverters are required to function within the specified range of grid frequency limits, which is typically set at ±1 Hz according to the standards. If the grid frequency deviates beyond these limits, either going above or below the range, the inverter must be swiftly disconnected from the grid within a maximum period of 0.2 s.

2.14.2. Harmonic limits

The standards define limits for harmonic distortions in both currents and voltages. These limits specify the maximum allowable odd and even harmonic content in the output current of the inverter. To ensure compliance with these standards, Table 2.7 provides the specific limits for individual harmonics as well as the THD. This helps regulate and control the harmonic distortions produced by the inverter, ensuring that they remain within acceptable levels as outlined in the standards. (IEC 61727; IEEE Std 519; IEEE Std 1547).

Table 2.7. Harmonic limits

Individual odd harmonic order h	**Percent (%)**
H < 11	4.0
11 ≤ h < 17	2.0
17 ≤ h < 23	1.5
23 ≤ h < 35	0.6
35 ≤ h <50	0.3
THD	5.0

2.15. Reactive Power Support

The voltage control mode of a PV inverter adjusts the output current by synchronizing the output voltage with the system. This enables it to inject reactive power as an auxiliary to the local distribution voltage. The control is achieved by varying the q-axis current (Hu et al., 2019). In case of voltage sag, grid inverters must comply with LVRT standards and inject reactive power to assist voltage recovery and grid stability. Reactive current injection during voltage sag follows specific guidelines in the grid code (Al-Shetwi et al., 2018; Cabrera-Tobar et al., 2016; Neumann and Erlich, 2012). In the Turkish grid code, under fault conditions with voltage fluctuations of more than ±10% at the grid connection, wind turbines, and solar inverters must immediately provide reactive current support up to 100% of nominal levels. This response should be provided within 60 ms, maintaining a margin of 10% for 1.5 s.

In the German grid code, medium and high voltage systems are required to have reactive power injection capability (Yang and Wenjieand, 2014) as summarized in Figure 2.17 together with LVRT for dynamic grid voltage support during voltage sag situations. The LVRT control is activated when the voltage drops below 0.9 per unit (p.u.), and the reactive current injection is determined by the magnitude of the voltage as in Equation 2.15.1. The parameters in equations are defined as follows; instantaneous voltage V, normal grid voltage V_N, initial voltage V_0, nominal current I_N, and q-axis current I_{q0} before grid fault and I_d is d-axis current, I_q is q-axis current. I_{qr} is required reactive current, I_{dr} is required active current.

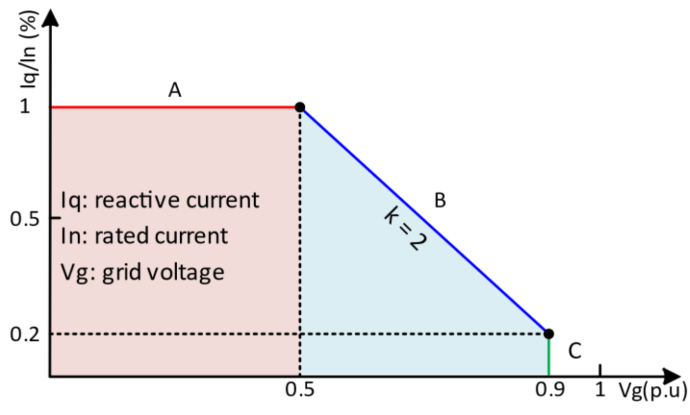

Figure 2.17. Reactive power support curve

$$I_{qr} = \begin{cases} \text{dead band} , & 0.9 \leq V \leq 1.1 \\ k * \left(\frac{V - V_0}{V_N}\right) + I_{q0}, & 0.5 \leq V \leq 0.9 \\ I_N + I_{q0} , & V \leq 0.5 \end{cases} , I_{dr} = \sqrt{{I_N}^2 - {I_q}^2} \quad (2.15.1)$$

This method ensures a consistent and stable peak current injection within the inverter, even during grid faults. In the event of a voltage sag, the inverter must provide the specified reactive power to assist voltage recovery according to the LVRT criteria.

2.16. Faults

Faults in the electrical grid refer to any type of abnormal condition or malfunction that can disrupt the normal functioning of the electrical power system. The grid-connected systems typically operate under balanced conditions, but grid faults can lead to unbalanced states due to natural interference, technical errors, or heavy load connections (Ammiche et al., 2018; Farhang et al., 2015). The analysis of operational faults in grid-connected systems includes two main methods: symmetrical fault and asymmetrical fault analysis (Lin et al., 2018). Symmetrical faults occur when all three-phase voltage drops have the same magnitude proportional to the fault severity and are typically associated with balanced three-phase faults. On the other hand, asymmetrical faults lead to severe unbalanced conditions with unequal phase voltage drops (Sadeghkhani et al., 2018).

Grid faults include line-to-line, single line-to-ground, double line-to-ground, open conductor faults, and balanced three-line faults. Effective protective measures are essential to prevent equipment damage during grid faults, especially to handle surge currents and short-circuit faults.

2.17. LVRT Strategies

It is of great importance to efficiently transfer the energy produced from RESs to the grid (Ma et al., 2022). While the generated energy is transferred to the grid, many faults can occur in the grid and quickly disconnecting large-scale renewable power plant may cause voltage fluctuations in the grid and results in grid instability. To ensure grid stability, RES should remain connected to the grid at fault conditions in a specified time span. In addition, proper amount of reactive power must be injected to the grid according to the specified requirement (Jyoti Joshi et al., 2021).

LVRT is a feature of grid-connected PV systems and other renewable energy generators that allows them to continue operating during temporary dips or drops in the electrical grid voltage. LVRT enables these generators to remain operational during voltage dips and fluctuations, providing a more reliable and stable source of power to the grid (Jyoti Joshi et al., 2021). This feature is especially important in systems with high penetration of renewable energy sources, as it allows for the integration of more intermittent renewable sources, such as wind and solar, into the grid.

Fault ride-through control involves two primary approaches: modified control and external devices (Zeb et al., 2022). Modified inverter control (MIC) and calculation methods provide control without extra devices. Conversely, Flexible Alternating Current Transmission System Devices (FACTS) and Breaker Chopper Circuit (BCC) use external components to improve performance. Simulations are carried out in MATLAB/Simulink.

In the paper by (Al-Shetwi et al., 2018), an integrated control approach for a single-stage solar PV system to enhance its LVRT capability according to modern grid codes and Malaysian standards was developed. They utilized a current limiter as well as a DC chopper brake controller to mitigate high alternating currents and absorb excess DC voltage, improving system resilience during grid disturbances. Simulations are carried out in MATLAB/Simulink. The schematic used in this paper is given in Figure 2.18.

In the paper by (Nasiri et al., 2022), a cost-effective braking chopper and controller as shown in Figure 2.18 is developed for the continuous LVRT solution in single-stage grid-integrated PV systems. Simulations are carried out in MATLAB/Simulink.

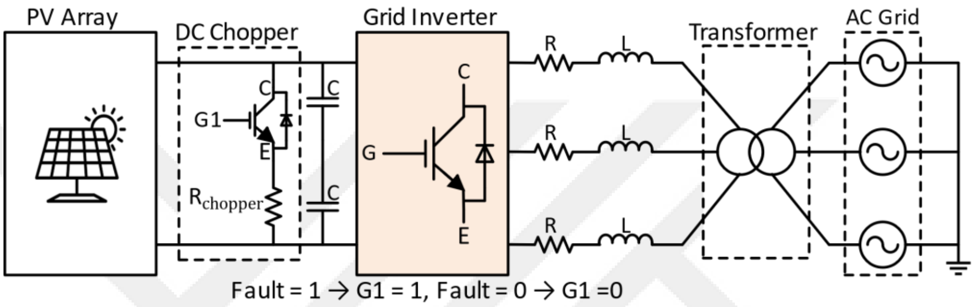

Figure 2.18. DC chopper model with RL filter

In the paper by (Ma et al., 2022), an innovative LVRT strategy utilizing an enhanced DDSRF-PLL and reactive current control strategy is proposed. The proposed strategy achieves stable DC voltage through a crowbar circuit. Simulations are carried out in MATLAB/Simulink. The schematic of the system used in this paper is given in Figure 2.19.

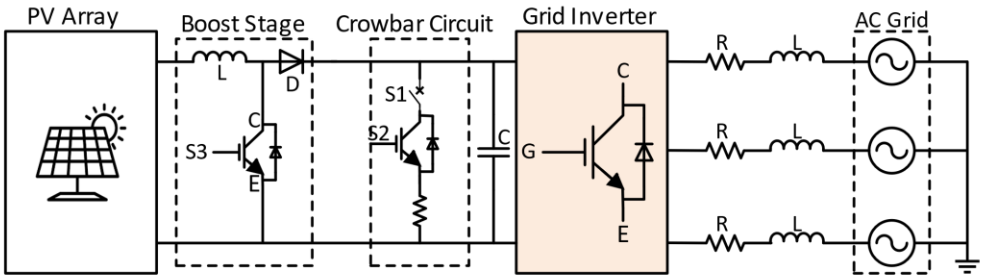

Figure 2.19. Crowbar model for two-stage system

In the paper by (Yang et al., 2017), a cost-effective control scheme addresses the challenges of LVRT operation in a two-stage single-phase grid-connected PV system. The method automatically regulates active power injection according to voltage drop and PV characteristics by moving the PV operation point to non-MPPT in faults. Simulations are carried out in MATLAB/Simulink.

In the paper by (Nithya and Roselyn, 2022), an innovative control strategy for LVRT capability in a grid-connected PV system presented. This strategy combines DC-link and MPPT controllers for normal operation and integrates a hybrid FRT approach with a series dynamic braking resistor (SDBR) and braking chopper for fault conditions. Simulations are carried out in MATLAB/Simulink. The paper by (Mohamed et al., 2019) an innovative hybrid control strategy for a two-stage grid-connected solar PV system using a braking chopper and a neutral-connected braking resistor presented. This approach aimed to mitigate LVRT issues by managing DC-link overvoltage and increasing the grid-side voltage sag resistance during faults. The paper by (Worku and Abido, 2015) proposes a grid-connected PV system with a supercapacitor energy storage system (SCESS) to enhance the FRT capability of the system and reduce power fluctuations.

In the paper by (Wen and Fazeli, 2019), a novel control strategy for 3-phase grid-connected PV systems, featuring an LVRT algorithm using mixed potential function to protect inverters from overcurrent issues during symmetric/asymmetric faults,

In the paper by (Sabir, 2019), a new energy management system for a grid-connected hybrid PV-FC source with LVRT capability is presented. The system meets the power demand, withstands symmetric/asymmetric voltage dips, and provides active/reactive power support to the grid. Constant active power is maintained during asymmetric dips. Simulations are carried out in MATLAB/Simulink.

In the paper by (Huka et al., 2018; Mirhosseini et al., 2015), a comprehensive LVRT strategy for grid-connected PV systems, addressing both balanced and unbalanced grid faults presented, also a power reduction approach manages the DC-link voltage to prevent excessive boost. Simulations are carried out in MATLAB/Simulink.

In the paper by (Jalilian et al., 2018), a DC-link bridge-type fault current limiter solution to improve the LVRT capability of grid-connected inverter is presented. The proposed technique provides limited AC fault currents during symmetrical/ asymmetrical fault scenarios and simulations studies performed in PSCAD/EMTDC.

In conclusion, LVRT implementation in single-stage and two-stage can be achieved through different methods, each with its advantages and challenges. Among external devices based FRT control; series dynamic braking resistors and BCC offer a cost advantage over FACTS due to having fewer switches and resistors. MIC-based methods, which do not require extra devices, are the most economical and efficient for FRT with grid code compatibility (Zeb et al., 2022). Continuous advancements in the field of renewable energy integration and power electronics are expected to bring more efficient and economically viable solutions for LVRT in grid-connected renewable power plants.

2.18. Summary

In this chapter, a comprehensive overview of the PV-FC hybrid systems, emphasizing design enhancements, international standards, power quality regulations, and grid connection requirements. It covers stand-alone and grid-connected systems, as well as both single-stage and two-stage power conversion. Additionally, a rigorous literature review is presented to support the understanding of PV-FC hybrid systems and LVRT strategies.

3. DESIGN OF PV-FC HYBRID SYSTEM

In this section, DC-link voltage, DC-link capacitor, PV array parameters, FC parameters, boost converter for PV and FC, and LCL filter design for an inverter are explained. The calculations and formulas are presented to determine the appropriate values for capacitors, inductors, currents, voltages, and other parameters necessary for the efficient and reliable operation of the system. Lastly detailed explanation of the overall inverter controller design is given. The system model is presented in Figure 3.1.

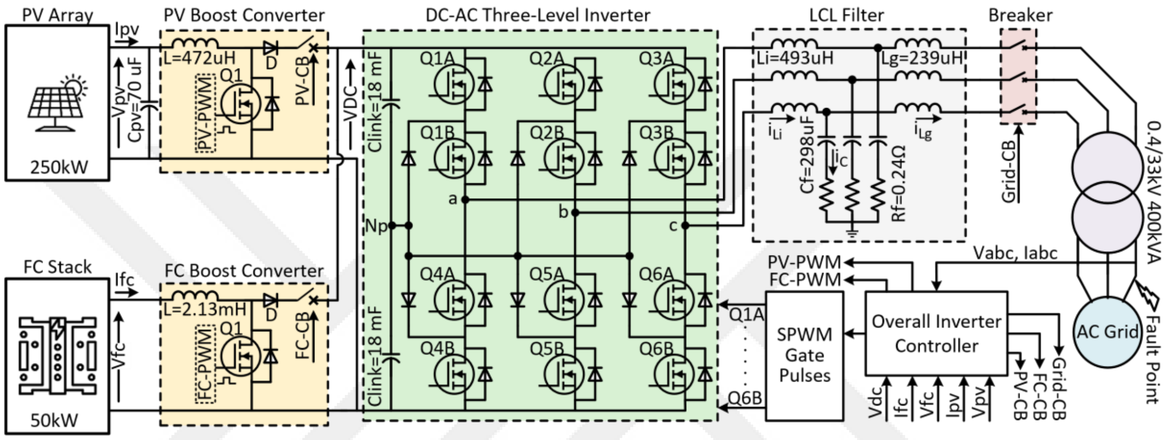

Figure 3.1. Structure of PV-FC hybrid power system with FRT capabilities

The parameters of the system are as follows: DC-link voltage is 800 V, inverter current is 515.5 A RMS, inverter switching frequency 1650 Hz, inverter line-to-line voltage is 400 V RMS, line-to-line grid voltage is 33 kV RMS. The nominal power output of the system is 300 kW, and the grid operates at a frequency of 50 Hz. Lastly, the grid connection is established with a line transformer with a capacity of 400 kVA and a voltage ratio of 0.4/33 kV.

3.1. DC-link Capacitor

Analyzing current and voltage waveforms on the inverter's DC side helps choose suitable capacitors based on voltage requirements, rms current, and harmonic components. Minimum DC-Link voltage is calculated with the formula (Quinn and Mohan, 1992).

$$V_{DCLINK} \geq 2 * \sqrt{2} * V_{PHASE,RMS} = 2 * \sqrt{2} * 230V = 653\ V \qquad (3.1.1)$$

Considering the minimum value of DC Link voltage $V_{DCLINK} = 800$ V is selected.

Correct selection of the DC bus capacitor is crucial to manage the required RMS current without overheating and to minimize ripple in the DC-link voltage (Quinn and Mohan, 1992). Based on a worst-case inverter efficiency of 85% and a maximum power of 300 kW, the RMS current through the inverter is calculated as in Equation 3.1.2 (Macit, 2020).

$$I_{INVRMS} = \frac{P_{INV}}{3 * V_{phaserms} * 0.85} = \frac{300000}{3 * 230 * 0.85} = 511.5 \text{ A} \quad (3.1.2)$$

The peak value of the inverter output current is calculated as in Equation 3.1.3.

$$I_{PEAK} = I_{INVRMS} * \sqrt{2} = 723.4 \text{ A} \quad (3.1.3)$$

Switch currents are crucial for rating the converter switches. Therefore, the switch's maximum allowable current rating must be greater than 723.4 A. The average value of the inverter output current is calculated as in Equation 3.1.4.

$$I_{INVAVG} = I_{INVRMS} * 0.9 = 460.35 \text{ A} \quad (3.1.4)$$

The voltage ripple value to restrict the DC-link voltage ripple to 5% of the DC-link voltage is calculated as in Equation 3.1.5 then C_{dclink} capacitor value is calculated (Kasal and Singh, 2011; Popa et al., 2016).

$$V_{ripple\_peak} = 0.05 * 800 = 40 \text{ V} \quad (3.1.5)$$

The value of the DC-link capacitor is determined through Equation 3.1.6.

$$C_{link} = \frac{I_{INVAVG}}{2 * \omega * V_{ripple\_peak}} = \frac{460.35}{2 * (2 * \pi * 50) * 40} = 18 \text{ mF} \quad (3.1.6)$$

For proper operation, it is recommended that the rated voltage $V_{rateddc}$ of the system be at least 20% higher than the operating voltage as in Equation 3.1.7 (Popa et al., 2016).

$$V_{dcrated} \geq \%120 * V_{DCLINK} = 1.2 * 800 \geq 960 \text{ V} \quad (3.1.7)$$

3.2. PV Array Parameters

PV cells have limited individual output power. To meet voltage and power needs, several PV modules are combined in series or parallel to form an array. The PV model used for this installation is the Aiko-A460-MAH54Mb. The configuration includes 37 parallel arrays, each array consisting of 15 series-connected modules. The total power output of the PV array is determined by multiplying the parallel arrays (37) by the series modules per array (15) and the power of the module (460W). Figure 3.2 shows the I-V and P-V characteristics of the designed PV array.

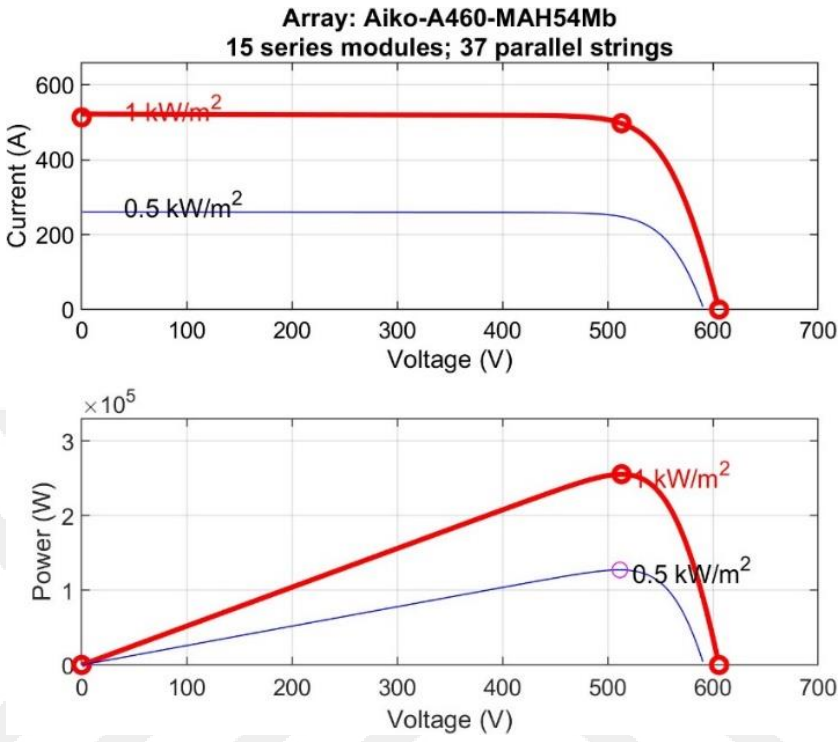

Figure 3.2. PV array I-V and P-V curve.

3.3. Fuel Cell Parameters

The FC system used is PEM type and designed to operate at 625 V operating voltage and provide 50 kW power output, nominal operating point, characterized by a current of 80 A and a voltage of 625 V, detailed parameters of FC stack presented in Table 3.1.

Table 3.1. FC parameters

Parameter	Value
Voltage at 0A and 1A [V_0(V), V_1(V)]	[900, 895]
Nominal operating point [I_{nom}(A), V_{nom}(V)]	[80, 625]
Maximum operating point [I_{end}(A), V_{end} (V)]	[280, 430]
Number of cells	900
Nominal stack efficiency (%)	55
Operating temperature (Celsius)	65
Nominal Air flow rate (lpm)	2100
Nominal supply pressure [Fuel (bar), Air (bar)]	[1.5, 1]
Nominal composition (%) [H2 O2 H2O(Air)]	[99.98, 21.1]

In Figure 3.3, the V-I and P-I curves show the performance of the FC used. Figure 3-(a) shows the voltage-current relationship, while Figure 3-(b) presents the power-current graphs. The product of current and voltage gives the FC stack power capacity. As seen in Figure 3.3, utilized FC shows optimum power output where voltage and current are aligned for maximum efficiency.

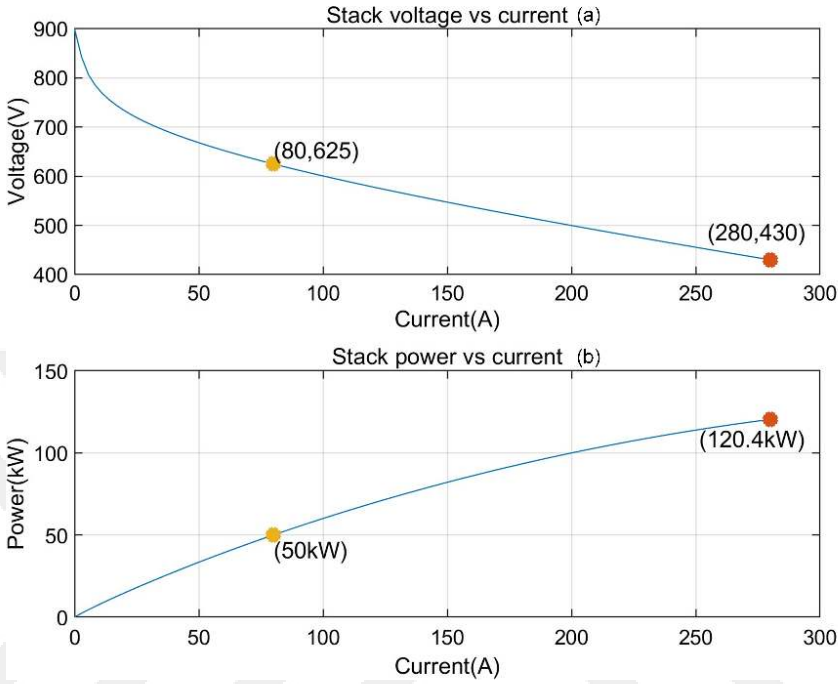

Figure 3.3. FC V-I and P-I curve

3.4. Boost Converter PV

The boost converter design procedures for continuous conduction mode operation and design considerations were discussed in Section 2.5. This section focuses on performing numerical calculations to determine the boost converter parameters specifically for this application. The design parameters of the boost converter for the PV array are given in Table 3.2.

Table 3.2. PV boost converter parameters

Boost Converter Parameter	**Value**
Typical input voltage (V_{IN})	513 V (Vmppt)
Desired output power (P_{out})	250 kW
Output voltage (V_{out})	800 V
Efficiency of converter (η)	0.9
Converter switching frequency (f_s)	8 kHz
Inductor current ripple percentage	10%

3.4.1. Calculation of Parameters

The output current calculated based on Equation 2.5.1.

$$I_{out} = \frac{250000}{800} = 312.5A$$

The maximum duty cycle calculated based on Equation 2.5.2:

$$D = 1 - \frac{513}{800} * 0.9 = 0.42$$

The inductor peak-to-peak ripple current calculated based on Equation 2.5.3.

$$\Delta I_L = 0.1 * 312.5 * \frac{800}{513} = 48.73 \text{ A}$$

The inductor value calculated based on Equation 2.5.5.

$$L = \frac{500 * (800 - 513)}{48.73 * 5000 * 800} = 472 \text{ uH}$$

The input filter capacitor C_{PV} is utilized in a PV inverter's boost stage to minimize power oscillations, reducing voltage ripple across the PV panel by balancing energy in continuous conduction mode. The nonlinear characteristics of the PV output are not taken into account for simplicity (Gao et al., 2009), V_{PV} is maximum PV voltage, ΔV_{PV} is 5% of V_{PV} selected, considering these criteria, the input capacitor value is calculated as in Equation 3.4.1.

$$C_{PV} \geq \frac{D_{max} * V_{PV}}{4 * \Delta V_{PV} * f_{sw} * L_{boostPV}} = \frac{0.42 * V_{PV}}{4 * 0.05 * 513 * 8000 * 2.8 \text{ mH}} = 70 \, uF \qquad (3.4.1)$$

3.5. Boost Converter FC

The boost converter design procedures for continuous conduction mode operation and design considerations were discussed in Section 2.5. This section focuses on performing numerical calculations to determine the boost converter parameters specifically for this application. The design parameters of the boost converter for the FC stack are given in Table 3.3.

Table 3.3. FC boost converter parameters

Boost Converter Parameter	**Value**
Typical input voltage (V_{IN})	625 V (Vmppt)
Desired output power (P_{out})	50 kW
Output voltage (V_{out})	800 V
Efficiency of converter (η)	0.9
Converter switching frequency (f_s)	8 kHz
Inductor current ripple percentage	10%

3.5.1. Calculation of Parameters

The output current is calculated based on Equation 2.5.1.

$$I_{out} = \frac{50000}{800} = 62.5 \text{ A}$$

The maximum duty cycle value is calculated based on Equation 2.5.2.

$$D = 1 - \frac{625}{800} * 0.9 = 0.296$$

The inductor peak-to-peak ripple current is calculated based on Equation 2.5.3.

$$\Delta I_L = 0.1 * 62.5 * \frac{800}{625} = 8 \text{ A}$$

The inductor value is calculated based on Equation 2.5.5.

$$L = \frac{500 * (800 - 625)}{8 * 8000 * 800} = 2.13 \text{ mH}$$

3.6. LCL Filter Design

The detailed design procedure and equations of the LCL filter are explained in Section 2.8. In this subsection, the numerical design procedure of LCL filter parameters for this specific system is calculated and the frequency response of the filter is evaluated with bode diagrams as present in Figure 3.4.

Table 3.4. LCL Filter design parameters

LCL Filter Parameter	Value
Nominal Power (P_n)	300 kW
DC-link Voltage (V_{DC})	800 V
Inverter Line Voltage (V_n)	400 V
Inverter Phase Voltage (V_{ph})	230 V
Grid Frequency (f_g)	50 Hz
Inverter Switching Frequency (f_{sw})	1650 Hz
Phase current ripple	10 %

3.6.1. Calculation of LCL Parameters

The base impedance is calculated based on Equation 2.8.1.

$$Z_b = \frac{V_n^2}{P_n} = \frac{400^2}{300000} = 0.533\ \Omega$$

The grid angular frequency is represented by ω_g. Base capacitance is calculated based on Equation 2.8.2.

$$C_b = \frac{1}{\omega_g * Z_b} = \frac{1}{(2 * \pi * 50) * 0.533} = 5.968\ \text{mF}$$

The filter capacitor is calculated based on Equation 2.8.3

$$C_f = C_b * 0.05 = 298\ \text{uF}$$

The maximum phase current is calculated based on Equation 2.8.4.

$$I_{maxphase} = \frac{P_n * \sqrt{2}}{3 * V_{ph}} = 612.372\ \text{A}$$

The maximum phase current ripple is chosen as 0.1 (10%) and calculated based on Equation 2.8.5.

$$\Delta I_{max} = 0.1 * I_{maxphase} = 0.1 * 612.372\ \text{A} = 61.237\ \text{A}$$

The inverter side inductor is calculated based on Equation 2.8.6

$$L_{inv} = \frac{V_{DC}}{16 * f_{sw} * dImax} = \frac{800}{16 * 1650 * 61.237} = 494 \text{ uH}$$

The grid side inductor value is calculated based on Equation 2.8.7 considering $k_a = 0.15$.

$$L_{grid} = \frac{\sqrt{\frac{1}{{k_a}^2} + 1}}{(\omega_{sw})^2 * C_f} = \frac{\sqrt{\frac{1}{0.15^2} + 1}}{(2 * \pi * f_{sw})^2 * 298 * 10^{-6}} = 239 \text{ uH}$$

The resonance frequency f_{res} is calculated based on Equation 2.8.8.

$$f_{res} = \frac{1}{2 * \pi} * \sqrt{\frac{L_{inv} + L_{grid}}{L_{inv} * L_{grid} * C_f}} \cong \frac{1}{2 * \pi} * 4559 \cong 725 \text{ Hz}$$

The resonance avoiding criteria is calculated based on Equation 2.8.9. To avoid resonance problems, the criteria in Equation 2.8.9 should be considered. If $f_{res} < 10 * f_g$: a greater k_a value, if $f_{res} > 0.5 * f_{sw}$: a smaller k_a value needs to be selected. In this example, 725 Hz meets the design criteria. The resistance in series with the filter capacitance is calculated based on Equation 2.8.10.

$$R_f = \frac{1}{3 * (2 * \pi * f_{res}) * C_f} = \frac{1}{3 * 4559 * 298 * 10^{-6}} = 0.245\ \Omega$$

The bode diagram of the filter is plotted in Figure 3.4.

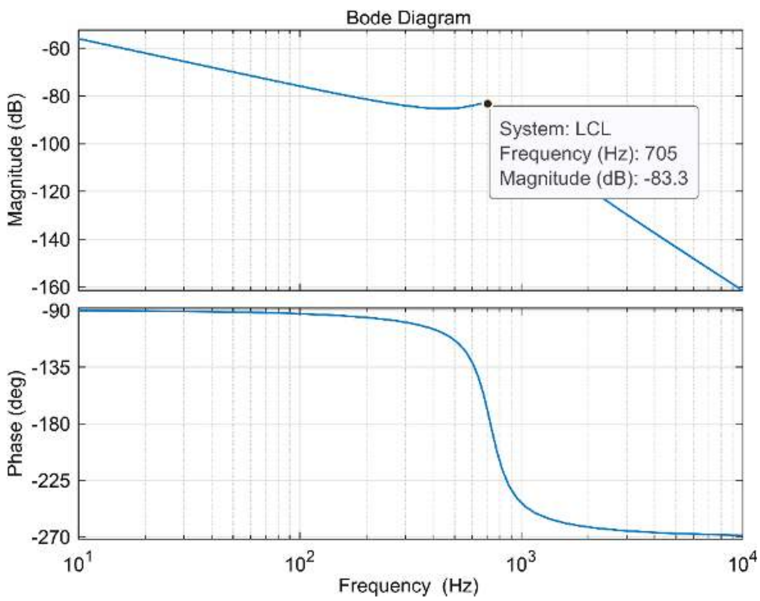

Figure 3.4. LCL filter bode diagram

3.7. Overall Inverter Controller

The overall inverter controller scheme consists of measurements, inverter current regulation, fault mode control, energy management, and PV/FC boost controllers. The general inverter controller is shown in Figure 3.5. A detailed description of the blocks of the inverter controller will be presented in this section.

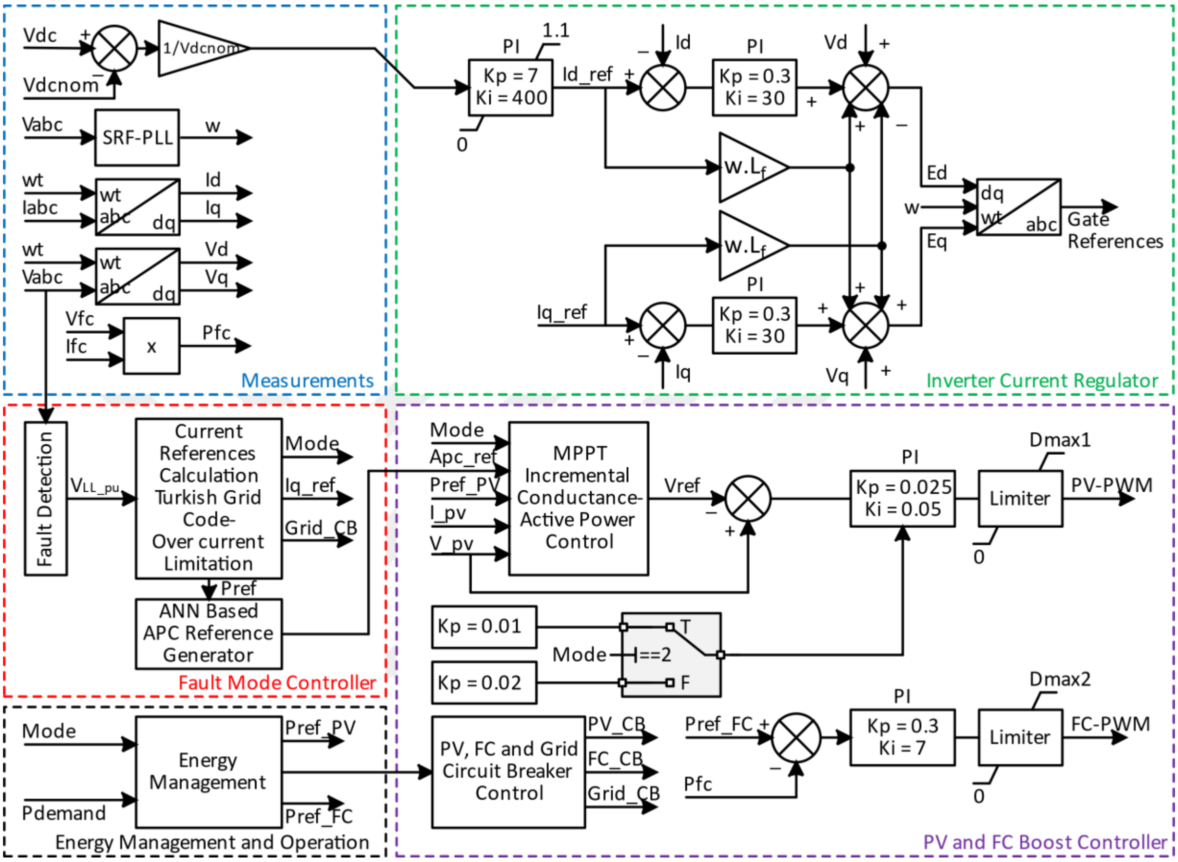

Figure 3.5. Overall control scheme

3.7.1. Measurements

Measurement blocks consist of SRF-PLL, grid voltages V_{abc}, grid currents I_{abc}, FC voltage V_{FC}, and FC current I_{FC} measurements. Inverter grid synchronization is done by SRF-PLL loop to get angular speed wt (in radians). Accurate phase estimation of the grid voltages is essential for precise injection of both active and reactive power (Aldbaiat et al., 2022). The SRF-PLL algorithm finds wide application in three-phase systems (Sevilmiş and Karaca, 2019) due its relatively simple design. The SRF-PLL converts abc phase voltages to dq rotating reference frame via Park's transformation for analysis (Kaura and Blasko, 1997) and, by use of Equation 3.7.1 and 3.7.2. In which we get V_d, V_q and I_d, I_q. This voltage and current are utilized in the inverter current controller to get reference dq0 vectors.

Park- Inverse Park transformations

The Park Transform converts three-phase abc time-domain components to direct, quadrature, and zero components in a rotating reference frame based on input angular position (wt in rad). Voltage vector abc/dq transformation is calculated as in Equation 3.7.1.

$$\begin{bmatrix} V_d \\ V_q \\ V_0 \end{bmatrix} = \frac{2}{3} \begin{bmatrix} \cos(wt) & \cos\left(wt - \frac{2\pi}{3}\right) & \cos\left(wt + \frac{2\pi}{3}\right) \\ \sin(wt) & \sin\left(wt - \frac{2\pi}{3}\right) & \sin\left(wt + \frac{2\pi}{3}\right) \\ \frac{1}{2} & \frac{1}{2} & \frac{1}{2} \end{bmatrix} \begin{bmatrix} V_a \\ V_b \\ V_c \end{bmatrix} \quad (3.7.1)$$

The current vector abc/dq transformation is calculated in Equation 3.8.2.

$$\begin{bmatrix} I_d \\ I_q \\ I_0 \end{bmatrix} = \frac{2}{3} \begin{bmatrix} \cos(wt) & \cos\left(wt - \frac{2\pi}{3}\right) & \cos\left(wt + \frac{2\pi}{3}\right) \\ \sin(wt) & \sin\left(wt - \frac{2\pi}{3}\right) & \sin\left(wt + \frac{2\pi}{3}\right) \\ \frac{1}{2} & \frac{1}{2} & \frac{1}{2} \end{bmatrix} \begin{bmatrix} I_a \\ I_b \\ I_c \end{bmatrix} \quad (3.7.2)$$

The voltage vector dq/abc (inverse park) transformation calculated in Equation 3.8.3.

$$\begin{bmatrix} V_a \\ V_b \\ V_c \end{bmatrix} = \begin{bmatrix} \cos(wt) & -\sin(wt) & 1 \\ \cos\left(wt - \frac{2\pi}{3}\right) & -\sin\left(wt - \frac{2\pi}{3}\right) & 1 \\ \cos\left(wt + \frac{2\pi}{3}\right) & -\sin\left(wt + \frac{2\pi}{3}\right) & 1 \end{bmatrix} \begin{bmatrix} V_d \\ V_q \\ V_0 \end{bmatrix} \quad (3.7.3)$$

3.7.2. Inverter Current Regulator

Current control is established within a frame that rotates at an angular velocity ω. Within this frame, two voltage equations define the voltage and current components (Liserre et al., 2005). The equations include the reference voltages $E_d(t)$ and $E_q(t)$, the total inductor internal resistance R_T and the inductance sum $L_f = L_{inv} + L_{grid}$. The measured currents are $i_d(t)$ and $i_q(t)$ and the measured voltages are $V_d(t)$ and $V_q(t)$ in dq frame. Lastly, the $i_d^*(t)$ and $i_q^*(t)$ represents reference currents in the dq frame. Ignoring the filter capacitor and resistors, the system is described by Equation 3.7. The inverter current controller is also visualized in Figure 3.5.

$$\begin{cases} E_d(t) = R_T * i_d(t) + L_f * \frac{d}{dt} * i_d(t) + V_d(t) - w * L_f * i_q^*(t) + w * L_f * i_d^*(t) \\ E_q(t) = R_T * i_q(t) + L_f * \frac{d}{dt} * i_q(t) + V_q(t) + w * L_f * i_q^*(t) + w * L_f * i_d^*(t) \end{cases} \quad (3.7.4)$$

These dq currents are controlled by two by two effectively tuned PI controllers to produce the voltages that should control these currents. The controller generates voltage references in the dq frame which are subjected to an Inverse Park transformation (dq0/abc) via Equation 3.7.4. This generates pulse signals for the three-level NPC converter switches using the applied reference voltage vector.

The nominal value of DC-link voltage is selected 800 V according to Equation 3.1.1, and this reference voltage compared with measured DC-link voltage V_{DC} and scaled by a factor of $1/Vdcnom$ then fed into a PI controller with $K_P = 7$ and $K_i = 400$ values, the output of the PI controller is limited to a minimum value of 0 and a maximum value of 1.1 to prevent over-current. The output of this controller used as an active power reference for the inverter current regulator $i_d^*(t)$.

3.7.3. PV and FC Boost Controller

The FC boost converter output power is regulated using a PI controller to vary the output power based on power reference supplied during both fault and normal operation. In the event of a grid failure, the PV array generates more power than is fed into the power grid. As a result, this excess power can lead to a significant increase in the DC-link voltage. This increase is a result of energy accumulation in the DC-link capacitors (Al-Shetwi et al., 2018). During normal operation, the PV array operates at operation point B as shown in Figure 3.6, the boost converter executes MPPT, the inverter performs DC-link voltage regulation, which is essential for the active power reference calculation, and it extracts maximum power from the PV array. During grid faults, MPPT stops, and DC-link voltage is managed by a PI controller as in Figure 3.5 to enable output power regulation by variable duty cycle control method based on voltage reference. This allows to curtail output power to handle the power imbalance during faults.

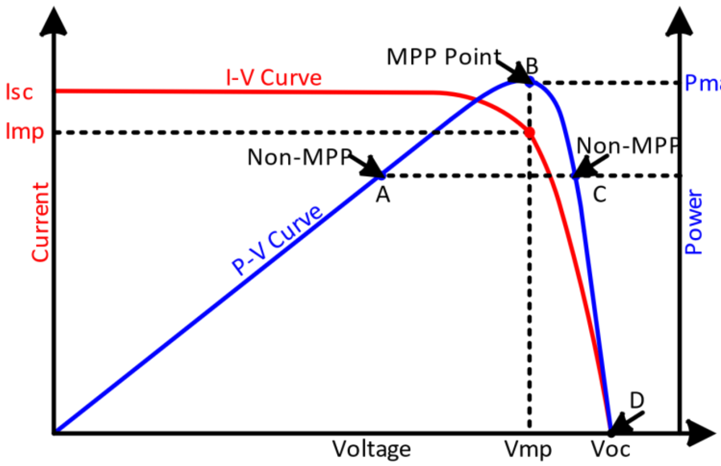

Figure 3.6. PV array operating curve

There is an active power curtailment method to reduce the PV power output, which can be achieved by moving the MPPT operating point from point (B) to point A or C in Figure 3.6. The paper by (Jyotia Joshi et al., 2021) compares non-MPPT modes for PV systems, finding poor dynamic but good steady-state response on the left side (A), and fast reachability with power oscillations on the right side (C). The proposed method solves power oscillations by utilizing an ANN-based power reference generator. In the event of a voltage sag, P and Q references are calculated according to Equation 2.15.1, and active power references and fed to the proposed ANN-based power reference generator to calculate the required voltage reference for current regulation. In the event of voltage sag, the proposed fault mode (red box) active power control scheme in Figure 3.7 is used. The modified INC method uses the normal mode (blue box) active power control scheme in Figure 3.7.

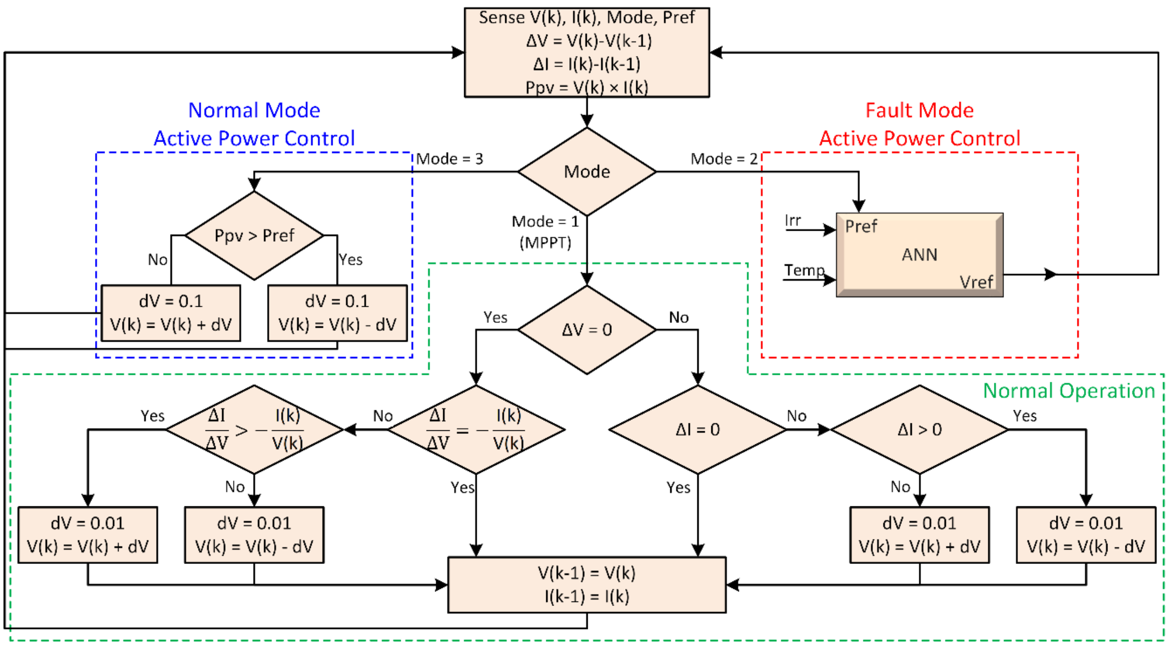

Figure 3.7. General active power control and MPPT

3.7.4. Energy Management System and Operation Scenarios

The general energy management strategy scheme is visualized in Figure 3.8. This management scheme runs the PV and FC systems in full power mode when demand is equal to maximum production. There are many works in the literature for energy management strategies; a PV-Battery hybrid system in (Bozkurt, 2022), a PV-FC-Battery hybrid system for off-grid systems in (Gugulothu et al., 2023), an energy management scheme including LVRT introduced in (An et al., 2023) and an algorithm for operation mode selection and collaborative control is presented. Considering these studies, the priority of the system is to utilize as much power as possible from the PV array since it has no storage, when the PV power generation drops below 10 kW the PV array is deactivated, and the FC continues to supply power according to demand.

During normal operation, the energy management system receives real P_{dem} and reactive power Q_{dem} demand from the transmission operator and PV array operate at operation point B as in Figure 3.6 and it extracts maximum power from the PV array. If the power demand is less than the PV maximum power, the system regulates PV power by moving towards to operation point to C point according to power demand or power reference. The energy management strategy is given in Figure 3.8.

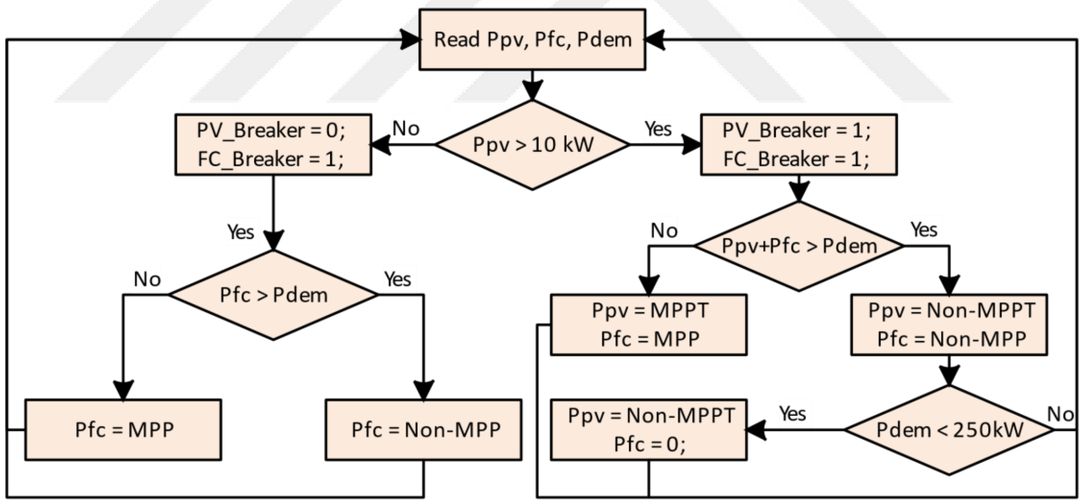

Figure 3.8. Energy management strategy

3.7.5. Proposed Fault Mode Controller

Fault detection

The proposed control employs the RMS method given in (Al-Shetwi et al., 2018) to detect voltage sag by monitoring d-q grid voltage components via the PLL. The line-to-line voltage V_{LL} is computed using Equation 3.7.5, without requiring extra hardware or transformations. Additionally, V_{LL} measurement is improved using a second-order low-pass filter with a 100 Hz natural frequency and 0.707 damping factor. This enhances clarity and stabilizes the reference signal.

$$V_{LL} = \sqrt{{V_d}^2 - {V_q}^2} \quad (3.7.5)$$

Current Reference Generation Based on Turkish Grid Code

In this thesis, the existing baseline generation based on the Turkish LVRT grid regulations in Section 2.13.1 is considered. According to specifications, the renewable power plant must remain connected to the grid for 0.15 s even if the line voltage drops to 0 % of the nominal voltage V_N. In addition, the grid voltage must return to 90 % of the pre-fault level within 1.5 s. A ratio $v(t) = 0.9/(1.5 - 0.15) = 0.66$ is applied to monitor grid voltage between 0.15 s and 1.5 s for compliance. Taking these features into account, the operation of the LVRT is shown in Figure 3.9.

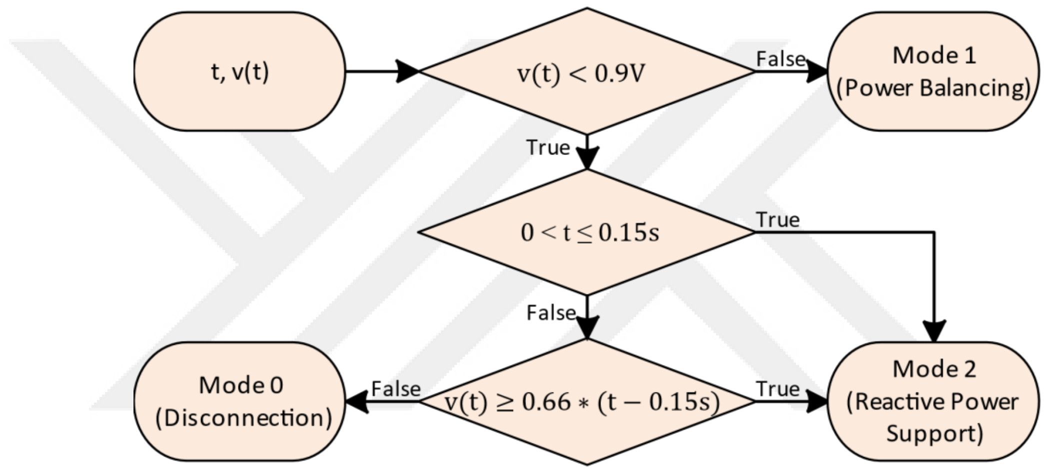

Figure 3.9. LVRT operation chart based on Turkish grid code

The system operates normally in the voltage range 0.9 to 1.1 p.u. and the inverter only injects active current. During a voltage collapse, the inverter is required to provide the specified reactive power to assist voltage recovery in accordance with LVRT requirements. According to Turkish renewable grid regulation, in case of voltage fluctuations of more than ±10 % at the grid connection, wind turbines, and solar inverters must immediately be able to provide up to 100 % rated current in reactive support sustained for 1.5 s, within 60 ms ±10. In this thesis ratio based on Equation 2.15.1 is preferred during faults.

ANN Based Active Power Generator

PV curve has a non-linear operating characteristic in the non-MPP region between the “B” and “D” points in Figure 3.6. An ANN model was constructed to extract non-MMP characteristics of the PV curve between “B” and “D” points. The idea behind this strategy is to find V_{ref} values corresponding to P_{ref} values in different power levels. The PV data extraction circuit in Figure 3.10 is constructed in MATLAB/Simulink to get training data.

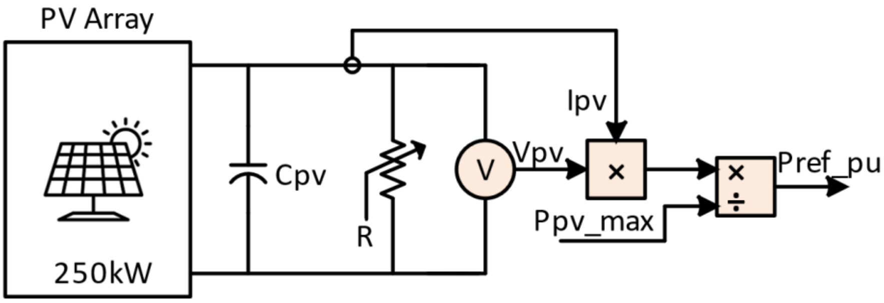

Figure 3.10. Train circuit

Firstly, the resistance value $V_{mp}/I_{mp} = 513.15/497.65 \approx 1.03\ \Omega$, which corresponds to approximately 1 Ω for operating the PV array at maximum power, is calculated. Starting from this resistance value, the resistance is increased in steps of 0.005. In addition, voltage references and their corresponding temperatures, solar irradiation levels and power references data are obtained for various resistance values. As a result, 4000 data were obtained. To enhance the randomness of the data, firstly the obtained values were mixed using the MATLAB random permutation command. Then obtained dataset of 4000 data points was divided into three separate sets as follows: 70 % of the data was allocated for training, while 15 % was assigned for both validation and test data. The MATLAB's neural network fitting tool is used for model training and model generation. A network with temperature (Temp), irradiation (Irr) and Pref inputs and Vref output constructed as in Figure 3.11.

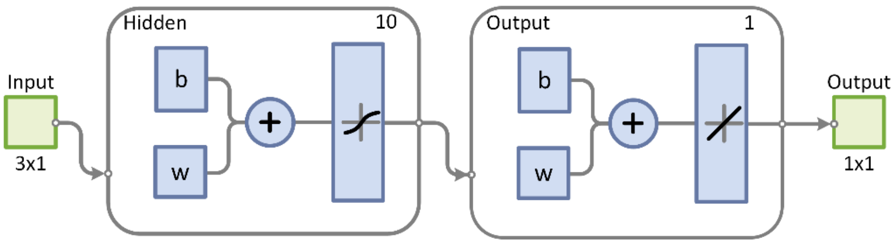

Figure 3.11. Proposed neural network structure.

The neural network has 10 hidden neurons, and the network is trained using the Levenberg Marquardt learning algorithm. According to the results in Figure 3.12, the model exhibits remarkable performance with high regression coefficients. In particular, the training data gives R=0.9998, validation R=0.9967 and testing R=0.998. The overall data is R=0.998. After the training process, the developed model was exported to MATLAB/Simulink for modeling purposes.

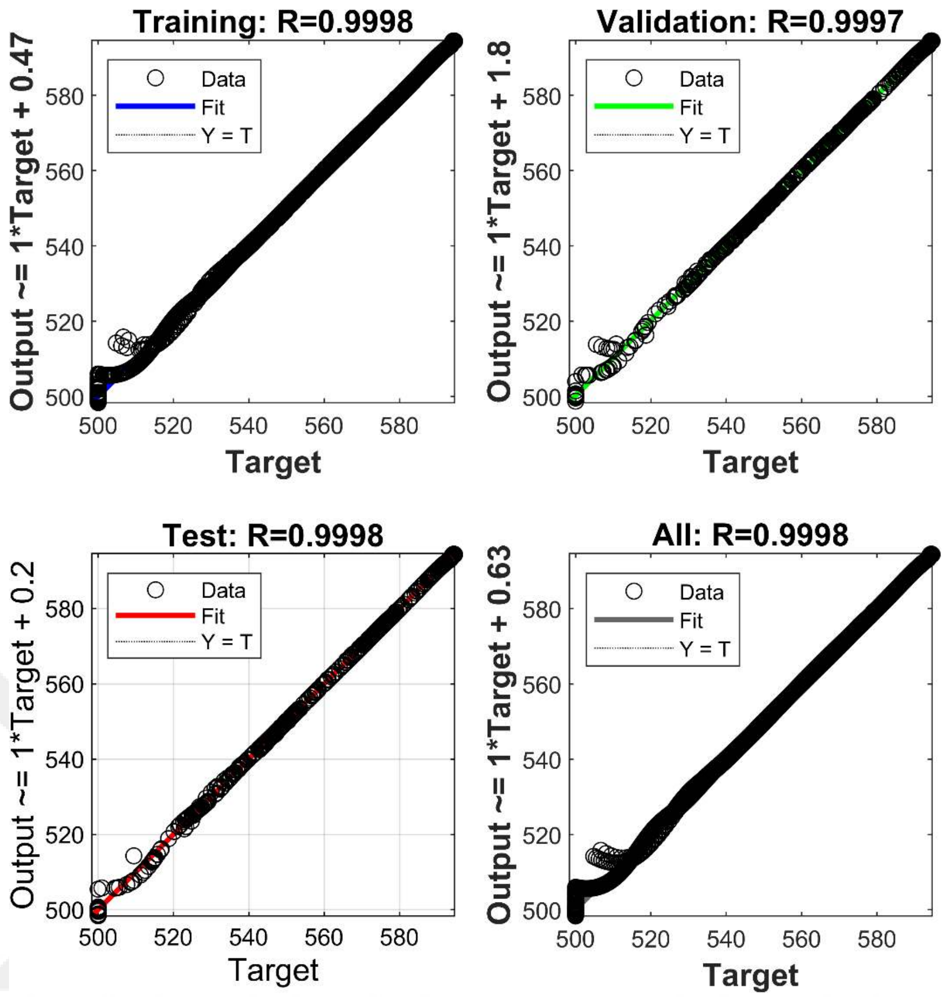

Figure 3.12. Regression graphs of the proposed model

The tracking performance of the model is evaluated through simulation using reference changes: 80 % from 0.1 to 0.2 s, 60 % from 0.2 to 0.3 s, 40 % from 0.3 to 0.4 s and 20 % from 0.4 to 0.5 s, followed by 20 % power increments every 0.1 s until full PV array capacity. Figure 3.13 validates the tracking capability and performance of the developed model.

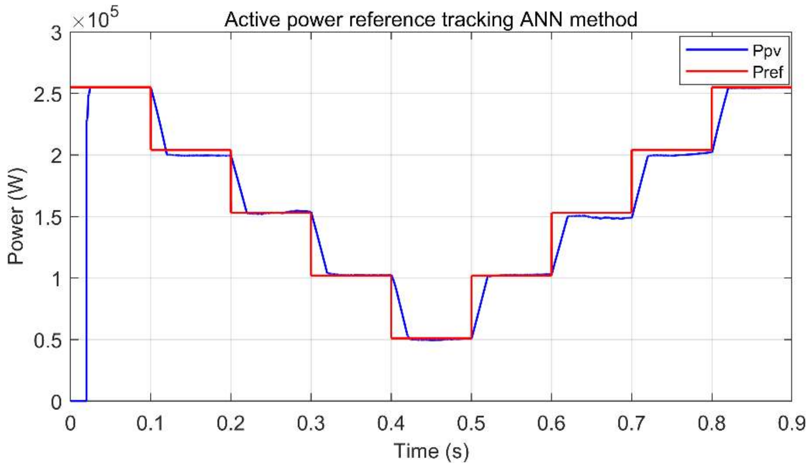

Figure 3.13. Tracking capability of developed ANN model

3.8. Summary

In this chapter, a detailed description of the PV-FC hybrid power system design is provided. It covers calculations and design considerations for DC-link capacitors, PV array parameters, FC parameters, boost converter parameter calculation for PV and FC, LCL filter design, and overall inverter controller design. The structure of the system and available control strategies are described in depth, including fault mode control, energy management, and the proposed ANN-driven non-MPPT mode active power generator adapted for PV operation.

4. RESULTS AND DISCUSSIONS

This section presents the simulation of the designed hybrid system, steady-state analysis, fault mode analysis, and a comparative study between the proposed ANN method and the modified INC approach highlighting the efficiency of the proposed method.

The designed PV-FC system's performance was evaluated through a series of tests under steady-state and dynamic conditions. Unlike the existing literature, the system is subjected to sequential faults to evaluate system performance under dynamic and transient conditions. This approach provides a comprehensive assessment of the system’s behavior. To evaluate the system's performance under dynamic conditions, sequential voltage sags are applied at different time intervals starting from a 75 % drop between 0.2 s and 0.4 s, a 50 % drop between 0.4 s and 0.6 s, and a 25 % drop between 0.6 s and 0.8 s. After 0.8 s, the grid voltage was restored to its normal range, considering test durations a total simulation time of 1 s was chosen. The specified procedure is carried out independently for various fault types such as: symmetrical three-line fault (Section 4.3.1), asymmetrical single line fault (Section 4.3.2), asymmetrical double line fault (Section 4.3.3) and line-to-line fault (Section 4.3.4). Evaluations of the system performance were performed for each case to ensure a consistent and meaningful analysis. Additionally, the system fault ride-through capability is tested at 500 W/m^2 irradiation in Section 4.4 to assess performance in a different level of solar irradiation.

4.1. System Operation Under 1000 W/m^2 Irradiation

Figure 4.1 illustrates the inverter operation output waveforms of the PV-FC system under 1000 W/m^2 irradiation condition. Figure 4.1-(a) shows grid-side phase voltages, Figure 4.1-(b) shows grid-side phase currents, Figure 4.1-(c) shows active and reactive power injected to the grid, and Figure 4.1-(d) shows the DC-link voltage for 1 s operation. The DC-link voltage has an initial peak of 888 V due to the initialization of the DC-link voltage controller, then remains at 800 V DC at steady state.

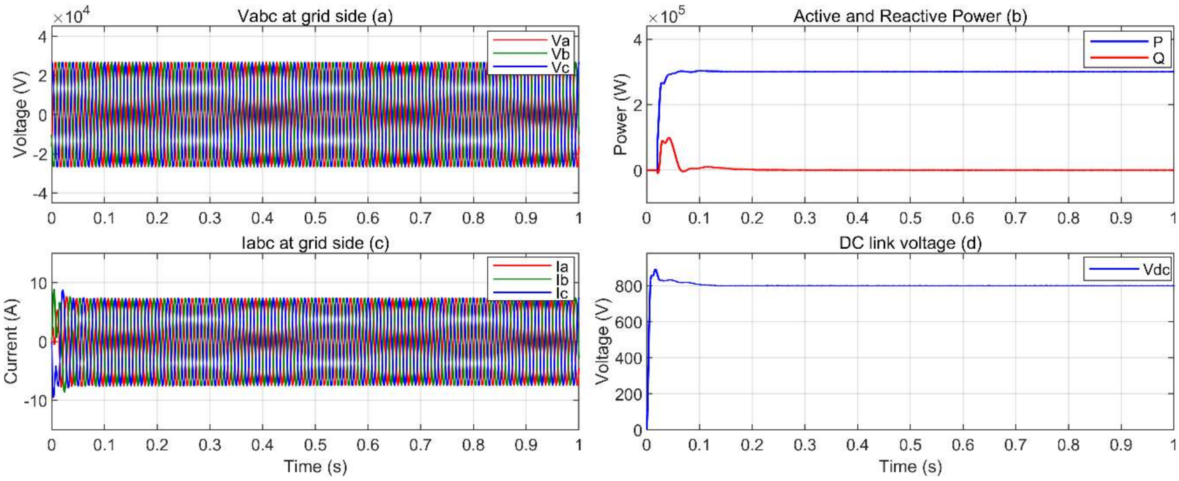

Figure 4.1. Inverter operation under 1000 W/m2 irradiation

In a stable operating state, Figure 4.2-(a) shows the injected phase currents, Figure 4.2-(b) current THD measurement, from this graph it can be seen THD level is consistently below 2 % and meets the design criteria, Figure 4.3-(c) shows the system efficiency which is measured approximately 98 % by dividing the average output power by the average input power.

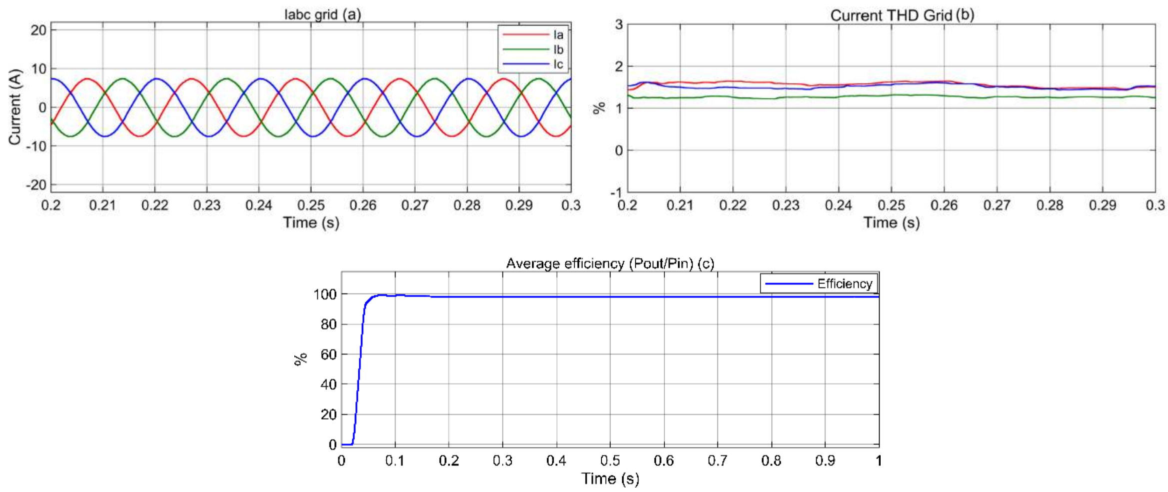

Figure 4.2. Phase currents, THD, and efficiency measurements under 1000 W/m^2 irradiation

4.2. System Operation Under 500 W/m^2 Irradiation

Figure 4.3 illustrates the inverter operation output waveforms of the PV-FC system under 500 W/m^2 irradiation condition. Specifically, Figure 4.3-(a) shows grid-side phase voltages, Figure 4.1-(b) shows grid-side phase currents, Figure 4.4-(c) shows active and reactive power injected to the grid, and Figure 4.1-(d) shows the DC-link voltage for 1 s operation.

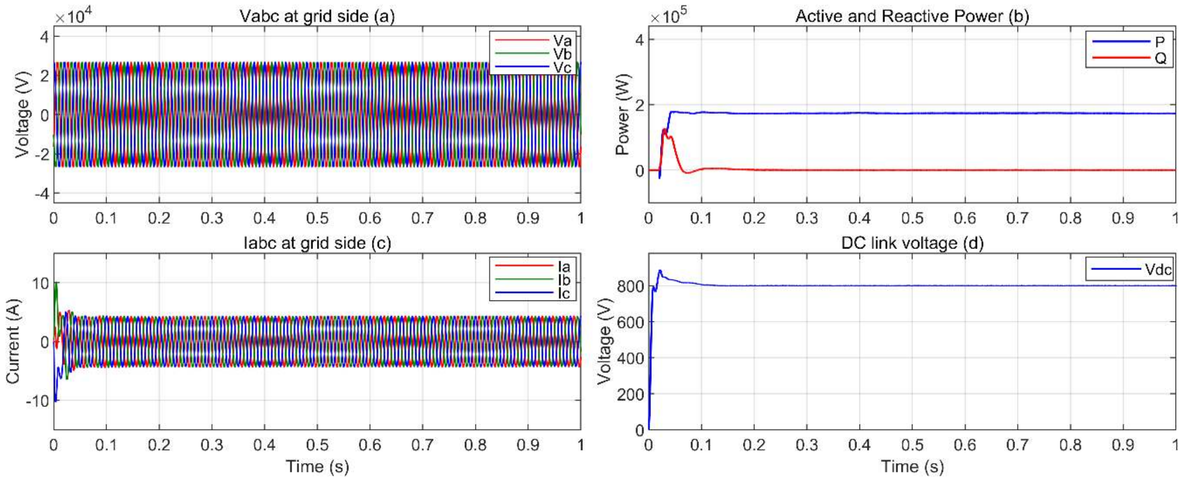

Figure 4.3. Inverter operation under 500 W/m² irradiation

In a stable operating state under 500 W/m² irradiation, Figure 4.4-(a) shows injected phase currents. Figure 4.4-(b) shows that current THD level is consistently below 2 % and meets the design criteria.

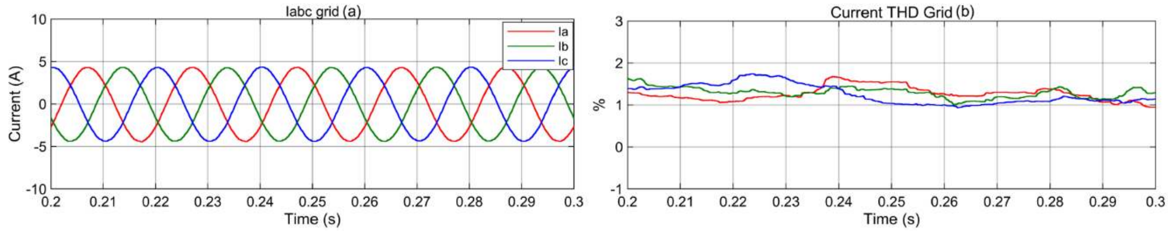

Figure 4.4. Phase currents and THD measurement under 500 W/m² irradiation

4.3. System Operation Fault Mode Analysis Under 1000 W/m² Irradiation

In this section, the system is subjected to symmetrical and asymmetrical voltage variations such as three-line to ground in Section 4.3.1, single line-to-ground in Section 4.3.2, double line-to-ground in Section 4.3.3, and line-to-line in Section 4.3.4 for 1000 W/m² irradiation. Fault scenario applied as follows; starting from 75 % voltage drop between 0.2-0.4 s, 50 % drop between 0.4-0.6 and 25 % drop between 0.6-0.8 s and return to nominal voltage at 0.8 s. This scenario applied both the conventional INC method and the proposed ANN method to make a performance comparison between these methods.

4.3.1. Three-Line to Ground Fault Under 1000 W/m² Irradiation

Figure 4.5 shows the modified INC strategy and Figure 4.6 shows the proposed control strategy results for a three-line symmetrical fault for 1000 W/m² irradiation. Figure 4.5-(a) shows the grid voltage level, Figure 4.5-(b) shows the active and reactive power injection into the grid during the fault, Figure 4.5-(c) shows the injected currents during the fault. Figure 4.5-(d) shows the DC-link voltage curve exhibits a minimum of 581 V and a peak of 1090 V during the fault.

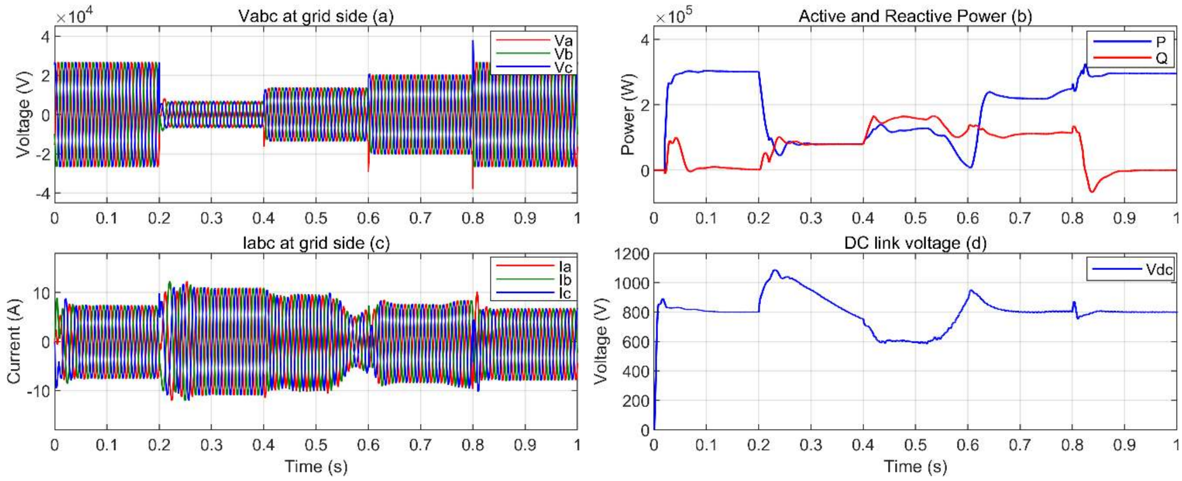

Figure 4.5. Symmetrical three-line fault modified INC strategy under 1000 W/m^2 irradiation

Figure 4.6-(a) shows the grid voltage level, Figure 4.6-(b) shows the active and reactive power injection into the grid during the fault, and Figure 4.6-(c) shows the injected currents during the fault. Furthermore, Figure 4.6-(d) shows the DC-link voltage curve exhibits a minimum of 732 V and a peak of 877 V during the fault. Comparing Figure 4.5-(c) with Figure 4.6-(c), the proposed method also shows better performance at limiting the currents.

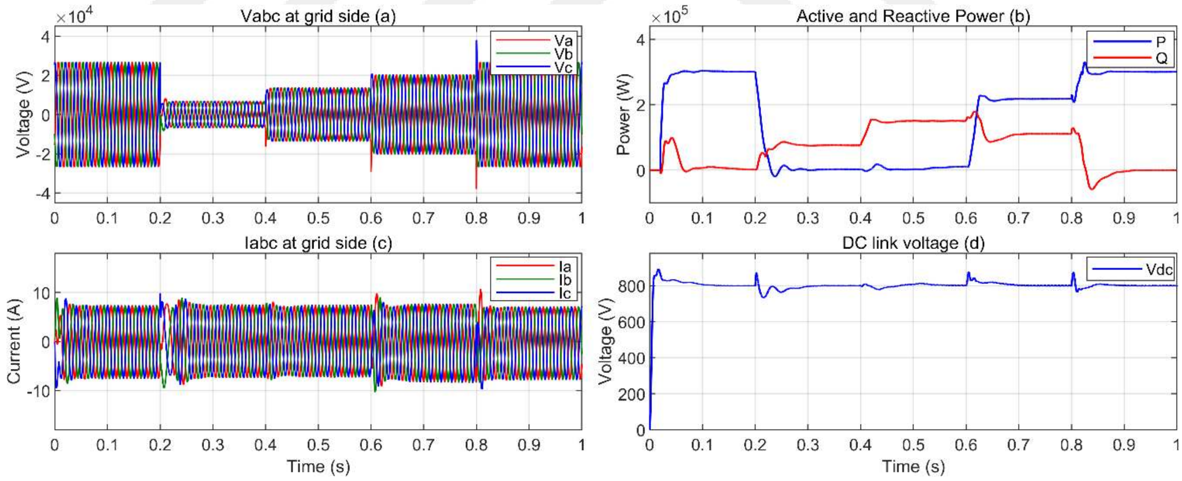

Figure 4.6. Symmetrical three-line fault ANN method under 1000 W/m^2 irradiation

4.3.2. Single Line-to-Ground Fault Under 1000 W/m^2 Irradiation

Figure 4.7 shows the modified INC strategy and Figure 4.8 shows the proposed control strategy results for single-line asymmetrical fault for 1000 W/m^2 irradiation. Figure 4.7-(d) shows the DC-link voltage curve exhibits a minimum of 618 V and a peak of 928 V during the fault.

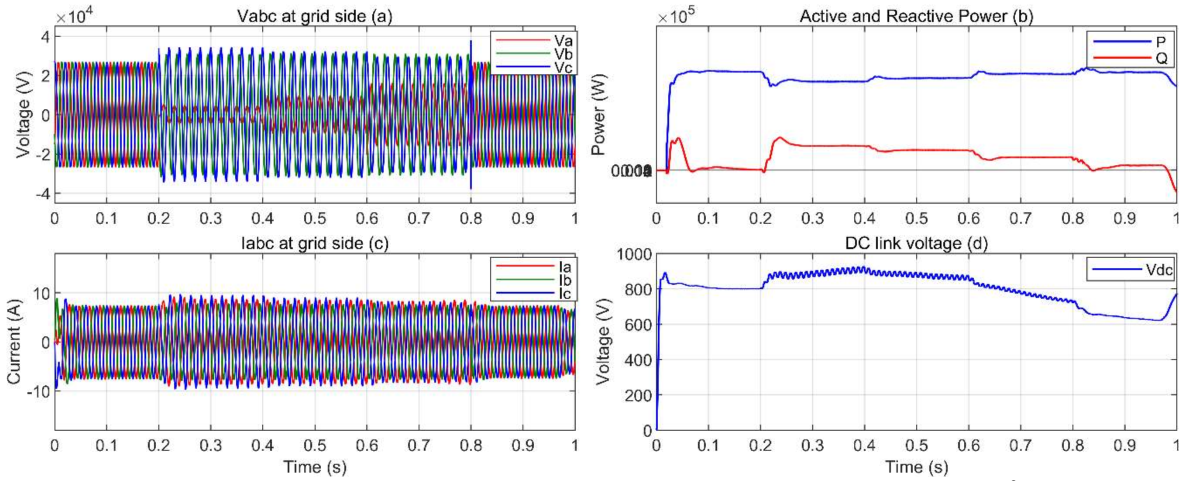

Figure 4.7. Asymmetrical single-line fault modified INC strategy under 1000 W/m^2 irradiation

Figure 4.8-(d) shows the DC-link voltage curve exhibits a minimum of 758 V and a peak of 850 V during the fault.

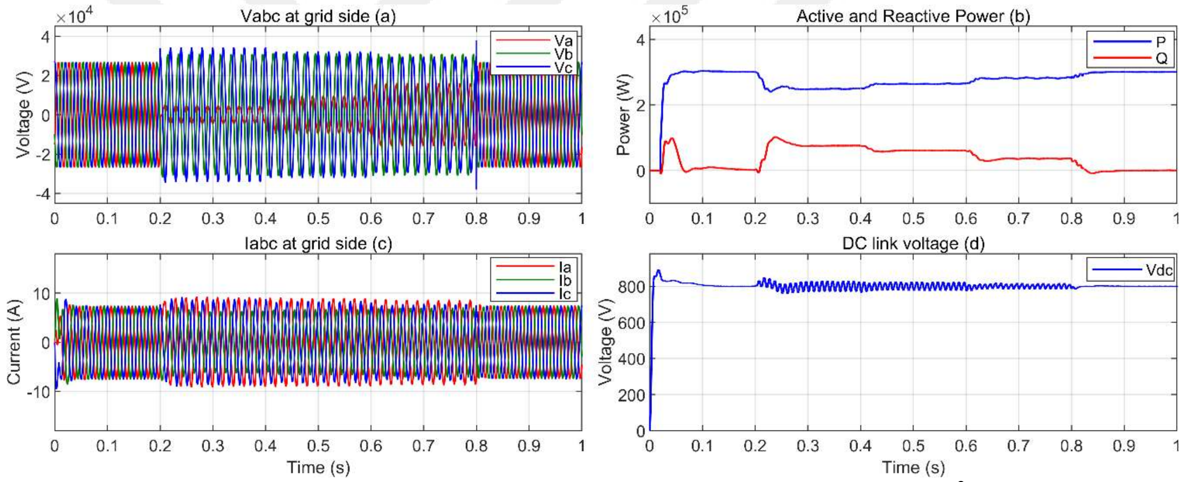

Figure 4.8. Asymmetrical single-line fault ANN method under 1000 W/m^2 irradiation

4.3.3. Double Line-to-Ground Under 1000 W/m^2 Irradiation

Figure 4.9 shows the modified INC strategy and Figure 4.10 shows the proposed control strategy results for double line asymmetrical fault for 1000 W/m^2 irradiation. Figure 4.9-(d) shows the DC-link voltage curve exhibits a minimum of 626V and a peak of 1034V during the fault.

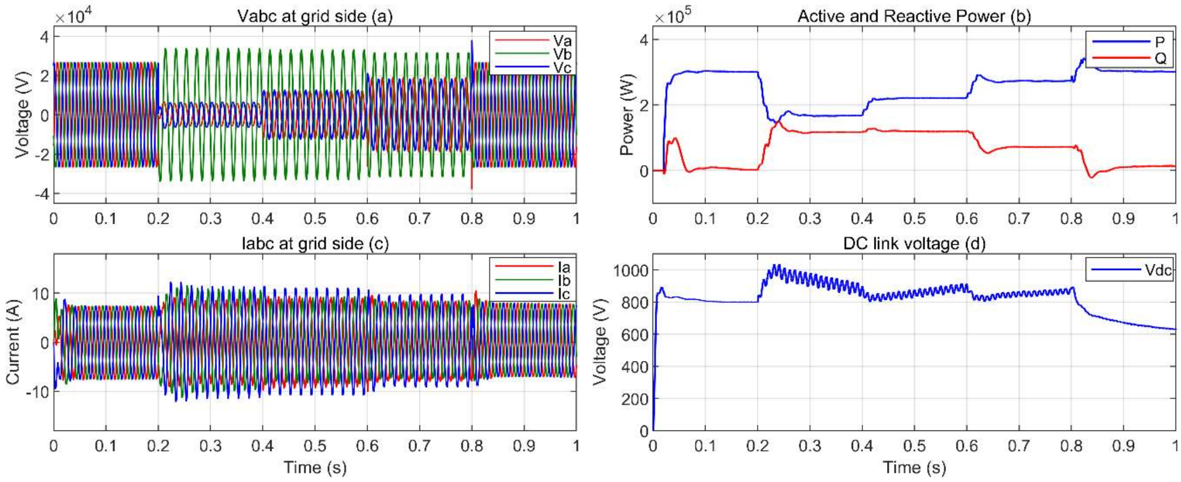

Figure 4.9. Asymmetrical double-line fault modified INC strategy under 1000 W/m² irradiation

Figure 4.10-(d) shows the DC-link voltage curve exhibits a minimum of 713 V and a peak of 858 V during the fault.

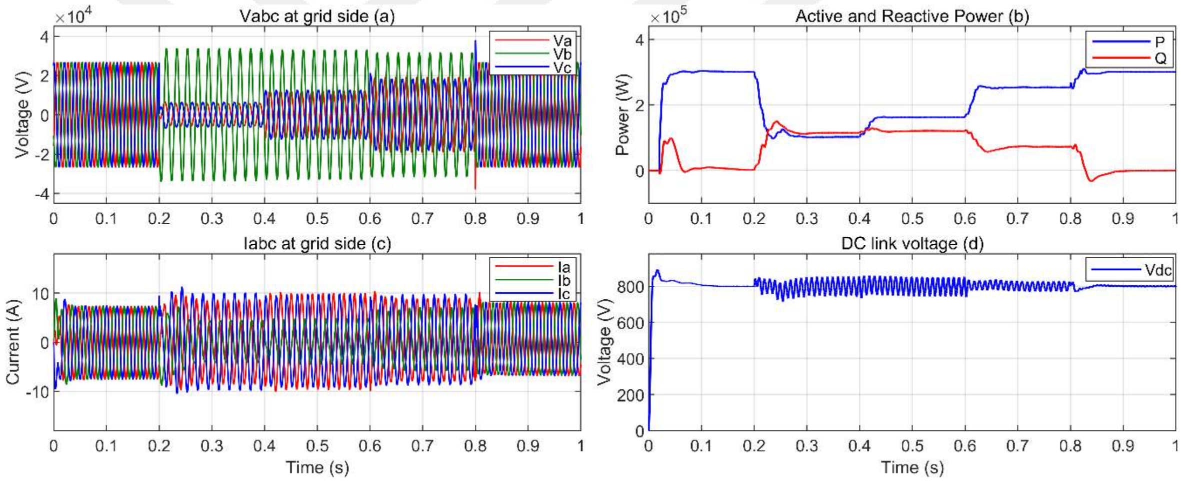

Figure 4.10. Asymmetrical double-line fault ANN method under 1000 W/m² irradiation

4.3.4. Line-to-Line Fault Under 1000 W/m² Irradiation

Figure 4.11 shows the modified INC strategy and Figure 4.12 shows the proposed control strategy results for line-to-line asymmetrical fault for 1000 W/m² irradiation. Figure 4.11-(d) shows the DC-link voltage curve exhibits a minimum of 655 V and a peak of 1050 V during the fault.

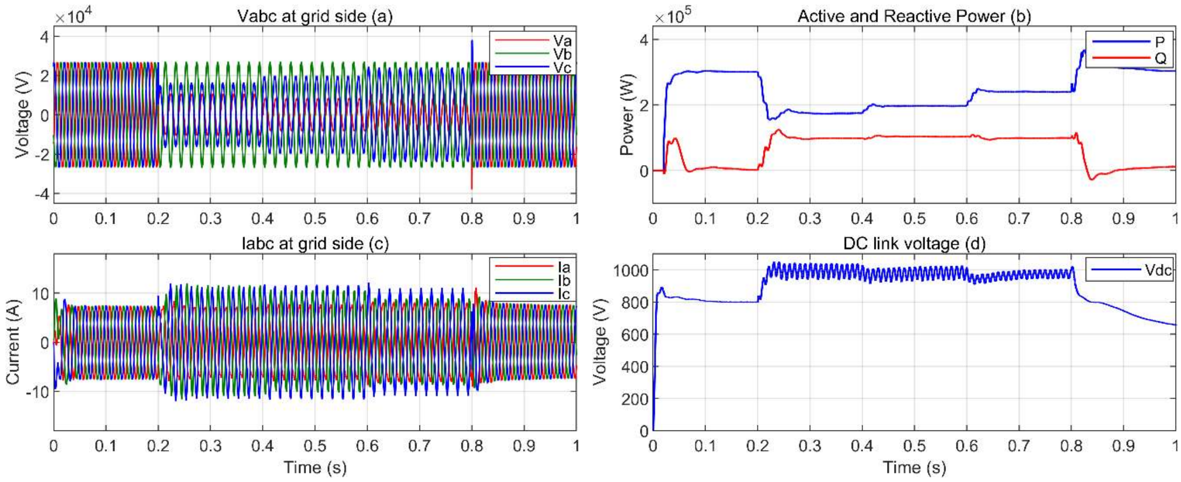

Figure 4.11. Asymmetrical line-to-line fault modified INC strategy under 1000 W/m^2 irradiation

Figure 4.12-(d) shows the DC-link voltage curve exhibits a minimum of 697 V and a peak of 881 V during the fault.

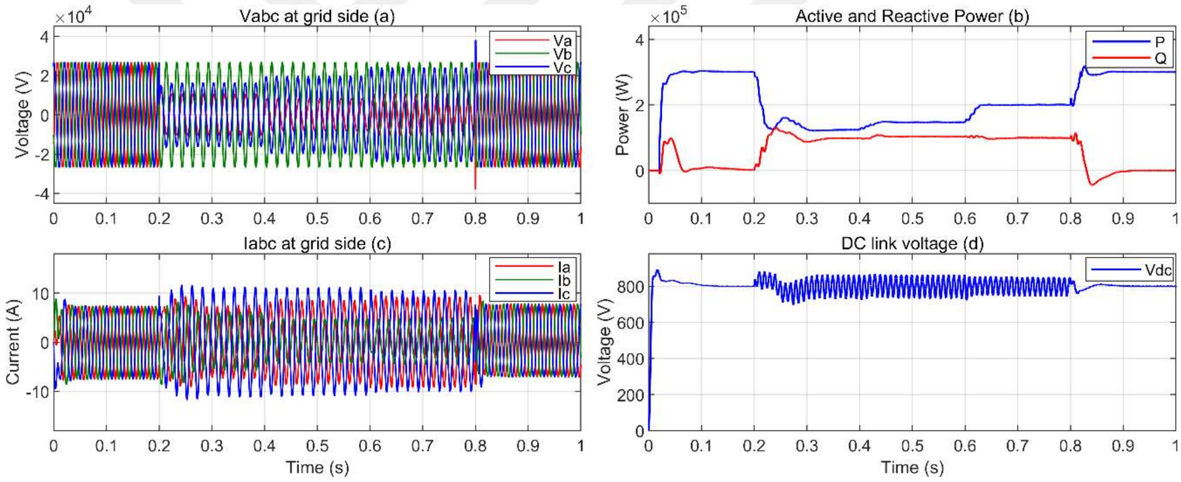

Figure 4.12. Asymmetrical line-to-line fault ANN method under 1000 W/m^2 irradiation

4.4. System Operation Fault Mode Analysis Under 500 W/m^2 Irradiation

In this section, the system is subjected to symmetrical and asymmetrical voltage variations such as three-line in Section 4.3.1, single-line in Section 4.3.2, double-line in Section 4.3.3, and line-to-line in Section 4.3.4 for 500 W/m^2 irradiation, starting from 75 % voltage drop between 0.2-0.4 s, 50 % drop between 0.4-0.6 and 25 % drop between 0.6-0.8 s and return to nominal voltage at 0.8 s.

4.4.1. Three-Line to Ground Fault Under 500 W/m^2 Irradiation

Figure 4.13 shows the modified INC strategy and Figure 4.14 shows the proposed control strategy results for three-line asymmetrical faults under 500 W/m^2 irradiation. Figure 4.13-(d) shows the DC-link voltage curve exhibits a minimum of 736 V and a peak of 877 V during the fault.

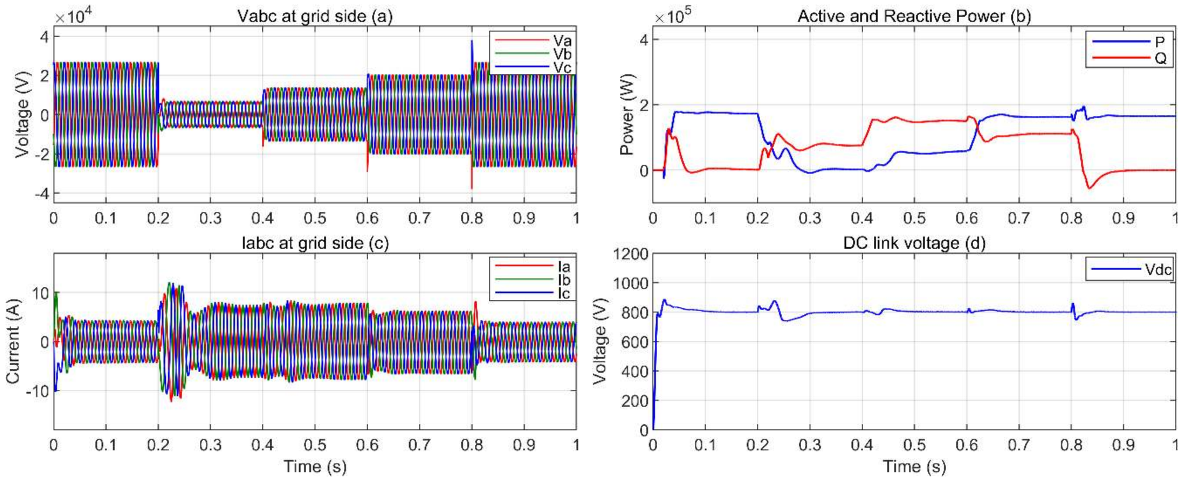

Figure 4.13. Symmetrical three-line fault modified INC strategy under 500 W/m^2 irradiation

Figure 4.14-(d) shows the DC-link voltage curve exhibits a minimum of 725 V and a peak of 868 V during the fault.

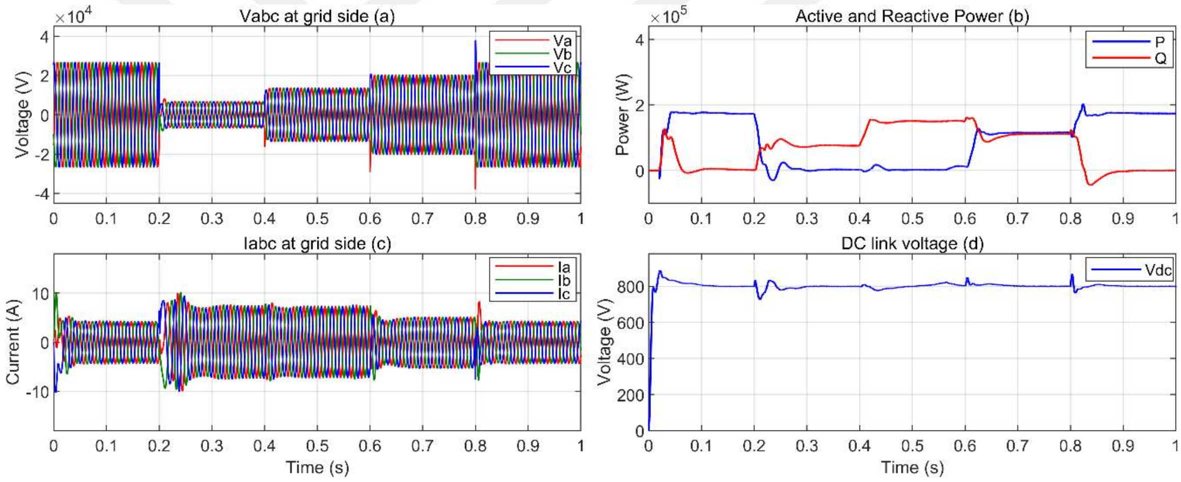

Figure 4.14. Symmetrical three-line fault ANN method under 500 W/m^2 irradiation

4.4.2. Single Line-to-Ground Fault Under 500 W/m^2 Irradiation

Figure 4.15 shows the modified INC strategy and Figure 4.16 shows the proposed control strategy results for single-line asymmetrical fault under 500 W/m^2 irradiation. Figure 4.15-(d) shows the DC-link voltage curve exhibits a minimum of 778 V and a peak of 850 V during the fault.

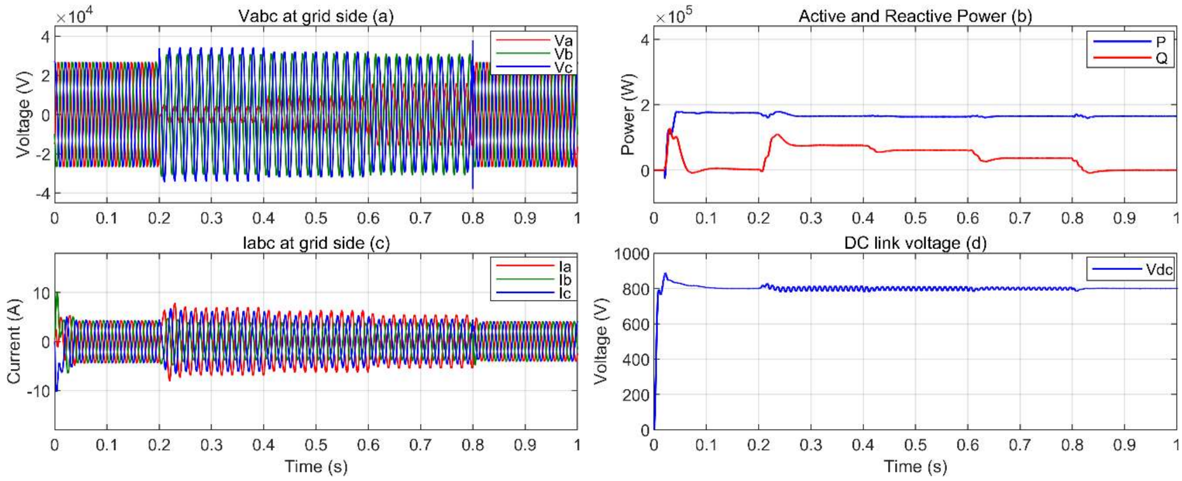

Figure 4.15. Asymmetrical single-line fault modified INC strategy under 500 W/m² irradiation

Figure 4.16-(d) shows the DC-link voltage curve exhibits a minimum of 767 V and a peak of 850 V during the fault.

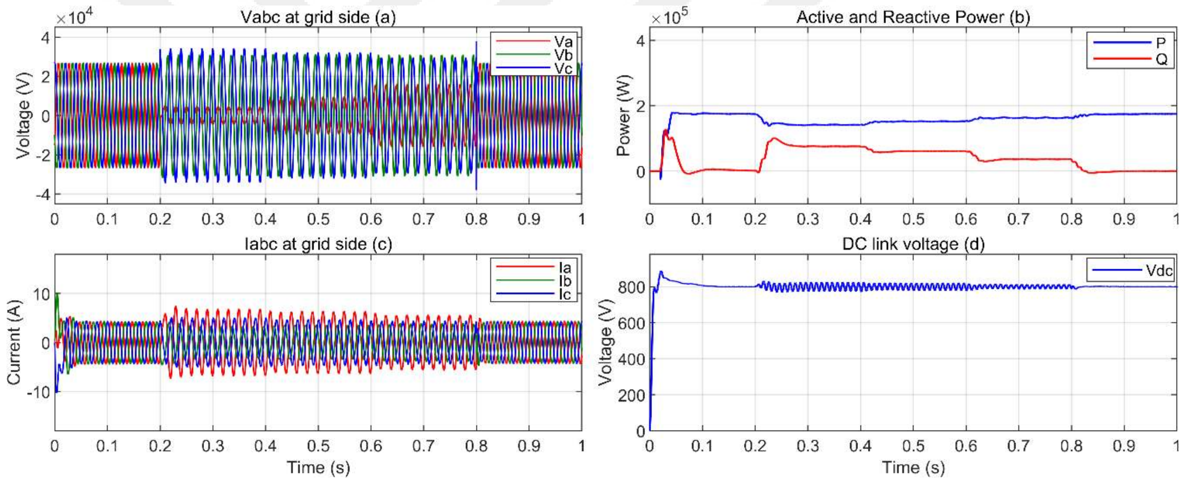

Figure 4.16. Asymmetrical single-line fault ANN method under 500 W/m² irradiation

4.4.3. Double Line-to-Ground Fault Under 500 W/m² Irradiation

Figure 4.17 shows the conventional modified INC strategy and Figure 4.18 shows the proposed control strategy results for double line asymmetrical fault for 500 W/m² irradiation. Figure 4.17-(d) shows the DC-link voltage curve exhibits a minimum of 746 V and a peak of 865 V during the fault.

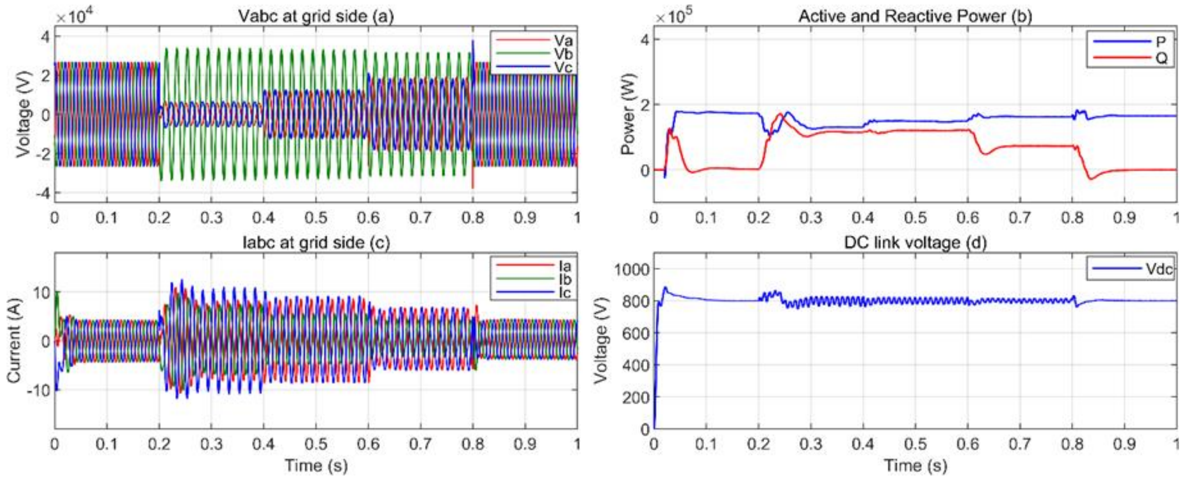

Figure 4.17. Asymmetrical double-line fault modified INC method under 500 W/m^2 irradiation

Figure 4.18-(d) shows the DC-link voltage curve exhibits a minimum of 744 V and a peak of 850 V during the fault.

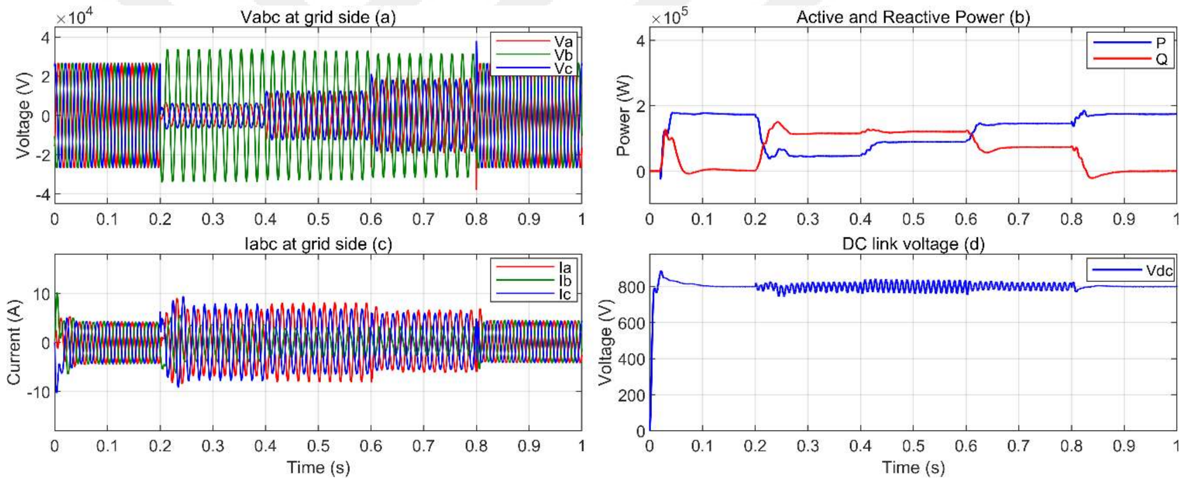

Figure 4.18. Asymmetrical double-line fault ANN method under 500 W/m^2 irradiation

4.4.4. Line-to-Line Fault Under 500 W/m^2 Irradiation

Figure 4.19 shows the conventional modified INC strategy and Figure 4.20 shows the proposed control strategy results for line-to-line asymmetrical fault for 500 W/m^2 irradiation. Figure 4.19-(d) shows the DC-link voltage curve exhibits a minimum of 741 V and a peak of 864 V during the fault.

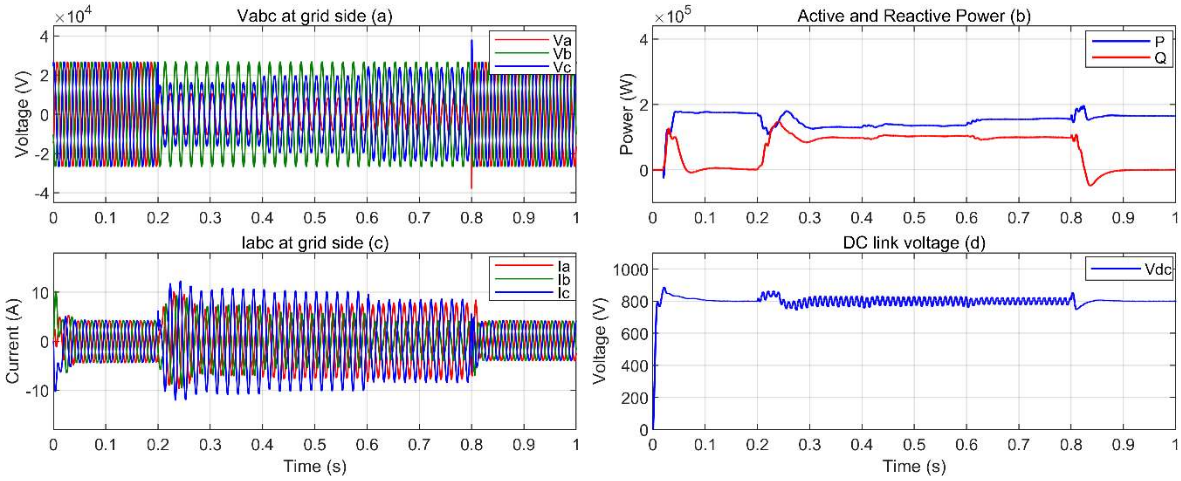

Figure 4.19. Asymmetrical line-to-line fault modified INC strategy under 500 W/m^2 irradiation

Figure 4.20-(d) shows the DC-link voltage curve exhibits a minimum of 735 V and a peak of 850 V during the fault.

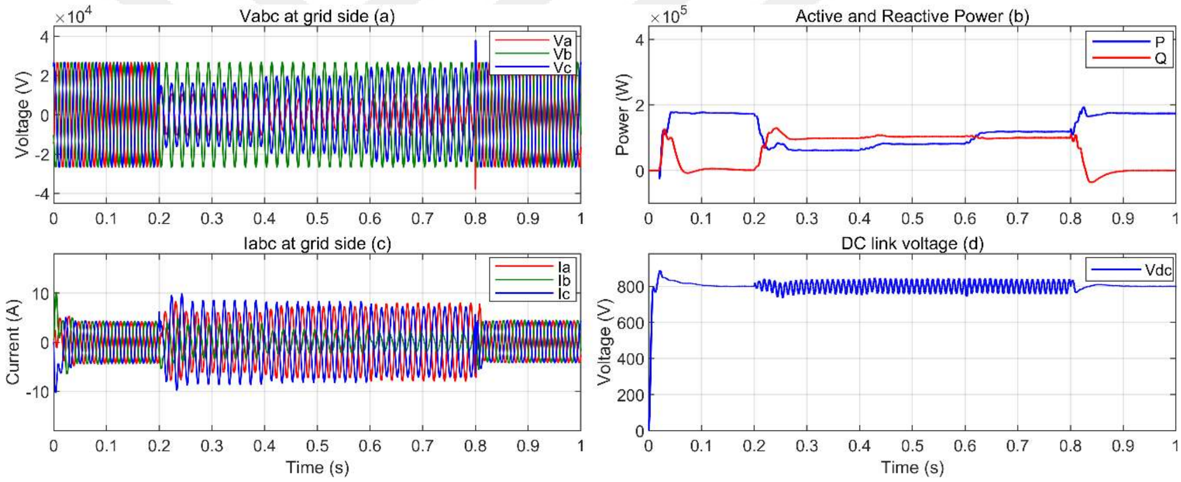

Figure 4.20. Asymmetrical line-to-line fault ANN method under 500 W/m^2 irradiation

4.5. Summary

By subjecting the system to dynamic scenarios, the study aimed to evaluate its resilience and ability to cope with varying fault conditions. The results obtained from Sections 4.1, 4.2, 4.3, and 4.3 provided valuable insights into the system's behavior during both steady-state and transient operations.

In addition, this section presents a numerical comparison between the modified INC method and the proposed ANN method, evaluating their performance under three-line-to-ground (TLG), single line-to-ground (SLG), double line-to-ground (DLG), and line-to-line (LL) fault. Results are summarized in Table 4.1 and Table 4.2.

Table 4.1 includes DC-link voltage peak and dip values (in volts) with percentage deviations from 800 volts, assessing faults under 1000 W/m^2 solar irradiation. Table 4.2 presents similar data for faults under 500 W/m^2 solar irradiation

Table 4.1. DC-Link voltage comparison under 1000 W/m^2 irradiation

Fault	**TLG**		**SLG**		**DLG**		**LL**	
Voltage	**Dip**	**Peak**	**Dip**	**Peak**	**Dip**	**Peak**	**Dip**	**Peak**
INC Method	581 V	1090 V	618 V	928 V	626 V	1034 V	655 V	1050 V
ANN Method	732 V	877 V	758 V	850 V	713 V	858 V	697 V	881 V
INC Deviation	27.4 %	36.3 %	22.8%	16 %	21.8 %	29.3 %	18.1 %	31.3 %
ANN Deviation	8.5 %	9.6 %	5.3 %	6.3 %	10.9 %	7.3 %	12.9 %	10.1 %

As seen in Table 4.1; for TLG faults, the ANN method exhibits a dip deviation of 8.5 % and a peak deviation of 9.6 %. In contrast, the conventional INC method shows significantly higher deviations with 27.45 % dip and 36.3 % peak deviations. As seen in Table 4.1 proposed method also exhibits superior performance under SLG, DLG, and LL faults

Table 4.2. DC-Link voltage comparison under 500 W/m^2 irradiation

Fault	**TLG**		**SLG**		**DLG**		**LL**	
Voltage	**Dip**	**Peak**	**Dip**	**Peak**	**Dip**	**Peak**	**Dip**	**Peak**
INC Method	736 V	877 V	778 V	850 V	746 V	865 V	655 V	864 V
ANN Method	725 V	868 V	767 V	850 V	744 V	850 V	735 V	850 V
INC Deviation	8 %	9.6 %	2.8 %	6.3 %	6.8 %	8.1 %	7.4 %	8 %
ANN Deviation	9.4 %	8.5 %	4.1 %	6.3 %	7 %	6.3 %	8.1 %	6.3 %

As shown in Table 4.2, when analyzing the TLG faults, the ANN method shows a peak deviation of 8.5 %, while the SLG faults show a peak deviation of 6.3 %, just like LL. In contrast, the INC method exhibits a peak deviation of 9.6 % for TLG, 6.3 % for SLG, 8.1 % for DLG and 8 % for DLG. These findings reveal that the proposed approach is better in reducing the peak deviations under 500 W/m^2 solar irradiation

5. CONCLUSIONS

In this thesis, a flexible active power control method using an artificial neural network is developed to improve the DC voltage stabilization of the PV -FC hybrid power system to overcome the AC side overcurrent during grid faults. This strategy performs well in limiting the DC voltage during faults and managing the AC-side inverter overcurrent. It also addresses active and reactive power control to comply with LVRT requirements under symmetrical and asymmetrical faults. Additionally, the combination of a multi-mode control approach and an energy management scheme optimizes power generation and utilization, ensuring efficient operation during both normal and fault scenarios.

This study also examined the effectiveness of ANN and modified INC approaches to mitigate overvoltage at DC-link voltage covering various fault types (TLG, SLG, DLG, and LL) and solar irradiation levels of 1000 W/m^2 and 500 W/m^2, as detailed in Section 4.5. The results consistently revealed the effectiveness of the proposed ANN method over the INC method, especially under 1000 W/m^2 irradiance. Across all fault types, the ANN method exhibits a maximum voltage deviation of 12.9 % or less, keeping it below 1000 (low-voltage power systems limit in IEEE1668-2017 standard) volts. Under 500 W/m^2 solar irradiation, the proposed system performs better in reducing the peak bias, with the highest peak limited to 9.4 %, while it performs similarly in reducing the voltage dip deviations. Overall, the proposed ANN method performs better than the INC method.

In this thesis, a comprehensive LCL filter design is presented accompanied by bode diagrams that provide insights into the performance and effectiveness of the filter. The LCL filter is a critical component that helps to reduce harmonic distortion and improve system performance, contributing to the overall reliability of the PV-FC hybrid system. In a steady-state condition, the measured current THD value of the developed system is less than 2 % which satisfies the 3 % harmonics limit. The simulation results presented in this thesis verify the efficiency and effectiveness of the proposed system and control strategies. At steady state and 1000 W/m^2 solar irradiation, the efficiency of the system is about 98 %. These results provide quantitative evidence of the system's ability to withstand voltage dips while maintaining stable operation and complying with the Turkish LVRT requirements and grid integration regulations.

In conclusion, this thesis comprehensively investigates the LVRT capabilities of a designed 300kW PV-FC hybrid system, demonstrates its dynamic response to different voltage sag depths, and verifies its ability to maintain the power quality standards with operational criteria set by the Turkish Energy Market Regulatory Authority.

In the future, with the increasing use of renewable energy sources, such studies will become even more important. The energy sector will continue to work on new technologies and control systems for a safe and stable transition to renewable energy.

REFERENCES

Abidi, H., Sidhom, L., Chihi, I., 2023. Systematic literature review and benchmarking for photovoltaic MPPT techniques. Energies (Basel) 16. https://doi.org/10.3390/en16083509

Aiko, 2023. N-Type ABC Black Hole Series AIKO-A-MAH54Mb PV Module. Aiko Solar Energy Technology.

Alaaeddin, M.H., Sapuan, S.M., Zuhri, M.Y.M., Zainudin, E.S., AL-Oqla, F.M., 2019. Photovoltaic applications: Status and manufacturing prospects. Renewable and Sustainable Energy Reviews. https://doi.org/10.1016/j.rser.2018.12.026

Aldbaiat, B., Nour, M., Radwan, E., Awada, E., 2022. Grid-Connected PV System with Reactive Power Management and an Optimized SRF-PLL Using Genetic Algorithm. Energies (Basel) 15. https://doi.org/10.3390/en15062177

Ali, A., Almutairi, K., Padmanaban, S., Tirth, V., Algarni, S., Irshad, K., Islam, S., Zahir, M.H., Shafiullah, M., Malik, M.Z., 2020. Investigation of MPPT Techniques under Uniform and Non-Uniform Solar Irradiation Condition-A Retrospection. IEEE Access 8, 127368–127392. https://doi.org/10.1109/ACCESS.2020.3007710

Alizadeh, S., Avami, A., 2021. Development of a framework for the sustainability evaluation of renewable and fossil fuel power plants using integrated LCA-emergy analysis: A case study in Iran. Renew Energy 179, 1548–1564. https://doi.org/10.1016/j.renene.2021.07.140

Al-Shetwi, A.Q., Sujod, M.Z., Blaabjerg, F., 2018. Low voltage ride-through capability control for single-stage inverter-based grid-connected photovoltaic power plant. Solar Energy 159, 665–681. https://doi.org/https://doi.org/10.1016/j.solener.2017.11.027

Al-Shetwi, A.Q., Sujod, M.Z., Blaabjerg, F., Yang, Y., 2019. Fault ride-through control of grid-connected photovoltaic power plants: A review. Solar Energy 180, 340–350.

Ammiche, M., Kouadri, A., Halabi, L.M., Guichi, A., Mekhilef, S., 2018. Fault detection in a grid-connected photovoltaic system using adaptive thresholding method. Solar Energy 174, 762–769. https://doi.org/https://doi.org/10.1016/j.solener.2018.09.024

An, C.G., Lee, H., Kim, T.G., Yi, J., Won, C.Y., 2023. A Study on Energy Management and Cooperative Control Considering LVRT in a Hybrid Microgrid. Energies (Basel) 16. https://doi.org/10.3390/en16114372

Ang, T.-Z., Salem, M., Kamarol, M., Das, H.S., Nazari, M.A., Prabaharan, N., 2022. A comprehensive study of renewable energy sources: Classifications, challenges and suggestions. Energy Strategy Reviews 43, 100939. https://doi.org/https://doi.org/10.1016/j.esr.2022.100939

Anzalchi, A., Sarwat, A., 2017. Overview of technical specifications for grid-connected photovoltaic systems. Energy Convers Manag 152, 312–327. https://doi.org/https://doi.org/10.1016/j.enconman.2017.09.049

Arar Tahir, K., Zamorano, M., Ordóñez García, J., 2023. Scientific mapping of optimisation applied to microgrids integrated with renewable energy systems. International Journal of Electrical Power & Energy Systems 145, 108698. https://doi.org/https://doi.org/10.1016/j.ijepes.2022.108698

Araujo, S.V., Engler, A., Sahan, B., 2007. LCL Filter design for grid-connected NPC inverters in offshore wind turbines, in: 2007 7th International Conference on Power Electronics. IEEE, pp. 1133–1138.

Attala, A., Taha, A.T.M., Ryad, A., 2014. PV, wind and fuel cell hybrid optimization generation for AL-Arish site. International Journal of Recent Development in Engineering and Technology 2.

Bajpai, P., Dash, V., 2012. Hybrid renewable energy systems for power generation in stand-alone applications: A review. Renewable and Sustainable Energy Reviews 16, 2926–2939. https://doi.org/https://doi.org/10.1016/j.rser.2012.02.009

Barbir, F., 2006. PEM Fuel Cells Chapter 2. https://doi.org/https://doi.org/10.1007/1-84628-207-1_2

Basnet, S., Deschinkel, K., Le Moyne, L., Cécile Péra, M., 2023. A review on recent standalone and grid integrated hybrid renewable energy systems: System optimization and energy management strategies. Renewable Energy Focus 46, 103–125. https://doi.org/https://doi.org/10.1016/j.ref.2023.06.001

Benda, V., Černá, L., 2020. PV cells and modules – State of the art, limits and trends. Heliyon. https://doi.org/10.1016/j.heliyon.2020.e05666

Bizon, N., Thounthong, P., 2021. Multi-Objective Energy Management Strategy for PV/FC Hybrid Power Systems. Electronics (Basel) 10. https://doi.org/10.3390/electronics10141721

Bollipo, R.B., Mikkili, S., Bonthagorla, P.K., 2021. Hybrid, optimal, intelligent and classical PV MPPT techniques: A review. CSEE Journal of Power and Energy Systems 7, 9–33. https://doi.org/10.17775/CSEEJPES.2019.02720

Bonthagorla, P.K., Mikkili, S., 2022. Performance Investigation of Hybrid and Conventional PV Array Configurations for Grid-connected/Standalone PV Systems. CSEE Journal of Power and Energy Systems 8, 682–695. https://doi.org/10.17775/CSEEJPES.2020.02510

Bozkurt, H., 2022. Optimal design of a hybrid PV-Battery system for on-grid applications. Çukurova University.

Breeze, P., 2018. Chapter 9 - Renewable Energy Combined Heat and Power, in: Breeze, P. (Ed.), Combined Heat and Power. Academic Press, pp. 77–83. https://doi.org/https://doi.org/10.1016/B978-0-12-812908-1.00009-2

Brito, M.A.G., Galotto, L., Sampaio, L.P., e Melo, G. de A., Canesin, C.A., 2013. Evaluation of the Main MPPT Techniques for Photovoltaic Applications. IEEE Transactions on Industrial Electronics 60, 1156–1167. https://doi.org/10.1109/TIE.2012.2198036

Büyük, M., Tan, A., Tümay, M., Bayindir, K.Ç., 2016. Topologies, generalized designs, passive and active damping methods of switching ripple filters for voltage source inverter: A comprehensive review. Renewable and Sustainable Energy Reviews. https://doi.org/10.1016/j.rser.2016.04.006

Cabrera-Tobar, A., Bullich-Massagué, E., Aragüés-Peñalba, M., Gomis-Bellmunt, O., 2016. Review of advanced grid requirements for the integration of large scale photovoltaic power plants in the transmission system. Renewable and Sustainable Energy Reviews 62, 971–987. https://doi.org/https://doi.org/10.1016/j.rser.2016.05.044

Çelik, Ö., 2019. Controller design and experimental verification of grid-connected microinverters for photovoltaic applications (Phd Thesis). Çukurova Universite, Adana.

Çelik, Ö., 2015. A novel hybrid mppt method for grid connected photovoltaic systems with partial shading conditions. Çukurova University.

Çelik, Ö., Yalman, Y., Tan, A., Bayındır, K.Ç., Çetinkaya, Ü., Akdeniz, M., Chaudhary, S.K., Høyer, M., Guerrero, J.M., 2022. Grid code requirements – A case study on the assessment for integration of offshore wind power plants in Turkey. Sustainable Energy Technologies and Assessments 52, 102137. https://doi.org/https://doi.org/10.1016/j.seta.2022.102137

Da Silva, S.A.Ol., Sampaio, L.P., De Oliveira, F.M., Durand, F.R., 2017. Feed-forward DC-bus control loop applied to a single-phase grid-connected PV system operating with PSO-based MPPT technique and active power-line conditioning. IET Renewable Power Generation 11, 183–193. https://doi.org/10.1049/iet-rpg.2016.0120

De Stasi, F., 2015. Application Report Working with Boost Converters.

Ding, G., Gao, F., Tian, H., Ma, C., Chen, M., He, G., Liu, Y., 2016. Adaptive DC-Link Voltage Control of Two-Stage Photovoltaic Inverter During Low Voltage Ride-Through Operation. IEEE Trans Power Electron 31, 4182–4194. https://doi.org/10.1109/TPEL.2015.2469603

Dorji, S., Wangchuk, D., Choden, T., Tshewang, T., 2020. Maximum Power Point Tracking of solar photovoltaic cell using Perturb & Observe and fuzzy logic controller algorithm for boost converter and quadratic boost converter. Mater Today Proc 27, 1224–1229. https://doi.org/https://doi.org/10.1016/j.matpr.2020.02.144

Dursun, M., Dosoglu, M.K., 2018. LCL Filter Design for Grid Connected Three-Phase Inverter. ISMSIT 2018 - 2nd International Symposium on Multidisciplinary Studies and Innovative Technologies, Proceedings. https://doi.org/10.1109/ISMSIT.2018.8567054

EMRA, 2022. Electric Network Regulation. Turkish Energy Market Regulation Association.

EN50160, 2023. Voltage characteristics of electricity supplied by public electricity networks.

Errouha, M., Derouich, A., Motahhir, S., Zamzoum, O., El Ouanjli, N., El Ghzizal, A., 2019. Optimization and control of water pumping PV systems using fuzzy logic controller. Energy Reports 5, 853–865. https://doi.org/https://doi.org/10.1016/j.egyr.2019.07.001

Falcone, P.M., Hiete, M., Sapio, A., 2021. Hydrogen economy and sustainable development goals: Review and policy insights. Curr Opin Green Sustain Chem 31, 100506. https://doi.org/https://doi.org/10.1016/j.cogsc.2021.100506

Farhang, J., Eydi, M., Asaei, B., Farhangi, B., 2015. Flexible strategy for active and reactive power control in grid connected inverter under unbalanced grid fault, in: 2015 23rd Iranian Conference on Electrical Engineering. pp. 1618–1623. https://doi.org/10.1109/IranianCEE.2015.7146478

FCTO, 2016. Fuel Cells [WWW Document]. Fuel Cell Technologies Office United States. URL https://www.energy.gov/eere/fuelcells/comparison-fuel-cell-technologies (accessed 6.30.23).

Felseghi, R.-A., Carcadea, E., Raboaca, M.S., TRUFIN, C.N., Filote, C., 2019. Hydrogen Fuel Cell Technology for the Sustainable Future of Stationary Applications. Energies (Basel) 12. https://doi.org/10.3390/en12234593

Gao, F., Li, D., Loh, P.C., Tang, Y., Wang, P., 2009. Indirect dc-link voltage control of two-stage single-phase PV inverter, in: 2009 IEEE Energy Conversion Congress and Exposition. pp. 1166–1172. https://doi.org/10.1109/ECCE.2009.5316399

Ghenai, C., Bettayeb, M., 2019a. Grid-Tied Solar PV/Fuel Cell Hybrid Power System for University Building, in: Energy Procedia. Elsevier Ltd, pp. 96–103. https://doi.org/10.1016/j.egypro.2018.12.025

Ghenai, C., Bettayeb, M., 2019b. Grid-Tied Solar PV/Fuel Cell Hybrid Power System for University Building. Energy Procedia 159, 96–103. https://doi.org/https://doi.org/10.1016/j.egypro.2018.12.025

Gilman, P., Dobos, A., Diorio, N., Freeman, J., Janzou, S., Ryberg, D., 2018. SAM Photovoltaic Model Technical Reference Update. National Renewable Energy Laboratory.

Gugulothu, R., Nagu, B., Pullaguram, D., 2023. Energy management strategy for standalone DC microgrid system with photovoltaic/fuel cell/battery storage. J Energy Storage 57. https://doi.org/10.1016/j.est.2022.106274

Hagh, M.T., Khalili, T., 2019. A review of fault ride through of PV and wind renewable energies in grid codes. Int J Energy Res. https://doi.org/10.1002/er.4247

Hauke, B., 2022. Basic Calculation of a Boost Converter's Power Stage.

Hawke, J., Enjeti, P., Palma, L., Sarma, H., 2011. A modular fuel cell with hybrid energy storage. IEEE Energy Conversion Congress and Exposition: Energy Conversion Innovation for a Clean Energy Future, ECCE 2011, Proceedings 2971–2976. https://doi.org/10.1109/ECCE.2011.6064169

Hosseini, S.M., Kanagaraj, N., Sadeghi, S., Yousefi, H., 2022. Midpoint and endpoint impacts of electricity generation by renewable and nonrenewable technologies: A case study of Alberta, Canada. Renew Energy 197, 22–39. https://doi.org/10.1016/j.renene.2022.07.033

Hu, S., Xiang, Y., Zhang, X., Liu, J., Wang, R., Hong, B., 2019. Reactive power operability of distributed energy resources for voltage stability of distribution networks. Journal of Modern Power Systems and Clean Energy 7, 851–861. https://doi.org/10.1007/s40565-018-0484-3

Huang, K., Luo, P., Liu, P., KIM, J.S., Wang, Y., Xu, W., Li, H., Gong, Y., 2022. Improving complementarity of a hybrid renewable energy system to meet load demand by using hydropower regulation ability. Energy 248, 123535. https://doi.org/https://doi.org/10.1016/j.energy.2022.123535

Huka, G.B., Li, W., Chao, P., Peng, S., 2018. A comprehensive LVRT strategy of two-stage photovoltaic systems under balanced and unbalanced faults. International Journal of Electrical Power & Energy Systems 103, 288–301. https://doi.org/https://doi.org/10.1016/j.ijepes.2018.06.014

IEA, 2023. Renewable Energy Market Update - June 2023. International Energy Agency.

IEA, 2022. Renewables 2022 Analysis and forecast to 2027. International Energy Agency.

IEA, 2021. Turkey 2021 - Energy Policy Review. International Energy Agency.

IEC 61727, 2004. Photovoltaic (PV) systems - characteristics of the utility interface. International Electro-technical Commission-IEC.

IEEE 1547, 2018. Standard for Interconnection and Interoperability of Distributed Energy Resources with Associated Electric Power Systems Interfaces. IEEE.

IEEE Std 519-1992, 1993. IEEE Recommended Practices and Requirements for Harmonic Control in Electrical Power Systems. IEEE Std 519-1992 1–112. https://doi.org/10.1109/IEEESTD.1993.114370

IEEE Std 519-2022, 2022. IEEE Standard for Harmonic Control in Electric Power Systems. IEEE Std 519-2022 (Revision of IEEE Std 519-2014) 1–31. https://doi.org/10.1109/IEEESTD.2022.9848440

IEEE Std 929-2000, 2000. IEEE Recommended Practice for Utility Interface of Photovoltaic (PV) Systems. IEEE Std 929-2000 i-. https://doi.org/10.1109/IEEESTD.2000.91304

IEEE Std 1547-2018, 2018. IEEE Standard for Interconnection and Interoperability of Distributed Energy Resources with Associated Electric Power Systems Interfaces. IEEE Std 1547-2018 (Revision of IEEE Std 1547-2003) 1–138. https://doi.org/10.1109/IEEESTD.2018.8332112

IEEE Std 1668-2017, 2017. IEEE Recommended Practice for Voltage Sag and Short Interruption Ride-Through Testing for End-Use Electrical Equipment Rated Less than 1000 V. IEEE Std 1668-2017 (Revision of IEEE Std 1668-2014) 1–85. https://doi.org/10.1109/IEEESTD.2017.8120227

IEEE Std 2800-2022, 2022. IEEE Standard for Interconnection and Interoperability of Inverter-Based Resources (IBRs) Interconnecting with Associated Transmission Electric Power Systems. IEEE Std 2800-2022 1–180. https://doi.org/10.1109/IEEESTD.2022.9762253

IRENA, 2023. Renewables 2023 Global Status Report Collection. REN21 Secretariat, Renewables in Energy Demand.

IRENA, 2022. Grid codes for renewable powered systems. International Renewable Energy Agency.

IRENA, 2012. Renewable energy technologies: cost analysis series. International Renewable Energy Agency.

Jalilian, A., Naderi, S.B., Negnevitsky, M., Hagh, M.T., 2018. Controllable DC-link bridge-type FCL for low voltage ride-through enhancement of converter interfaced DG systems. International Journal of Electrical Power & Energy Systems 95, 653–663. https://doi.org/https://doi.org/10.1016/j.ijepes.2017.09.022

Jayalath, S., Hanif, M., 2018. An LCL-Filter Design with Optimum Total Inductance and Capacitance. IEEE Trans Power Electron 33, 6687–6698. https://doi.org/10.1109/TPEL.2017.2754100

Joshi, Jyotia, Swami, A.K., Jately, V., 2021. Active Power Curtailment in PV Array Under LVRT Condition, in: Choudhury Sushabhan and Gowri, R. and S.P.B. and D.D.-T. (Ed.), Intelligent Communication, Control and Devices. Springer Singapore, Singapore, pp. 65–74.

Joshi, Jyoti, Swami, A.K., Jately, V., Azzopardi, B., 2021. A Comprehensive Review of Control Strategies to Overcome Challenges during LVRT in PV Systems. IEEE Access. https://doi.org/10.1109/ACCESS.2021.3109050

Kala, P., Arora, S., 2017. A comprehensive study of classical and hybrid multilevel inverter topologies for renewable energy applications. Renewable and Sustainable Energy Reviews. https://doi.org/10.1016/j.rser.2017.02.008

Kasal, G.K., Singh, B., 2011. Voltage and frequency controllers for an asynchronous generator-based isolated wind energy conversion system. IEEE Transactions on Energy Conversion 26, 402–416. https://doi.org/10.1109/TEC.2010.2102029

Kaura, V., Blasko, V., 1997. Operation of a phase locked loop system under distorted utility conditions. IEEE Trans Ind Appl 33, 58–63. https://doi.org/10.1109/28.567077

Kemp, J.M., Millstein, D., Kim, J.H., Wiser, R., 2023. Interactions between hybrid power plant development and local transmission in congested regions. Advances in Applied Energy 10, 100133. https://doi.org/https://doi.org/10.1016/j.adapen.2023.100133

Khalid, A., Stevenson, A., Sarwat, A.I., 2021. Overview of technical specifications for grid-connected microgrid battery energy storage systems. IEEE Access 9, 163554–163593. https://doi.org/10.1109/ACCESS.2021.3132223

Kish, G.J., Lee, J.J., Lehn, P.W., 2012. Modelling and control of photovoltaic panels utilising the incremental conductance method for maximum power point tracking. IET Renewable Power Generation 6, 259–266. https://doi.org/10.1049/ip-gtd:19951577

Kjaer, S.B., Pedersen, J.K., Blaabjerg, F., 2005. A review of single-phase grid-connected inverters for photovoltaic modules. IEEE Trans Ind Appl 41, 1292–1306. https://doi.org/10.1109/TIA.2005.853371

KOSPO, 2021. World's largest hydrogen fuel cell power plant. Korean Southern Power. https://doi.org/https://doi.org/10.1016/S1464-2859(21)00602-7

Lin, X., Han, Y., Yang, P., Wang, C., Xiong, J., 2018. Low-Voltage Ride-Through Techniques for Two-Stage Photovoltaic System under Unbalanced Grid Voltage Sag Conditions, in: 2018 IEEE 4th Southern Power Electronics Conference (SPEC). pp. 1–8. https://doi.org/10.1109/SPEC.2018.8636016

Liserre, M., Blaabjerg, F., Hansen, S., 2005. Design and control of an LCL-filter-based three-phase active rectifier. IEEE Trans Ind Appl 41, 1281–1291. https://doi.org/10.1109/TIA.2005.853373

Ma, W., Gao, H., Song, H., Zhang, Y., 2022. Grid-Connected Photovoltaic LVRT Strategy Based on Improved DDSRF-PLL and Reactive Power Control, in: 2022 12th International Conference on Power and Energy Systems (ICPES). pp. 831–837. https://doi.org/10.1109/ICPES56491.2022.10072847

Macit, E., 2020. Design and control of three phase grid connected PV system with 1 MW power capacity. Gaziantep University.

Maradin, D., 2021. Advantages and disadvantages of renewable energy sources utilization. International Journal of Energy Economics and Policy 176–183. https://doi.org/doi:10.32479/ijeep.11027

Marqusee, J., Becker, W., Ericson, S., 2021. Resilience and economics of microgrids with PV, battery storage, and networked diesel generators. Advances in Applied Energy 3, 100049. https://doi.org/https://doi.org/10.1016/j.adapen.2021.100049

Mirhosseini, M., Pou, J., Agelidis, V.G., 2015. Single- and Two-Stage Inverter-Based Grid-Connected Photovoltaic Power Plants With Ride-Through Capability Under Grid Faults. IEEE Trans Sustain Energy 6, 1150–1159. https://doi.org/10.1109/TSTE.2014.2347044

Mohamed, S.R., Aruna Jeyanthy, P., Devaraj, D., 2019. Low Voltage Ride-Through Capability Enhancement of Grid-Connected Photovoltaic Systems- A Hybrid Control Approach, in: 2019 IEEE International Conference on Clean Energy and Energy Efficient Electronics Circuit for Sustainable Development (INCCES). pp. 1–6. https://doi.org/10.1109/INCCES47820.2019.9167719

Mohsin, M., Taghizadeh-Hesary, F., Panthamit, N., Anwar, S., Abbas, Q., Vo, X.V., 2021. Developing Low Carbon Finance Index: Evidence From Developed and Developing Economies. Financ Res Lett 43, 101520. https://doi.org/https://doi.org/10.1016/j.frl.2020.101520

Morey, M., Gupta, N., Garg, M.M., Kumar, A., 2023. A comprehensive review of grid-connected solar photovoltaic system: Architecture, control, and ancillary services. Renewable Energy Focus 45, 307–330. https://doi.org/https://doi.org/10.1016/j.ref.2023.04.009

Motapon, S.N., Tremblay, O., Dessaint, L.-A., 2009. A generic fuel cell model for the simulation of fuel cell vehicles, in: 2009 IEEE Vehicle Power and Propulsion Conference. pp. 1722–1729. https://doi.org/10.1109/VPPC.2009.5289692

Nabae, A., Takahashi, I., Akagi, H., 1981. A New Neutral-Point-Clamped PWM Inverter. IEEE Trans Ind Appl 518–523.

Nasiri, M., Arzani, A., McCormack, S.J., 2022. A simple and effective grid-supporting low voltage ride-through scheme for single-stage photovoltaic power plants. Solar Energy 232, 248–262. https://doi.org/https://doi.org/10.1016/j.solener.2021.11.052

Neumann, T., Erlich, I., 2012. Modelling and control of photovoltaic inverter systems with respect to German grid code requirements, in: 2012 IEEE Power and Energy Society General Meeting. pp. 1–8. https://doi.org/10.1109/PESGM.2012.6345310

Nithya, C., Roselyn, J.P., 2022. Multimode Inverter Control Strategy for LVRT and HVRT Capability Enhancement in Grid Connected Solar PV System. IEEE Access 10, 54899–54911. https://doi.org/10.1109/ACCESS.2022.3175872

Noman, A.M., Al-Shamma'a, A.A., Addoweesh, K.E., Alabduljabbar, A.A., Alolah, A.I., 2017. A Survey on Two Level and Cascaded Multilevel Inverter Topologies for Grid Connected PV System, in: IECON 2017 - 43rd Annual Conference of the IEEE Industrial Electronics Society.

Nyamathulla, S., Chittathuru, D., Muyeen, S.M., 2023. An Overview of Multilevel Inverters Lifetime Assessment for Grid-Connected Solar Photovoltaic Applications. Electronics (Switzerland). https://doi.org/10.3390/electronics12081944

OECD, 2022. Green Economy Transition in Eastern Europe, the Caucasus and Central Asia. OECD Green Growth Studies. https://doi.org/https://doi.org/10.1787/c410b82a-en

Osman, A.I., Chen, L., Yang, M., Msigwa, G., Farghali, M., Fawzy, S., Rooney, D.W., Yap, P.S., 2023. Cost, environmental impact, and resilience of renewable energy under a changing climate: a review. Environ Chem Lett. https://doi.org/10.1007/s10311-022-01532-8

Paliwal, P., Patidar, N.P., Nema, R.K., 2014. Planning of grid integrated distributed generators: A review of technology, objectives and techniques. Renewable and Sustainable Energy Reviews 40, 557–570. https://doi.org/https://doi.org/10.1016/j.rser.2014.07.200

Paska, J., Biczel, P., Kłos, M., 2009. Hybrid power systems – An effective way of utilising primary energy sources. Renew Energy 34, 2414–2421. https://doi.org/https://doi.org/10.1016/j.renene.2009.02.018

Patil, T.G., Asokan, S., 2017. Comparative analysis of calculation of solar panel efficiency degradation, in: 2017 Third International Conference on Science Technology Engineering & Management (ICONSTEM). pp. 522–525. https://doi.org/10.1109/ICONSTEM.2017.8261377

Pishvaee, M.S., Mohseni, S., Bairamzadeh, S., 2021. Chapter 1 - An overview of biomass feedstocks for biofuel production, in: Pishvaee, M.S., Mohseni, S., Bairamzadeh, S. (Eds.), Biomass to Biofuel Supply Chain Design and Planning Under Uncertainty. Academic Press, pp. 1–20. https://doi.org/https://doi.org/10.1016/B978-0-12-820640-9.00001-5

Podder, A.K., Roy, N.K., Pota, H.R., 2019. MPPT methods for solar PV systems: a critical review based on tracking nature. IET Renewable Power Generation 13, 1615–1632. https://doi.org/10.1049/iet-rpg.2018.5946

Popa, D.-L., Nicolae, M.-S., Nicolae, P.-M., Popescu, M., 2016. Design and Simulation of a 10 MW Photovoltaic Power Plant using MATLAB and Simulink, in: 2016 IEEE International Power Electronics and Motion Control Conference (PEMC). Varna, Bulgaria, pp. 378–383. https://doi.org/DOI: 10.1109/EPEPEMC.2016.7752027

Priyadarshi, N., Padmanaban, S., Bhaskar, M.S., Blaabjerg, F., Holm-Nielsen, J.B., Azam, F., Sharma, A.K., 2020. A Hybrid Photovoltaic-Fuel Cell-Based Single-Stage Grid Integration with Lyapunov Control Scheme. IEEE Syst J 14, 3334–3342. https://doi.org/10.1109/JSYST.2019.2948899

Quinn, C.A., Mohan, N., 1992. Active filtering of harmonic currents in three-phase, four-wire systems with three-phase and single-phase non-linear loads. Conference Proceedings - IEEE Applied Power Electronics Conference and Exposition - APEC 829–836. https://doi.org/10.1109/APEC.1992.228328

Rahman, S., Saha, S., Haque, M.E., Islam, S.N., Arif, M.T., Mosadeghy, M., Oo, A.M.T., 2022. A framework to assess voltage stability of power grids with high penetration of solar PV systems. International Journal of Electrical Power & Energy Systems 139, 107815. https://doi.org/https://doi.org/10.1016/j.ijepes.2021.107815

Rashad, A., Kamel, S., Jurado, F., 2017. Chapter 2 - The Basic Principles of Wind Farms, in: Gharehpetian, G.B., Mousavi Agah, S.M. (Eds.), Distributed Generation Systems. Butterworth-Heinemann, pp. 21–67. https://doi.org/https://doi.org/10.1016/B978-0-12-804208-3.00002-9

Rashid, M.H., 2011. Power Electronics Handbook Third Edition.

Reca-Cardeña, J., López-Luque, R., 2018. Chapter 9 - Design Principles of Photovoltaic Irrigation Systems, in: Yahyaoui, I. (Ed.), Advances in Renewable Energies and Power Technologies. Elsevier, pp. 295–333. https://doi.org/https://doi.org/10.1016/B978-0-12-812959-3.00009-5

Reddy, B.R.S., Reddy, V.C.V., Kumar, M.V., 2023. Modelling and analysis of DC-DC converters with AI based MPP tracking approaches for grid-tied PV-fuel cell system. Electric Power Systems Research 216. https://doi.org/10.1016/j.epsr.2022.109053

Revathy, S.R., Kirubakaran, V., Rajeshwaran, M., Balasundaram, T., Sekar, V.S.C., Alghamdi, S., Rajab, B.S., Babalghith, A.O., Anbese, E.M., 2022. Design and Analysis of ANFIS – Based MPPT Method for Solar Photovoltaic Applications. International Journal of Photoenergy 2022, 9625564. https://doi.org/10.1155/2022/9625564

Rezk, H., Kanagaraj, N., Al-Dhaifallah, M., 2020. Design and Sensitivity Analysis of Hybrid Photovoltaic-Fuel-Cell-Battery System to Supply a Small Community at Saudi NEOM City. Sustainability 12. https://doi.org/10.3390/su12083341

Reznik, A., Simoes, M.G., Al-Durra, A., Muyeen, S.M., 2014. LCL Filter design and performance analysis for grid-interconnected systems. IEEE Trans Ind Appl 50, 1225–1232. https://doi.org/10.1109/TIA.2013.2274612

Rodríguez, J., Lai, J.S., Peng, F.Z., 2002. Multilevel inverters: A survey of topologies, controls, and applications. IEEE Transactions on Industrial Electronics 49, 724–738. https://doi.org/10.1109/TIE.2002.801052

Roy, A.K., Basak, P., Biswal, G.R., 2019. Low voltage ride through capability enhancement in a grid-connected wind/fuel cell hybrid system via combined feed-forward and fuzzy logic control. IET Generation, Transmission and Distribution 13, 2866–2876. https://doi.org/10.1049/iet-gtd.2019.0021

Sabir, A., 2019. A novel low-voltage ride-through capable energy management scheme for a grid-connected hybrid photovoltaic-fuel cell power source. International Transactions on Electrical Energy Systems 29. https://doi.org/10.1002/etep.2713

Sadeghkhani, I., Golshan, M.E.H., Mehrizi-Sani, A., Guerrero, J.M., 2018. Low-voltage ride-through of a droop-based three-phase four-wire grid-connected microgrid. IET Generation, Transmission and Distribution 12, 1906–1914. https://doi.org/10.1049/iet-gtd.2017.1306

SBP, 2022. Strategy Budget Presidency, Presidential Annual Program for 2023. Official Gazette dated 25 October 2022 and numbered 31994 repeated.

Sevilmiş, F., Karaca, H., 2019. Performance analysis of SRF-PLL and DDSRF-PLL algorithms for grid interactive inverters. International Advanced Researches and Engineering Journal 3, 116–122. https://doi.org/10.35860/iarej.412250

Shafiullah, M., Ahmed, S.D., Al-Sulaiman, F.A., 2022. Grid Integration Challenges and Solution Strategies for Solar PV Systems: A Review. IEEE Access 10, 52233–52257. https://doi.org/10.1109/ACCESS.2022.3174555

Shang, L., Guo, H., Zhu, W., 2020. An improved MPPT control strategy based on incremental conductance algorithm. Protection and Control of Modern Power Systems 5, 14. https://doi.org/10.1186/s41601-020-00161-z

Shezan, S.K.A., Saidur, R., Hossain, A., Chong, W.T., Kibria, M.A., 2015. Performance analysis of solar-wind-diesel-battery hybrid energy system for KLIA Sepang station of Malaysia, in: IOP Conference Series: Materials Science and Engineering. Institute of Physics Publishing. https://doi.org/10.1088/1757-899X/88/1/012074

Soto, E.A., Bosman, L.B., Wollega, E., Leon-Salas, W.D., 2022. Analysis of Grid Disturbances Caused by Massive Integration of Utility Level Solar Power Systems. Eng 3, 236–253. https://doi.org/10.3390/eng3020018

Sun, Y., Gao, B., Yao, Y., Fang, J., Zhang, M., Zhou, Y., Chen, H., Yang, L., 2014. Effects of feedstock type, production method, and pyrolysis temperature on biochar and hydrochar properties. Chemical Engineering Journal 240, 574–578. https://doi.org/https://doi.org/10.1016/j.cej.2013.10.081

TETC, 2023. Installed Power Report December 2022. Turkish Electricity Transmission Corporation.

Thirunavukkarasu, M., Sawle, Y., Lala, H., 2023. A comprehensive review on optimization of hybrid renewable energy systems using various optimization techniques. Renewable and Sustainable Energy Reviews 176, 113192. https://doi.org/https://doi.org/10.1016/j.rser.2023.113192

Trapani, K., Millar, D.L., 2013. Proposing offshore photovoltaic (PV) technology to the energy mix of the Maltese islands. Energy Convers Manag 67, 18–26. https://doi.org/https://doi.org/10.1016/j.enconman.2012.10.022

Velvizhi, G., Nair, R., Goswami, C., Arumugam, S.K., Shetti, N.P., Aminabhavi, T.M., 2023. Carbon credit reduction: A techno-economic analysis of “drop-in” fuel production. Environmental Pollution. https://doi.org/10.1016/j.envpol.2022.120507

Wen, H., Fazeli, M., 2019. A low-voltage ride-through strategy using mixed potential function for three-phase grid-connected PV systems. Electric Power Systems Research 173, 271–280. https://doi.org/https://doi.org/10.1016/j.epsr.2019.04.039

Worku, M.Y., Abido, M.A., 2015. Grid-connected PV array with supercapacitor energy storage system for fault ride through, in: 2015 IEEE International Conference on Industrial Technology (ICIT). pp. 2901–2906. https://doi.org/10.1109/ICIT.2015.7125526

Xu, S., Huang, W., Wang, H., Zheng, W., Wang, J., Chai, Y., Ma, M., 2023. A Simultaneous Diagnosis Method for Power Switch and Current Sensor Faults in Grid-Connected Three-Level NPC Inverters. IEEE Trans Power Electron 38, 1104–1118. https://doi.org/10.1109/TPEL.2022.3200721

Xu, Y.-P., Ouyang, P., Xing, S.-M., Qi, L.-Y., khayatnezhad, M., Jafari, H., 2021. Optimal structure design of a PV/FC HRES using amended Water Strider Algorithm. Energy Reports 7, 2057–2067. https://doi.org/https://doi.org/10.1016/j.egyr.2021.04.016

Yang, F., Yang, L., Ma, X., 2014. An advanced control strategy of PV system for low-voltage ride-through capability enhancement. Solar Energy 109, 24–35. https://doi.org/https://doi.org/10.1016/j.solener.2014.08.018

Yang, Y., Sangwongwanich, A., Liu, H., Blaabjerg, F., 2017. Low voltage ride-through of two-stage grid-connected photovoltaic systems through the inherent linear power-voltage characteristic, in: 2017 IEEE Applied Power Electronics Conference and Exposition (APEC). pp. 3582–3588. https://doi.org/10.1109/APEC.2017.7931212

Yang, Y.C., Wenjieand, B.F., 2014. Advanced Control of Photovoltaic and Wind Turbines Power Systems, in: Orłowska-Kowalska Teresa and Blaabjerg, F. and R.J. (Ed.), Advanced and Intelligent Control in Power Electronics and Drives. Springer International Publishing, Cham, pp. 41–89. https://doi.org/10.1007/978-3-319-03401-0_2

Zeb, K., Islam, S.U., Khan, I., Uddin, W., Ishfaq, M., Curi Busarello, T.D., Muyeen, S.M., Ahmad, I., Kim, H.J., 2022. Faults and Fault Ride Through strategies for grid-connected photovoltaic system: A comprehensive review. Renewable and Sustainable Energy Reviews 158, 112125. https://doi.org/https://doi.org/10.1016/j.rser.2022.112125

Zhao, J., Patwary, A.K., Qayyum, A., Alharthi, M., Bashir, F., Mohsin, M., Hanif, I., Abbas, Q., 2022. The determinants of renewable energy sources for the fueling of green and sustainable economy. Energy 238, 122029. https://doi.org/https://doi.org/10.1016/j.energy.2021.122029

CURRICULUM VITAE

Ramazan MACİT, completed his undergraduate education at Selçuk University, Department of Electrical and Electronics Engineering in 2019 with high honors. After graduating from his undergraduate education in 2019, he worked as a research assistant in the Department of Electrical and Electronics Engineering at Toros University in Mersin between 2020-2023. He is currently working as a research assistant at Eskişehir Technical University, Department of Electrical and Electronics Engineering in Eskişehir (2023). His research interests include Electrical Energy and Power Systems, Power Electronics, Circuits and Systems Theory, Renewable Energy systems and applications.